A Study of Suspended-Membrane and Acoustic Techniques for the

Determination of the Mechanical Properties

of Thin Polymer Films

by

Jeffrey Yen Pan

S.B., Electrical Engineering, Massachusetts Institute of Technology (1987)
S.M., Electrical Engineering, Massachusetts Institute of Technology (1987)

submitted in partial fulfillment
of the requirements for the degree of

Doctor of Philosophy
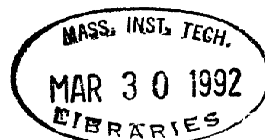
at the

Massachusetts Institute of Technology

October 1991

© Massachusetts Institute of Technology, 1991

Signature of Author⎯⎯⎯⎯⎯⎯⎯⎯⎯⎯⎯⎯⎯⎯⎯⎯⎯⎯⎯⎯⎯⎯⎯⎯⎯⎯⎯⎯⎯⎯
Department of Electrical Engineering
October 1991

Certified by⎯⎯⎯⎯⎯⎯⎯⎯⎯⎯⎯⎯⎯⎯⎯⎯⎯⎯⎯⎯⎯⎯⎯⎯⎯⎯
Professor Stephen D. Senturia
Barton L. Weller Professor of Electrical Engineering
Thesis Supervisor

Accepted by⎯⎯⎯⎯⎯⎯⎯⎯⎯⎯⎯⎯⎯⎯⎯⎯⎯⎯⎯⎯⎯⎯⎯⎯⎯⎯⎯⎯⎯
Professor Campbell L. Searle
Chairman, Department Committee on Graduate Students

A Study of Suspended-Membrane and Acoustic Techniques for the Determination of the Mechanical Properties of Thin Polymer Films

by

Jeffrey Yen Pan

Submitted to the Department of Electrical Engineering on September 30, 1991 in partial fulfillment of the requirements for the degree of Doctor of Philosophy

ABSTRACT

This thesis addresses the need for a set of techniques with which the mechanical properties of thin polymer films used in microelectronics can be accurately determined. This need comes from both the reliability concerns of the semiconductor industry as well as the microsensor design community. The variability of the mechanical properties of polymer films with temperature, humidity, processing, and direction requires modifications to typical measurement techniques to quantify. A number of candidate measurement methods are available. Among them are methods measuring wafer curvature, release-structure deformation, suspended-membrane deformation, resonant-structure behavior, acoustic-wave propagation, and uniaxial loading.

This study focuses on two promising techniques and explores ways of making them more suitable for the ask of measuring the effect of these variations. In addition, some limits on the techniques are also explored. These two techniques involve the measurement of membrane deformation and surface-acoustic-wave propagation.

Measurement of the pressure-deflection behavior of suspended membranes has already proved useful for determining the biaxial modulus and the residual stress in thin films. The capabilities of this technique have been extended with modifications in four key areas: sample measurement and positioning, data analysis and modeling, sample fabrication, and environmental control during testing. These modifications have improved the repeatability to ±3% and the accuracy to ±9%. With this good repeatability, control of the humidity, temperature, and processing conditions which the samples are exposed to now enables the measurement of the variation of biaxial modulus and residual stress of polyimide films with these parameters.

Development of the acoustic methods is conducted to investigate their applicability to the problem of measuring the degree of mechanical anisotropy in thin polyimide films. Validation of the results from optimized suspended-membrane measurements with independent acoustic tests is also undertaken. Once confirmed, the two methods are used together to measure the swelling parameter of polyimide films.

ACKNOWLEDGEMENTS

I would first like to thank my friends, my parents, and my brother for giving me the moral support and encouragement I needed to complete this thesis. I particularly thank Michelle for helping me through the personal challenges involved in pursuing a doctorate.

Three and a quarter years ago I joined Prof. Senturia's research group for a number of reasons, not the least of which was to meet and interact with a group of students and faculty at MIT that I had heard exciting things about from my friends. Now that I am finishing my degree, I would like to thank them all for making this not only a successful, but also an unforgettable experience.

I would especially like to thank my advisor, Prof. Stephen Senturia, for providing direction and counsel without impairing my own individuality and creativity. He has helped me in every aspect of my professional development from improving my technical writing skills to providing advice on how to find a job. It's only with hindsight that I can now see how truly committed he is to making sure his students learn the skills necessary to succeed.

I would also like to express my deepest gratitude to several people who helped me greatly by providing equipment and software necessary to complete this thesis. Dr. Daniel Oates and Robert Konieczka at MIT Lincoln Laboratory provided components and experience in packaging surface-acoustic-wave (SAW) devices. Prof. Eric Adler and Jacek Slaboszewicz, both from McGill University, furnished the multilayer SAW simulation software. Prof. Charles Sodini and Prof. Martin Schmidt, both from MIT, loaned me a network analyzer and digital oscilloscope respectively.

Considering my relative inexperience in semiconductor processing, the help I received from the staff and my fellow graduate students in the MIT Microsystems Technology Laboratories was invaluable. David Volfson and

3

TABLE OF CONTENTS

LIST OF FIGURES

LIST OF TABLES

CHAPTER I: INTRODUCTION

A. Motivation

Recent trends in the semiconductor industry indicate that improved packaging of integrated circuits into multi-chip modules and high-density-interconnect circuits will become an integral contributor to system performance improvements over the next few years [1, 2]. As in any aspect of semiconductor technology, materials science plays an important role in driving the technology. In packaging, however, the ability to control the deposition of the material and to tailor its electrical properties is not enough. As outlined by Tummala in [2], control of the mechanical properties is also required to achieve reliability in package designs.

The goal of this thesis is the development of a set of techniques for measuring mechanical properties interesting to a package designer. Because the properties to be measured are intimately related to the material of interest, improper selection of a material to be studied in this thesis can limit the usefulness of the methods developed. For this reason the materials investigated were restricted to polyimide films as described in the next section. This is an acknowledgement of both the key roles in packaging that polyimide plays as flexible substrates, insulating layers, interlevel dielectrics, passivation layers, and planarization layers [3, 4], as well as the wide range of mechanical behavior from viscoelasticity to brittle fracture exhibited by polymers in general [5]. Because polymer properties can vary dramatically with temperature, moisture, time, and processing, typical measurement techniques must be adapted to permit measurement and control of these factors.

Suspended-membrane techniques will be modified to measure swelling behavior, thermal expansion, viscoelasticity, and elastic moduli and residual stress as a function of processing in the polyimide films. An acoustic technique

11

will be used to determine mechanical anisotropy and to measure water absorption in the thin films. Necessary modifications of the two measurement techniques will be described in detail and results of measurements conducted on several commercial DuPont and Hitachi polyimides will be presented.

B. Materials

Polymers have played a key role in the field of packaging [3]. Polyimide, in particular, is an attractive material for many applications because of its excellent thermal stability, low dielectric constant, ease of deposition, low conductivity, and controllable etchability [4].

Polyimide is a condensation product of dianhydrides and diamines as shown in Figure 1.1 [6, 7]. In this figure, the R and R' groups of the monomers are often composed of many rings, and it is this high degree of backbone ring character in polyimides that contributes to its excellent properties [8, 9]. In DuPont Pyralin® 2555, which is the primary focus of this thesis, the dianhydride is benzophenone-tetracarboxylicdianhydride (BTDA) and the diamine is a mixture of metaphenylenediamine (MPDA) and oxydianiline (ODA) as shown in Figure 1.2. This polyimide is popular as an interlevel dielectric in double-level metal processes as well as in multichip modules.

dianhydride   diamine   polyamic acid
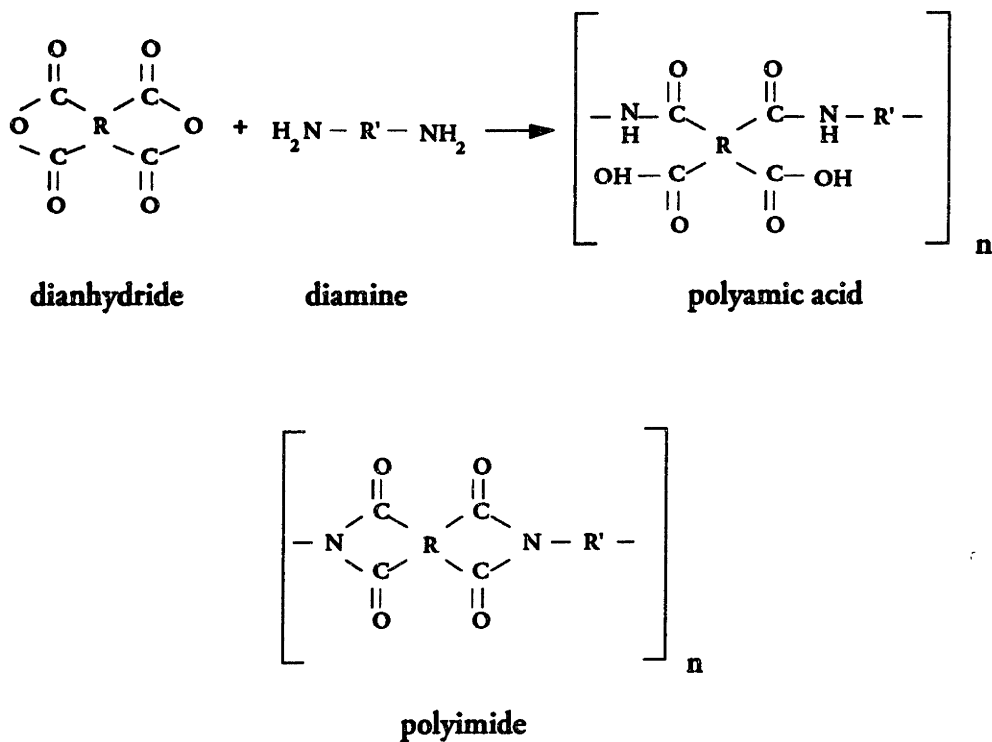
polyimide

Figure 1.1: Steps to formation of polyimide.

dianhydride   diamine

benzophenonetetracarboxylic   oxydianiline   metaphenylenediamine
dianhydride (BTDA)   (ODA)   (MPDA)
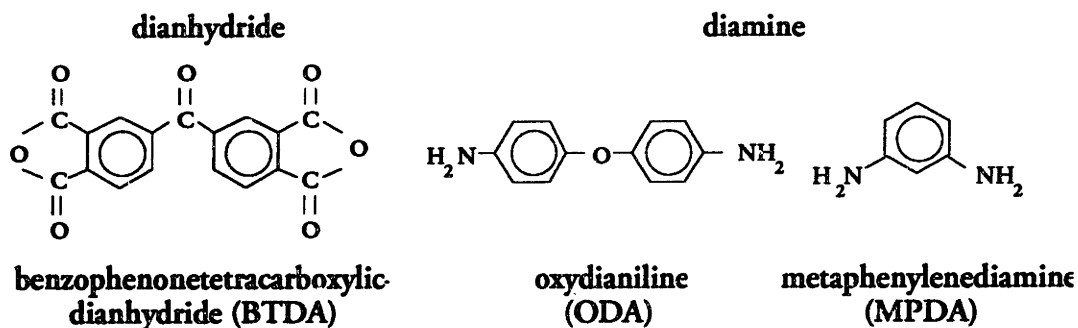
Figure 1.2: Chemical composition of dianhydride and diamines of DuPont Pyralin®
2555 polyimide.

The 2555 is supplied by DuPont as a polyamic acid formed by the reaction of

the dianhydride and the diamines in the solvent N-methylpyrrolidone (NMP).

Adhesion promoter, containing 0.5% γ-aminopropyltriethoxysilane in a 95%

methanol-5% water mixture, is spun onto the substrate just prior to polyimide

deposition. The polyamic acid is then poured onto the substrate and a uniform,

to within 1%, thickness of roughly 3 μm formed by spinning the substrate at

speeds in excess of 2000 rpm for 60 seconds. Thicker films are formed by applying additional coats without adhesion promoter. The nominal cure cycle involves a b-stage cure after each coat at 160° C for 30 minutes, which removes most of the solvent and completes roughly half of the imidization, followed by an anneal at 400° C for 90 minutes to complete the imidization [9].

In addition to the DuPont Pyralin® 2555, several films of other polyimides were supplied by Raychem for suspended-membrane measurements only. These other polyimides include Hitachi PIQ13 and the low-thermal expansion polyimides Hitachi PIQL100 and DuPont Pyralin® 2611. These films were nominally soft baked at 120° C for 90 seconds and cured at 400° C in a track furnace for an undisclosed amount of time. Measurement results on these polyimides are given in Chapter 2.

Finally, several films of DuPont Pyralin® 2556, a diluted version of 2555, were fabricated by Susan Noe for joint investigation of the effect of multiple cure cycles on the optical and mechanical properties [10]. The effects of the multiple cure cycles on 2556 are also discussed in Chapter 2.

A table given in Chapter 8 summarizes all the measurement results measured as part of this thesis.

C. Mechanical Properties of Interest

Numerous techniques already exist for measuring adhesion, thickness, density, elastic moduli, residual stress, and hardness of a given thin film sample. Given in Table I is a partial list of some of the more common methods of measuring each property. The large number of available methods for measuring each property is testimony to the amount of effort already undergone to develop mechanical property measurement techniques.

Each of the properties given in the table, however, are first order properties. That is, a single measurement, which is sometimes destructive, is sufficient to

14

provide a value for the property. For polymers, however, each of the properties can vary by several orders of magnitude depending on a number of other factors such as temperature, humidity, time, processing, etc [5]. A more useful measurement for polymers thus quantifies these effects by comparing the results of many experiments to determine the second-order properties as given in Table II. These are the mechanical properties that are measured in this thesis.

TABLE I
Mechanical properties and associated measurement techniques

Mechanical Property	Measurement Technique	Destructive?	Ref
adhesion	peel	Y	[11]
	pull-off	Y	[12]
	blister	Y	[13]
	island blister	Y	[14]
	acoustic	Y/N	[15-19]
thickness	stylus	Y	[20]
	reflectance-spectroscopy	N	[21]
	optical prism-coupling	N	[21]
	ellipsometry	N	[21]
	acoustic	N	[22]
mass/density	microbalance	N	[20]
	resonance	Y	[23]
	acoustic	N	[24]
residual stress	wafer curvature	N	[25]
	resonance	Y	[23, 26]
	membrane	Y	[27, 28]
	acoustic	N	[29]
elastic constants	uniaxial	Y	[30-32]
	membrane	Y	[33-35]
	acoustic	N	[36-39]
hardness	indenter	Y	[30, 40]

In order to measure these properties, a set of experiments must be carried out with only the parameter of interest varying. To conduct controlled experiments, all experiments should be conducted on the same sample of material and under

conditions similar to those under which it is used, i.e. without releasing residual stress in the film. Looking back at Table I, the question of whether a technique is destructive or not is now recognized as a potential limit to its effectiveness in measuring the second-order properties. If the measurement is not destructive, the precision, or resolution, of the technique limits the ability to measure second-order properties. This is because repeated measurements can be conducted on a single sample. If the measurement is destructive, the accuracy of the technique limits second-order resolution because several samples must be compared. Improvements in precision and accuracy of measurement methods are necessary to characterize polymer properties.

TABLE II

Additional mechanical properties found from measurements of the variation of mechanical parameters with experimental conditions

Mechanical Parameter	Experimental Variable	Mechanical Property
strain	temperature	coefficient of thermal expansion
strain	moisture	coefficient of hygroscopic expansion (swelling)
elastic constants	time	viscoelasticity aging
elastic constants	strain	yield
any	processing substrate	degree of cure
any	direction	anisotropy
any	position	multilayer/gradients

Of the properties listed in Table II, two have traditionally been difficult to measure for thin films because of a lack of a good non-destructive test for elastic moduli and residual stress: anisotropy of the elastic constants and swelling. Mechanical anisotropy in thin films is important to high-density-interconnect

designers because their structures are becoming increasingly three-dimensional in nature instead of the planar geometries of the past [2]. Swelling is important because of its impact on feature distortion and possibly more practically because of bubbling beneath hard masks when subject to temperatures in excess of the boiling point of the absorbed species [41].

From Table I, four techniques are available for measuring elastic moduli: uniaxial, membrane, resonance, and acoustic. Four techniques exist for measuring residual stress: wafer curvature, resonance, membrane, and acoustic. Of the three techniques that are common to both, the resonance techniques can be ruled out because they presently need to be done in a vacuum, so variations of humidity are not possible. The remaining two methods are reviewed briefly in the next two sections.

D. The Suspended-Membrane Technique
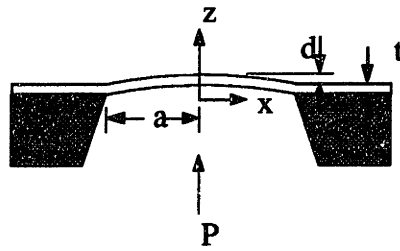
Figure 1.3: Deflection of a suspended membrane in response to an applied pressure.

The suspended-membrane, or load/deflection, method involves measurement of the center deflection of a membrane as a function of applied pressure as in Figure 1.3. For membranes with radius more than 200 times larger than the thickness, modeling of the mechanics [28, 32, 34, 42, 43] yields the relationship between the pressure, p, and the deflection, d:

$$p = \frac{C_1 t}{a^2} \sigma_o d + \frac{C_2 f(v) t}{a^4} \frac{E}{1-v} d^3 \qquad (1.1)$$

17

where a is the radius/half-edge length of the membrane, t the thickness, E the Young's modulus, ν the in-plane Poisson Ratio, σ_o the residual stress, and E/(1-ν) the biaxial modulus. The dimensionless constants C_1 and C_2 and the dimensionless function f(ν) are geometry and model dependent and given in Chapter 2. The function f(ν) is a slowly varying function of ν, changing only 6% for a variation of ν from 0.3 to 0.5 [43].

Beams [28], Bromley [27], Allen [34], and Maseeh [35, 44] have shown that the residual stress and biaxial modulus* of a thin film can be found through such experiments. The lure of the technique is that residual strain is measurable, so properties which affect it, such as thermal expansion coefficients and hygroscopic expansion coefficients, can be found from a series of such experiments. In order to obtain such data from a load/deflection experiment, however, it is necessary to improve the accuracy of the methods so that small effects become experimentally resolvable.

E. Acoustic Techniques

Acoustic techniques have been useful in determining the elastic constants of thin piezoelectric films. Wagers measured the properties of PVF$_2$ [45]. Carlotti examined ZnO [46]. Tsubouchi used the method to characterize AlN [39]. Their utility in measuring the properties of non-piezoelectric thin films has also been shown by Hickernell [47], Jelks [38], Frohlich [48], and Tittmann [49]. This thesis will extend the range of materials tested using these techniques to non-piezoelectric polymer thin films. The accuracy of the method will be compared against the suspended-membrane measurement techniques.

To determine the degree of mechanical symmetry in the film, modifications to the acoustic method are proposed. The use of modes other than the lowest-

---

* Biaxial modulus is found only to within a factor of f(ν). ν is often assumed to be 0.4 and a possible 3% error assumed.

18

order Rayleigh-like mode will be explored to enhance sensitivity to in-plane shear. With this modification, the five independent elastic constants of a transversely isotropic film can be found.

Another benefit of choosing acoustic methods to complement the suspended-membrane techniques is that mass loading of the surface-acoustic-wave oscillators has been shown by Wohltjen [24, 50] to be an effective technique for measuring mass uptake and diffusion coefficients.

F. Outline of Thesis

In Chapter 2 improvements that have been made to the modelling, fabrication, instrumentation, and data analysis of the suspended-membrane measurement will be detailed. Taking advantage of the improved reproducibility of the experiment, results of experiments to measure the effect of humidity, temperature, and processing on the mechanical properties will be presented. Limitations to the accuracy of the method will be explored.

Chapter 3 will begin describing the acoustic methods by providing background material on how acoustic waves can be excited and how the properties of interest can influence the propagation. Chapter 4 will build upon Chapter 3 by describing aspects of acoustic methods specific to the measurement of the mass uptake of a polymer film as a function of relative humidity. Chapter 5 will continue with the acoustic methods by describing aspects specific to the measurement of the elastic constants of a thin film.

Also in Chapter 5, the assumptions of isotropy in the polyimide film will be removed, and the acoustic methods are used to probe the degree of symmetry in the film. In Chapter 6, the results of both the suspended-membrane experiments and the acoustic measurements will be investigated together to confirm the accuracy of the measurements and to find values for the swelling parameter of the polyimide films. In Chapter 7, the knowledge gained from the previous

19

chapters is applied to the characterization of a single batch of simultaneously prepared 2555 films and the results presented. Chapter 8 will summarize, provide a table of properties measured, and draw conclusions based on this thesis work.

CHAPTER II: SUSPENDED-MEMBRANE METHODS

A. Previous Work on Suspended-Membranes

A number of authors have already shown the usefulness of suspended-membrane methods for measuring thin-film mechanical properties [27, 28, 33-35, 42-44, 51-53]. The technique has suffered from accuracy problems, however, that limit its effectiveness. The equation relating the pressure p and the deflection d is:

$$p = \frac{C_1 t}{a^2} \sigma_o d + \frac{C_2 f(v) t}{a^4} \frac{E}{1-v} d^3 \qquad (2.1)$$

where a is the radius/half-edge length of the membrane, t the thickness, E the Young's modulus, v the in-plane Poisson Ratio, σ_o the residual stress, and E/(1-v) the biaxial modulus.

The load-deflection method consists of five basic blocks as shown in Figure 2.1. Furthermore, FEM modeling by Maseeh [35] has shown that whereas in square membranes the maximum stress is located at the edge midpoints, the highest stress in circular geometries is in the center. The preferred membrane shape is thus circular in order to reduce sensitivity to membrane edge variations.

Considering equation (2.1), which is the result of analytical modeling of membrane deformation, it is apparent that a number of potential sources of error exist in this measurement. First, a number of geometry factors must be measured accurately. Since the radius of the membrane is raised to the fourth power, any inaccuracy in the measurement of the radius affects the extracted modulus four times as much. The thickness appears only linearly in the equation, so the effect of an error in thickness measurement appears directly. This indicates that the ability to accurately manufacture and measure circular membranes is one critical source of error.
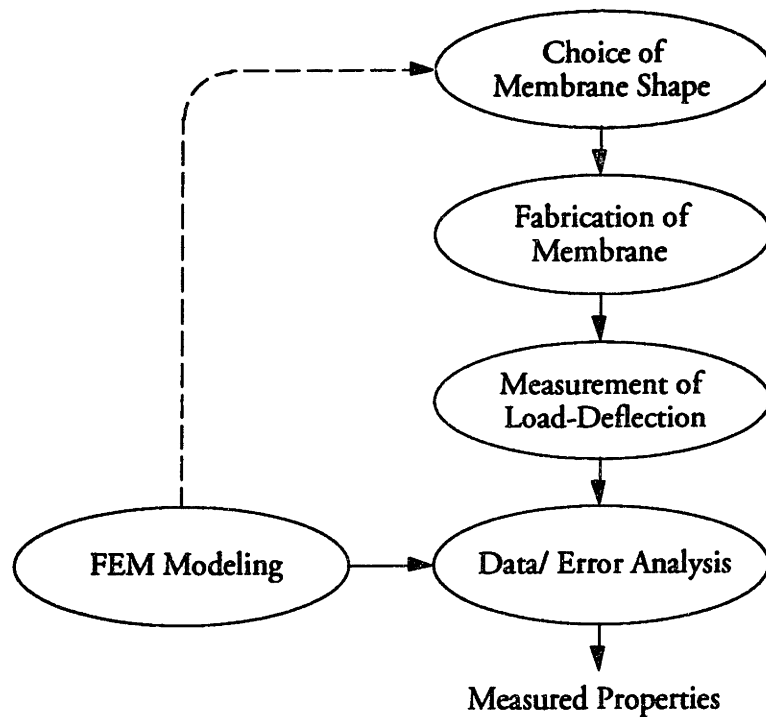
Figure 2.1: Basic elements of load-deflection method.

Another problem area is finding the applicable range of validity of the models. First, the factors C_1, C_2, and $f(v)$ are model and geometry dependent. Second, polymers are known to be viscoelastic [5]. Time-dependence and inelastic behavior is not accounted for in the models, so equation (2.1) is not suited for loading beyond the linear elastic limit. Third, the models are derived with an assumption that bending stiffness can be neglected. This assumption reaches a limit when the radius of the membrane becomes less than 200 times the thickness [42].

Finally, the suspended-membrane techniques are insensitive to out-of-plane properties. Furthermore, only the tensile stresses can be measured and the biaxial modulus of the film can only be found to within a function of the Poisson ratio. The in-plane Poisson ratio is still difficult to extract. Allen [54] has proposed that correlating the load-deflection results from circular and rectangular suspended membranes should yield the in-plane Poisson Ratio, but initial experiments have

22

failed due to the previously stated inaccuracies in the method. Improvements to the technique may eventually make the Poisson Ratio measurement viable.

In order to improve the accuracy and reproducibility of the suspended-membrane methods, improvements had to be made in the four key areas identified above: fabrication of the samples, measurement and testing of the samples, data analysis, and modeling.

B. Improving the Accuracy of Suspended-Membrane Models

In order to improve the accuracy of the models used to analyze load-deflection data, numerical load-deflection experiments were performed using finite-element analysis and the residual stress and biaxial modulus extracted according to equation (2.1). The extracted values were then compared against the parameters of the experiment to determine the accuracy of the models. In the event of a difference, the constants C_1 and C_2 and the dimensionless function $f(v)$ were adjusted to eliminate the error. Subsequent tests were then done to verify their values. Through such an analysis, Lin [42, 43, 55] showed that the values of these constants for circular and square membranes are as given in Table III.

The results of a similar numerical analysis of rectangular membranes for which the length is greater than eight times the width are also listed. ADINA (ADINA Engineering Inc., Watertown, MA) running on a Sun-4 workstation was the FEM program used to analyze the membranes. One quarter of a membrane with length 2", width 1/4", thickness 5 μm, and circular ends was simulated with 1296 four-noded shell elements. The input file is given in Appendix C.

TABLE III
Modeled values of C_1, C_2, and $f(v)$ for square, rectangular and circular membranes.

Membrane Shape	C_1	C_2	$f(v)$
Circular	4.0	2.67	$0.957 - 0.208v$
Square	3.41	1.37	$1.446 - 0.427v$
Rectangular	2.0	1.33	$(1+v)^{-1}$

The values of the constants in equation (2.1) are important for a number of reasons. First, the accuracy of the extracted properties is directly dependent on their accuracy. Second, the values given in Table III mark a dramatic departure from the values used by previous researchers in the field [28, 33, 34, 53]. Those initial models were derived from analytical models alone and their inaccuracy resulted from an inaccuracy of the assumed deflected shape. Using a microscope with a calibrated xy-stage, the deflected shape of a square membrane was measured and compared with the modeled shapes, as shown in Figure 2.2 [43]. The excellent agreement between the FEM calculated and the measured shapes confirms the accuracy of the FEM derived constants.
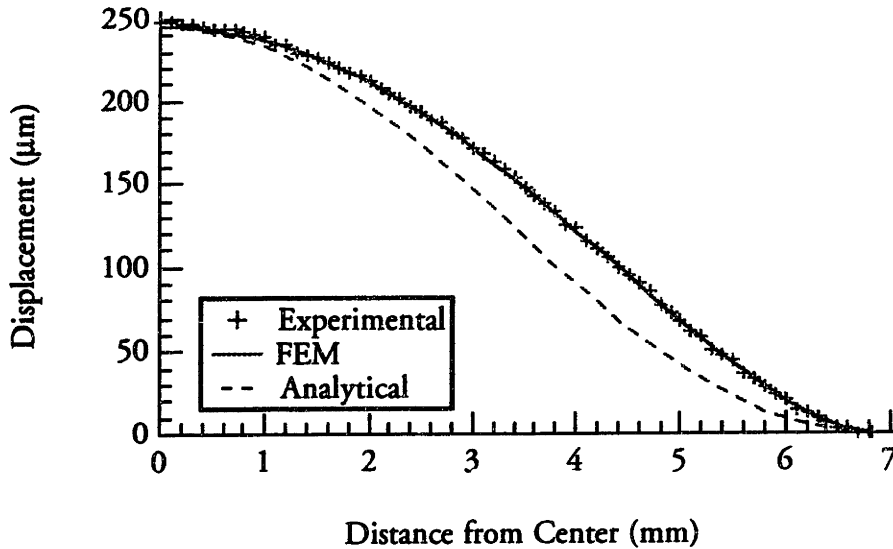
Figure 2.2: Experimental deflected shape vs. FEM results and analytical model for diagonal of square membrane.

The third reason the new values are important is that it very clearly reminds us of the need to verify the results of load-deflection experiments with independent measurements. Without the independent confirmation of the models with finite element analysis, we would have no way of knowing that the analytically derived values were incorrect.

Finally, armed with the more accurate models, the proposal by Allen [54] to compare the results from square and rectangular membranes to calculate a value for the in-plane Poisson ratio of the film becomes more viable. By taking the ratio of $C_2f(v)$ for the circular membranes versus the value for rectangular membranes, Figure 2.3 can be derived, which can in principle be used to find the in-plane Poisson ratio, as explained later.
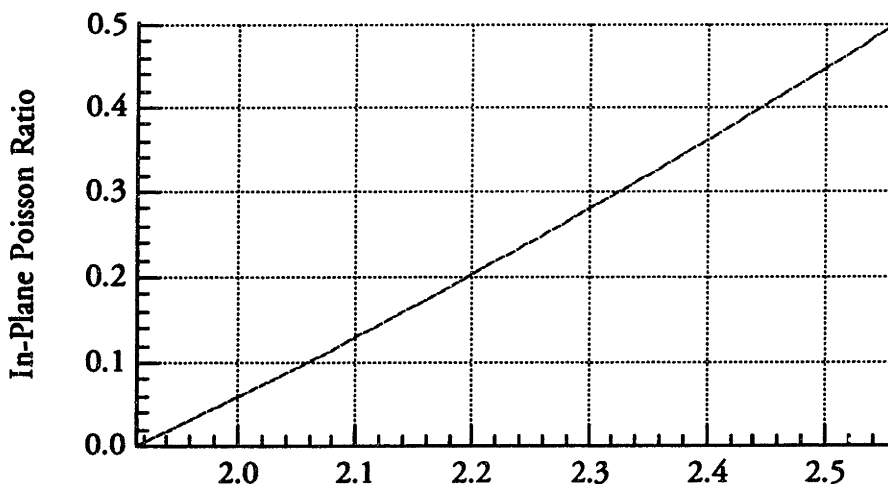
$$\frac{[C_2f(v)]_{circular}}{[C_2f(v)]_{rectangular}}$$

Figure 2.3: Chart for finding the in-plane Poisson ratio from the ratio of measured $C_2f(v)$ for circular membranes to that for rectangular membranes.

C. Simplifying the Fabrication of Suspended Membranes

The first step in conducting load-deflection measurements is to fabricate the suspended membrane. Three requirements arise for the suspended membranes that are used. First, the residual stress in the film must be preserved throughout

the fabrication. Second, we must be able to make accurate circular membranes. Third, for the samples obtained from our sponsors, the process must begin with polyimide films spun-cast onto plain five-inch silicon wafers.

Many of the fabrication processes use anisotropic etchants of silicon to provide an attractive method for making square or rectangular membranes [27, 34], but the process is complicated and cannot easily form circular geometries. Furthermore the alkaline etchants attack polyimide, so the membrane is typically formed by first depositing the film onto silicon diaphragms and then plasma etching the silicon diaphragm to leave just the film supported by the silicon wafer [34]. This process is not compatible with previously mentioned requirement that the process begin with polyimide films spun-cast onto plain five-inch silicon wafers.

A simpler fabrication process [35, 44] starts with the bonding of a circular support ring to the top side of a coated two-inch silicon wafer with an epoxy resin. The ring and the epoxy are then overcoated with black wax. Etching the entire silicon wafer in a 6:1:1 mixture of $HF:HNO_3:CH_3COOH$ [56] then transfers the stress to the supporting ring. The acid mixture does not attack the polyimide film.

Attempts to extend this technique to five-inch diameter silicon wafers and more brittle films failed for two reasons. First, the extended etch times of the larger wafer made it impossible to sufficiently protect the epoxy from the etch. Most of the time either the black wax de-adhered or the HF diffused through the polyimide film to attack the epoxy. Second, the pressure of the etch against the free-standing membranes was sufficient to shatter those formed from brittle materials. Minimization of the exposure of the epoxy to the silicon etch, and the provision of positive support for the membrane throughout the process were the primary goals for our improved process.

In our improved process, a silicon wafer, coated on one side with the film of interest, is clamped into a teflon jig (See Figures 2.4 and 2.5). A window in one side of the jig defines the eventual membrane's size, shape, and position. The teflon jig masks the surrounding areas from the etch and provides positive support for the membrane after its release. A 6:1:1 mixture of $HF:HNO_3:CH_3COOH$ is poured into the well formed by the jig and the silicon wafer to etch the exposed silicon. Upon rinsing, the wafer is removed from the jig, and the membrane is complete. The residual stress is supported by the unetched portion of the silicon wafer throughout the process.
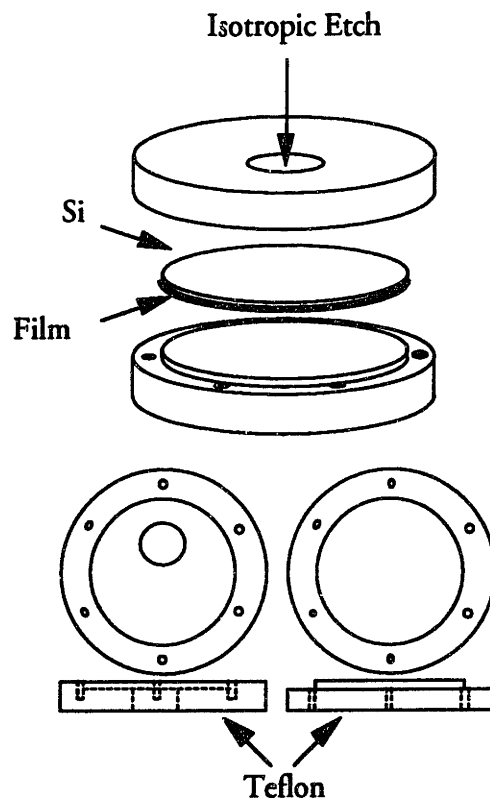
Figure 2.4: Jig for fabricating suspended membranes

Using this technique, 19-mm-radius circular membranes have been made from eight different polyimides ranging in thickness from 2 μm to 50 μm. A variation of less than 0.5 mm in the radius of the membranes was measured. 25-

27

mm-diameter membranes have also been successfully fabricated from 50-mm-diameter wafers demonstrating that a silicon ring as little as 12-mm wide is capable of supporting the film. 50-mm x 6-mm rectangular membranes have also been made to demonstrate the flexibility in the geometry that this technique allows.
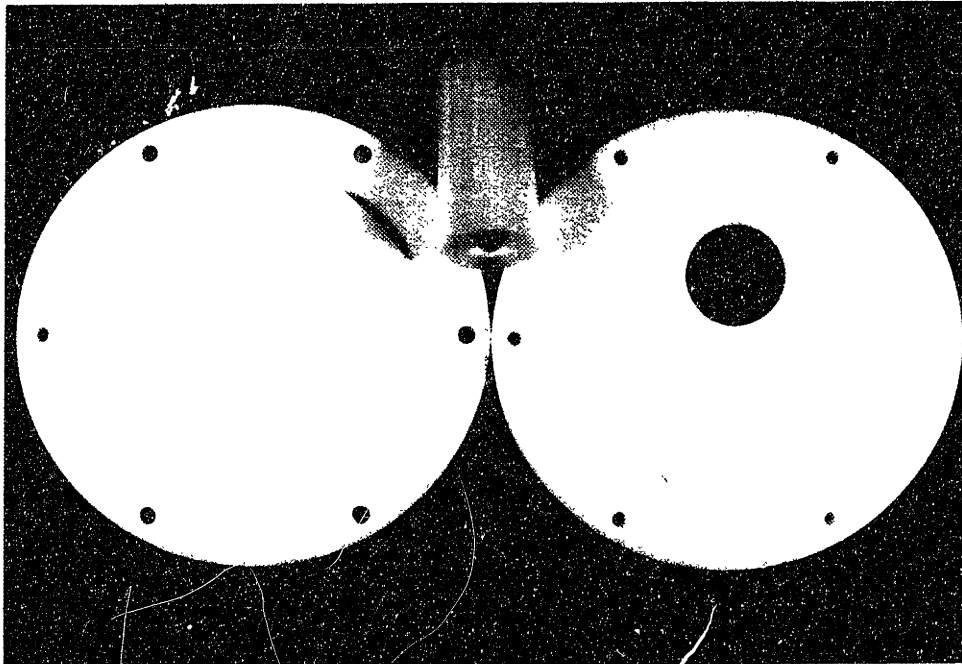
Figure 2.5: Photo of jig for fabricating suspended membranes

In order to improve the accuracy of the radius of our circular mechanical test samples, a precisely machined, 12.7-mm-radius Vespel® ring is bonded to the membrane with epoxy [44]. The surface in contact with the film is tapered to help prevent the flow of the low-viscosity epoxy past the inner radius of the ring. The teflon jig is used to carefully lower the ring into place on the membrane as in Figure 2.6. When the film is cut away from the silicon support, the residual stress is transferred to the ring. Mounting the ring to an aluminum plate completes the fabrication of the mechanical test site. Figures 2.7 and 2.8 detail the stages of membrane fabrication.
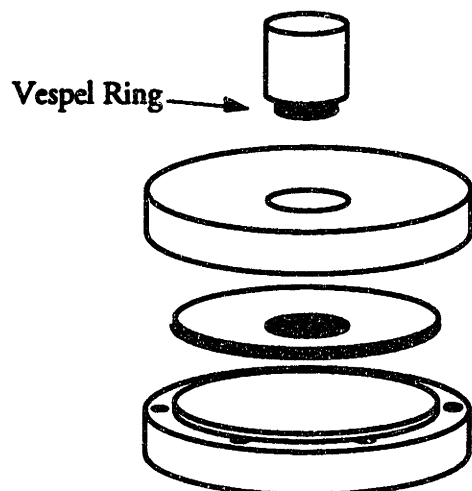
Figure 2.6: Using jig as an aid in epoxying Vespel rings to suspended membrane.
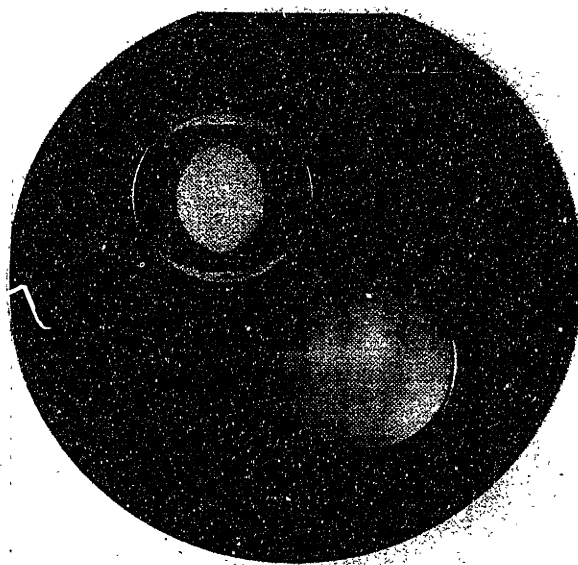
Figure 2.7: Photo of etched silicon wafer with mounted Vespel® ring.
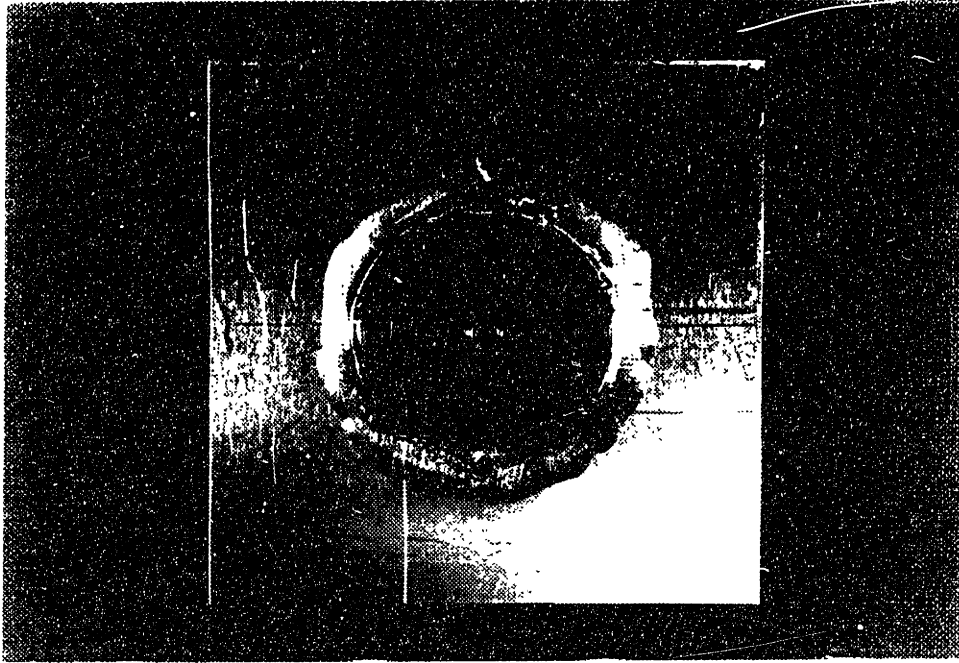
Figure 2.8: Photo of membrane mounted onto aluminum plate, ready for testing

D. Equipment for Measuring the Response to Pressure Loading

The primary requirement in setting up the measurement system was to choose instruments that would measure all of the parameters in equation (2.1). The system is shown in Figure 2.9. A Nikon UM-2 measuring microscope equipped with two Boeckeler model 9598 digital micrometers connected to a Metronics Quadra-Chek II digital readout box was used to measure the dimensions of the membranes. The maximum error in each axis for the calibrated x-y stage was less than 3 μm. The radius measurements were accurate to about 10 μm. The thicknesses of the films were taken from Dektak measurements and were estimated to be accurate to 2%.

The samples, mounted on aluminum plates, were clamped into a custom-designed pressurizing jig machined from aluminum for testing (see Figure 2.10) under controlled humidity. An O-ring seals against the aluminum plate for the pressure seal. A cover slip of glass permits tracking of the center deflection of the

membrane with the microscope and also forms a humidity control chamber over the top of the membrane. Dry air (dewpoint < -45° C) was combined with air bubbled through water and the dewpoint of the resulting mixture measured to supply the humidity-controlled air to the jig (see Figure 2.11). Using this method, the relative humidity during testing could be controlled to within 2% from less than 0.2%, which will be considered 0%, to 60%. Figure 2.12 shows the mounted membrane undergoing testing.
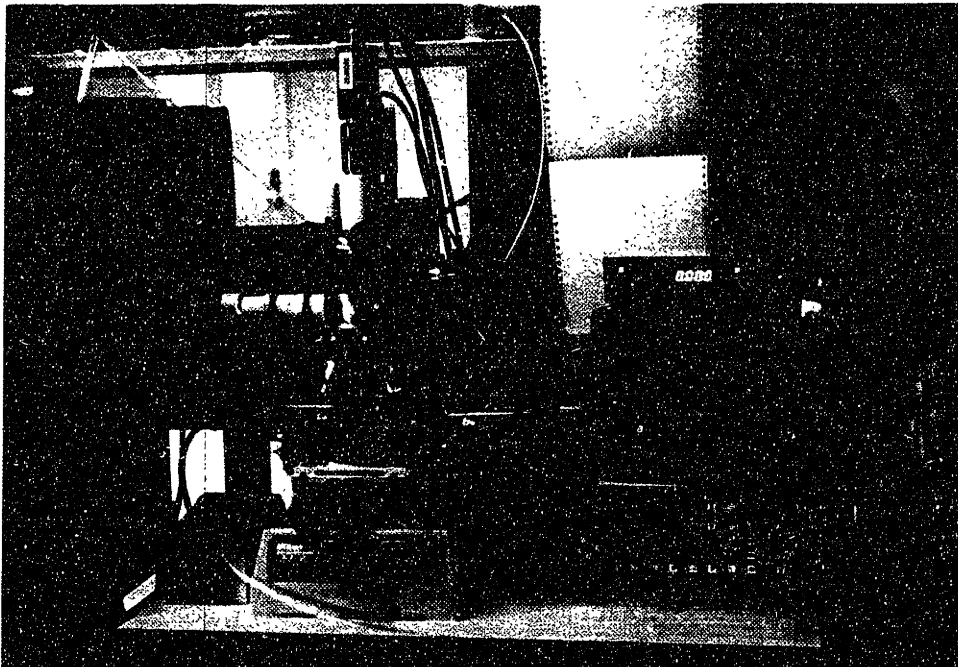
Figure 2.9: Photo of microscope and measurement system for load-deflection measurements
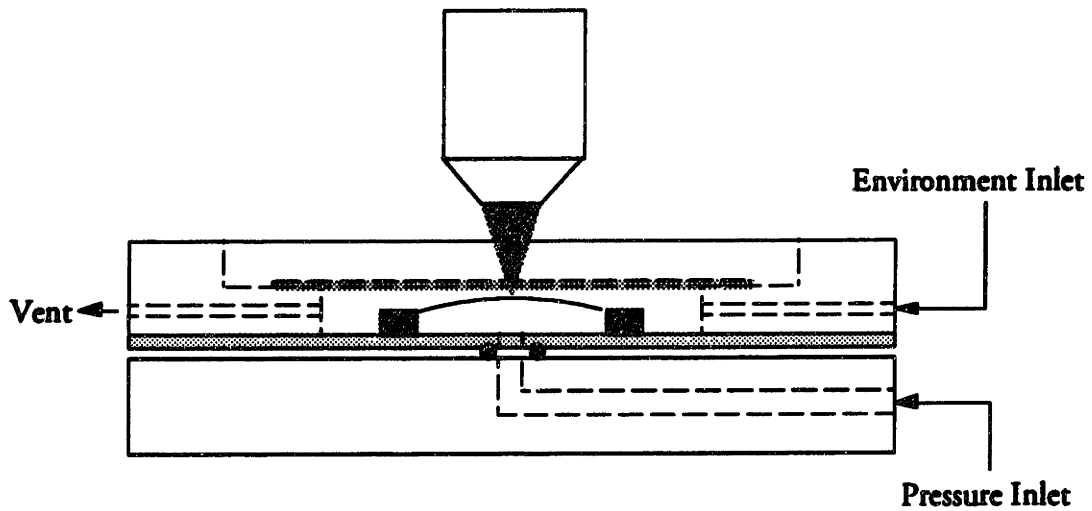
Figure 2.10: Jig for holding suspended membranes for testing.
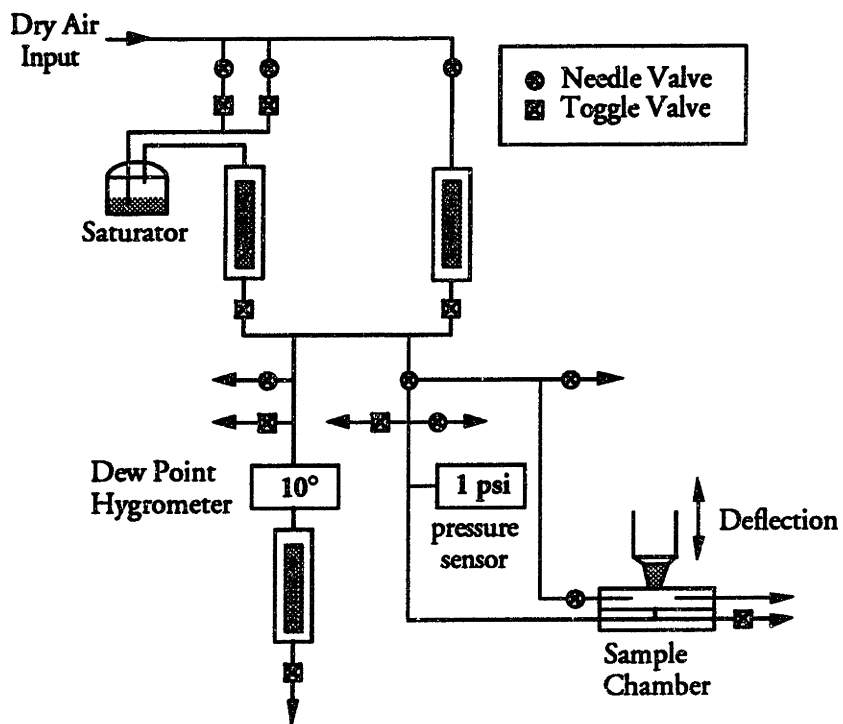
Figure 2.11: System used to control humidity of air flowing into test chamber.

Figure 2.12: Photo of mounted membrane undergoing testing

Computational routines inside the Quadra-Chek II were used to locate the center of the membrane under test. Center deflections resulting from varying pressure loads for each membrane were then measured with the microscope [33, 34, 43, 52]. The pressure was incremented to yield deflections in 50 μm steps up to a maximum of 1 mm for the 12.7-mm-radius membranes. A 40X objective with a numerical aperture of 0.5 provided the sub-micron depth of focus needed to locate the surface of the membranes. A 543-series Mitutoyo digimatic indicator was used to track the z-axis movement of the microscope head. The total measurement error in the deflection was less than 2 microns. Pressure readings from 0 to 5 psi ± 0.02 psi were converted to voltages with a Microswitch 142PC05G pressure sensor powered by a Hewlett Packard 6114A Precision Power Supply. The voltage was measured with a Hewlett Packard 3478A Multimeter. The multimeter was connected to an IBM PC-AT with a National Instruments AT-GPIB IEEE-488 compatible board. The z-axis micrometer and a footswitch were linked to the PC through a serial interface box.

A computer program written in BASIC acquired, printed, and stored the data from the micrometer and the multimeter in response to a footswitch signal from the user that the surface of the membrane was in focus (see Appendix B). Figure 2.13 is a schematic drawing of the measurement system. Figure 2.14 shows typical data from a load-deflection experiment, plotted as p/d vs. d^2.

IEEE-488
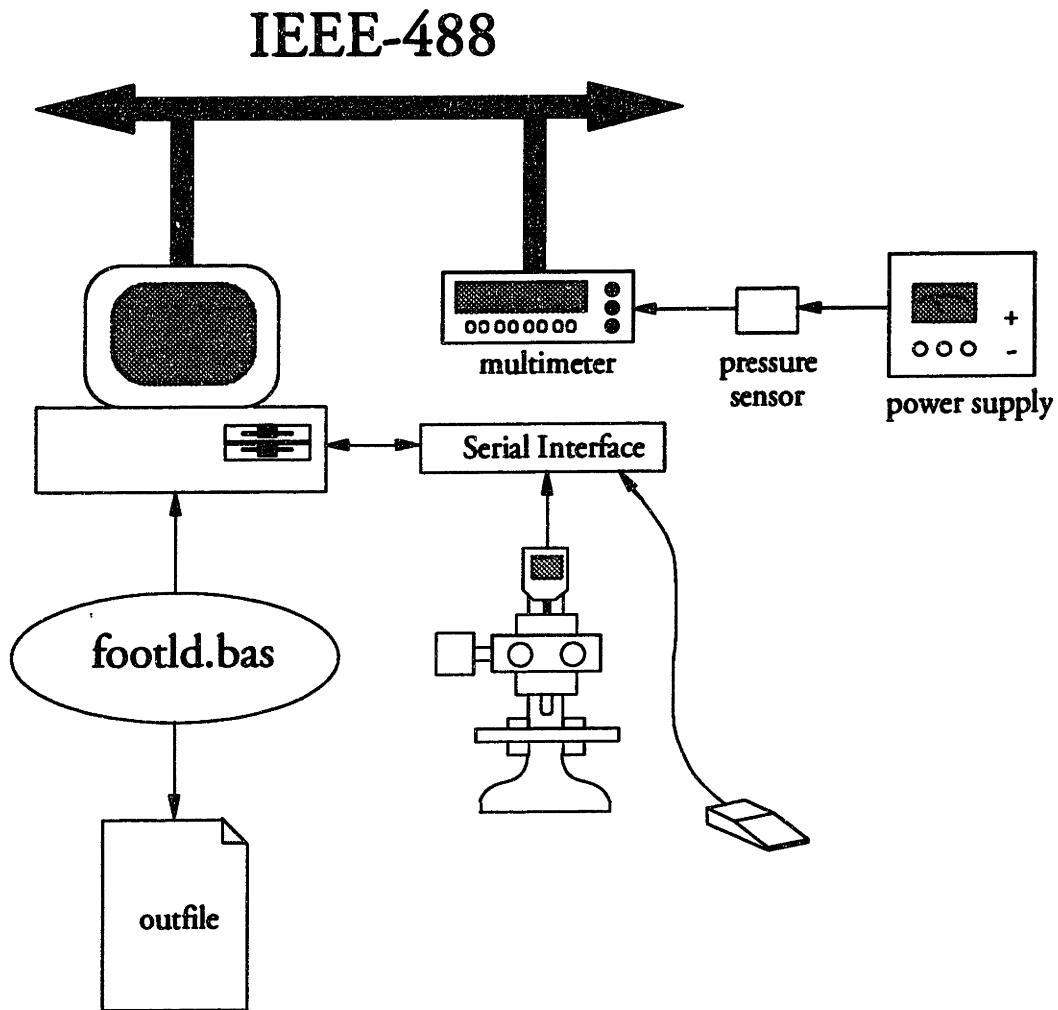
Figure 2.13: Semiautomated load-deflection test system.
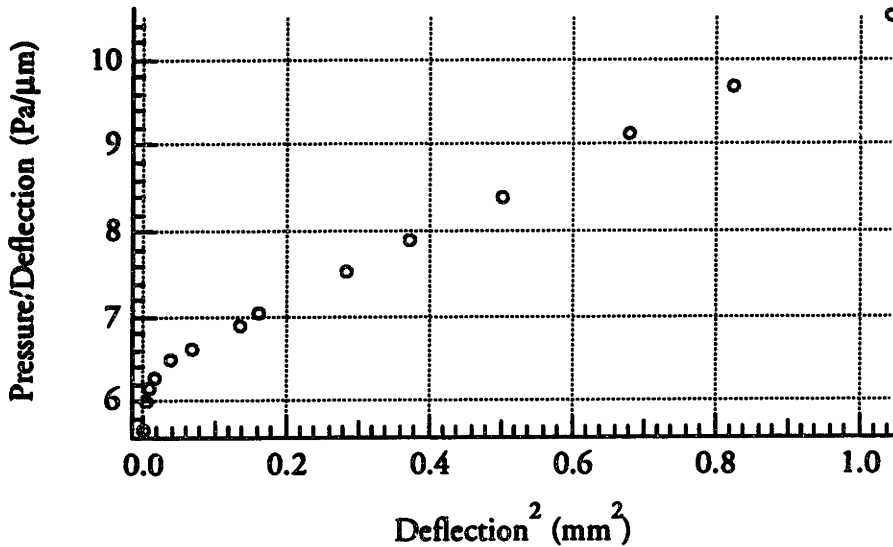
Figure 2.14: Typical pressure-deflection data from a load-deflection experiment.

E. Data Reduction and the Extraction of the Mechanical Properties

As evident from equation (2.1), plotting p/d vs. d^2 should yield a straight line. The residual stress can then be extracted from the intercept and the biaxial modulus from the slope of the least-squares-best-fit line. This is the method used in [42]. Occasionally, however, the experimental data can look like it does in Figure 2.14, with a slight curvature at low deflections. This curvature is due to pressure measurement offset errors, on the order of 0.02 psi, introduced by the presence of a positive pressure on the top side of the membrane or errors during the calibration of the sensor. The positive pressure is needed to control the humidity of the air surrounding the membrane under test.

Least-squares fitting, with b_0, and b_1 as the fitting parameters, to an equation of the form:

$$\frac{p}{d} = b_0 + b_1 d^2 \tag{2.2}$$

can be thought of as a weighted least-squares fitting to (2.1) with the weighting equal to 1/d. This would tend to emphasize the points at low deflections, where

the error is most evident. To avoid this problem, a more reliable equation to fit to is:

$$p = b_0 d + b_1 d^3 + p_0 \qquad (2.3)$$

where p_0 is now an explicit fit parameter to account for the pressure and deflection offset errors, and is included only when it is statistically significant.

The residual stress and biaxial modulus can be extracted from the fitted values of b_0 and b_1 by comparison with (2.1). The equations are:

$$\sigma_o = \frac{b_o a^2}{C_1 t} \qquad (2.4a)$$

$$\frac{E}{1-v} = \frac{b_1 a^4}{C_2 f(v) t} \qquad (2.4b)$$

As explained earlier, since $f(v)$ is a slowly varying function of v, we simply substitute an estimated value of 0.4 in $f(v)$ to extract the biaxial modulus when a measurement of the Poisson ratio has not been made. The resulting error is $\pm3\%$. Alternatively, when b_1 is known for both a circular and a rectangular membrane, the ratio of $b_1 a^4/t$ for the two geometries yields the ratio of $C_2 f(v)$ needed to use Figure 2.3.

From (2.4a) and (2.4b), it should be clear that the resolution of the measurement of a given membrane is dependent on the precision with which b_0 and b_1 can be found. Using a 95% confidence level and a routine collection of 15 to 20 pressure-deflection points, the uncertainty in b_0 and b_1 is approximately $\pm2\%$. The details of computing the values for b_0 and b_1 and their errors are given in Appendix B. The pressure offset error, p_0, when statistically significant, is usually less than 0.02 psi which compares favorably with the error specified for our Microswitch pressure sensor.

The accuracy of the values of residual stress and biaxial modulus is controlled by the accuracy with which the thickness and geometry are determined, as well

as by modeling errors. The estimated error in thickness is ±2% due to thickness variation across the membrane as well as measurement errors. The modeling error is on the order of 1% in stress and 2% in modulus found by comparing the results of different finite element computations [55]. The dominant error is the radius measurement because of the squared dependence of stress on its value and the fourth-power dependence of the modulus. The estimated 2% error in geometry measurement leads to a 4% error in stress and 8% error in modulus. Assuming the errors are uncorrelated, the total squared error is the sum of the individual squared errors. This leads to an accuracy of ±9% in biaxial modulus and ±5% in stress.

One final concern is the effect of humidity on the mechanical properties. Our apparatus can only control humidity to ±2%, so assuming linear swelling, the mechanical properties at a given humidity can only be resolved to 3%, and accurately measured to 9% in modulus and to 5% in stress.

F. Experimental Results: Humidity Effects

TABLE IV
Process conditions for polyimide film samples.

Polyimide	spin parameters	b-stage	anneal	# layers/ thickness
DuPont 2555	2000 rpm 60 secs	160° C 30 minutes	400°C 90 minutes	2 6.15 μm
DuPont 2556	4500 rpm 60 secs	180° C 3 minutes	375°C 40 minutes	2 2 μm

Films of 2555 and 2556 were prepared according to Table IV. Samples of Hitachi PIQ13, Hitachi PIQL100, and DuPont Pyralin® 2611 were supplied on five-inch silicon wafers by our sponsors. The thicknesses, measured with a Dektak profilometer, were 7.65 μm, 5.65 μm, and 19.3 μm respectively The process parameters for the wafers were not provided, but similar production films are b-cured at 160° C for 2-3 minutes and annealed at 400° C for an undisclosed amount of time in a track furnace.

The results of measurements of the effect of humidity on the five polyimide films are given in Tables V and VI. The radii of the circular membranes were nominally 12.7 mm. The data taken for a 2555 film are graphed in Figures 2.15 and 2.16. No variation in biaxial modulus with humidity is listed for 2555 because the value found was not statistically significant. The error bars are calculated according to Appendix B using a confidence level of 95%. All experiments were conducted at room temperature, which varied from 20° to 22° C. In each case, the samples were kept in a bell jar with desiccant for at least 24 hours before testing. After mounting the sample in the jig, dry air (RH < 0.2%) was flowed through the jig for at least eight hours to thoroughly dry out the sample. Subsequently, the RH was raised in approximately 20% increments, and the sample allowed to equilibrate for eight hours before remeasuring.
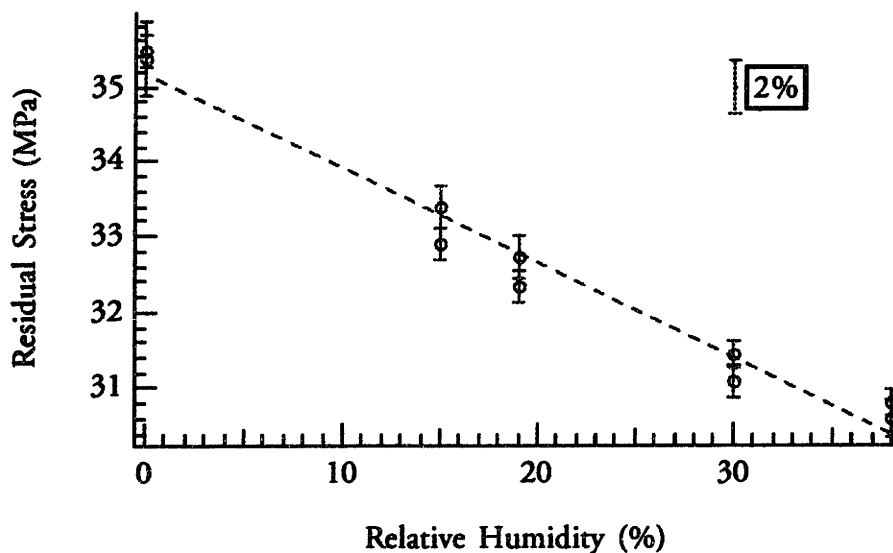
Figure 2.15: Measured residual stress at 20° C as a function of relative humidity for DuPont PI2555 film.
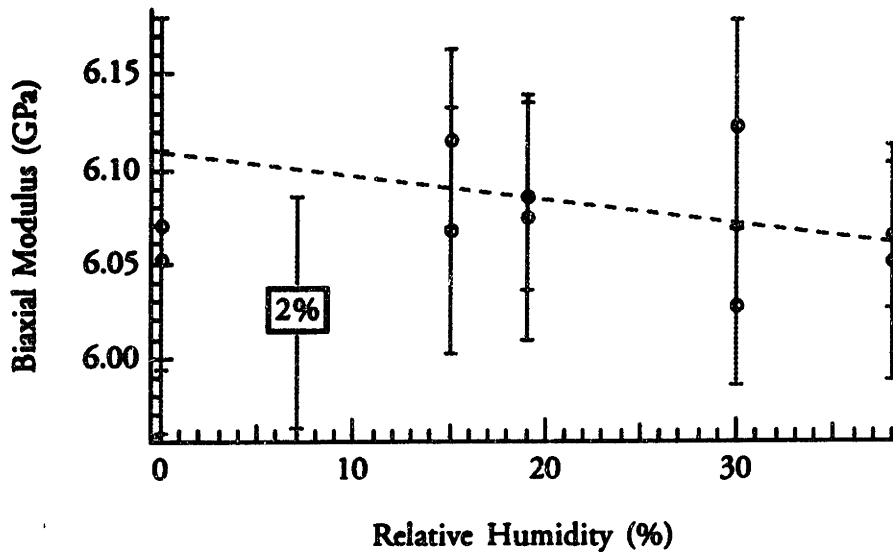
Figure 2.16: Measured biaxial modulus at 20° C as a function of relative humidity for DuPont PI2555 film.

Equilibration of the residual stress usually occurred within the first hour, whereas the biaxial modulus required as much as eight hours to equilibrate. The long equilibration times are much longer than the diffusion times measured by other researchers [57, 58], but have been found to be necessary for these mechanical tests. This could indicate either a problem with the transport of moisture into or out of the film once it is mounted in the testing jig or a slow internal mechanical relaxation process involving moisture in the polyimide.

For all the polyimides, both the residual stress and the biaxial modulus decreased with increasing humidity. The errors for the values are computed for a 95% confidence level given eight measurements on the same membrane in the humidity range from 0 % to 60%, and do not include the estimates of geometry and modeling errors. When a Poisson ratio of 0.4 is assumed, the measured values of modulus at 0% RH for the PIQ13 and PIQL100 films agree to within the measurement error with published values of Young's modulus of 3.3 GPa and 11 GPa respectively [59]. The rate of change of the residual strain as a function

of relative humidity for DuPont PI2555 is 0.0021% strain/%RH and compares very well with the published value of 0.0022% strain/% RH for Vespel [60].

TABLE V
Measured effect of humidity on the residual stress and modulus of thin polyimide films.

Polyimide	Residual Stress (MPa) at 0% RH	Biaxial Modulus (GPa) at 0% RH	Variation of Stress with Humidity (kPa/%RH)	Variation of Modulus with Humidity (MPa/%RH)
Hitachi PIQ13	36.1 ± 1	6.17 ± 0.06	-120 ± 26	-6.2 ± 1.5
Hitachi PIQL100	11.5 ± 0.4	17.7 ± 0.1	-47 ± 12	-7.3 ± 2.9
DuPont PI2555	35.2 ± 0.4	6.08 ± 0.04	-130 ± 18	---
DuPont PI2556	28.1 ± 0.9	6.40 ± 0.09	-150 ± 33	-8.0 ± 3.3
DuPont PI2611	34.8 ± 0.7	14.4 ± 0.1	-89 ± 18	-5.5 ± 2.8

TABLE VI
Measured effect of humidity on the residual strain of thin polyimide films.

Polyimide	Residual Strain (%) at 0% RH	Variation of Strain with Humidity (%/%RH)
Hitachi PIQ13	0.59 ± 0.02	-0.0014 ± 0.0006
Hitachi PIQL100	0.065 ± 0.003	-0.00025 ± 0.00008
DuPont PI2555	0.58 ± 0.01	-0.0021 ± 0.0004
DuPont PI2556	0.44 ± 0.009	-0.0019 ± 0.0003
DuPont PI2611	0.24 ± 0.006	-0.00054 ± 0.0002

We also measured the load-deflection behavior of several 50 mm x 6 mm rectangular membranes of Hitachi PIQ13 for comparison against the circular results. The residual stress varied from 28 MPa to 33 MPa. Using Figure 2.3 and the circular results, the extracted values of Poisson ratio varied from 0.3 to 0.5. The large variation is due to our inability to accurately control the width of the

40

rectangular membrane to better than 5%. From the above error analysis, this would indicate an uncertainty in the measured residual stress of 10% and the extracted modulus of 20%. The circular results are only accurate to 10%, so the Poisson ratio estimate is only measured to within 30%. With more precise rectangular membranes, made using anisotropic etchants such as potassium hydroxide [27, 34], the Poisson ratio measurement should be more accurate.

G. Experimental Results: Temperature Effects

In order to carry out a temperature-controlled experiment, two Chromalox CIR-1013 cartridge heaters and a WTJ-12-M-24 washer thermocouple from Omega Engineering were mounted into the load-deflection test jig shown in Figure 2.10. The thermocouple and heaters were controlled with a Eurotherm Type 822 controller. Table VII shows how the stress and modulus for a PIQL100 membrane changed with a 20° C rise in temperature. The stress seemingly rose with the increase in temperature, but this is believed to be due to the mismatched thermal expansion coefficients of the film and the Vespel® ring. The large apparent decrease in modulus is tentatively attributed to softening of the five-minute epoxy used to hold the ring onto the aluminum plate. A room-temperature test of the sample three months later indicated that the stress remained elevated, whereas the modulus approximately returned to its original value. This leads us to believe that the softening of the five-minute epoxy allowed the thermal-expansion-coefficient mismatch between the aluminum and the ring to impart an additional thermal stress on the ring. The increase in radius, although within the experimental error of the measurement, happens to indicate an increase in residual strain of 0.03%. When this is multiplied by the biaxial modulus, the residual stress increase is found to be about 5 MPa. The actual difference is 4.6 MPa.

TABLE VII
Apparent effect of temperature cycling on the stress and biaxial modulus of a PIQL100 membrane w/Vespel® ring on an aluminum plate.

Membrane Radius (μm)	Temperature (° C)	Residual Stress σ_o (MPa)	Biaxial Modulus $E/(1-v)$ (GPa)	Residual Strain $\sigma_o/[E/(1-v)]$
12879	22	12.3	16.7	0.073%
	42	20.1	15.3	0.13%
12883	23	16.9	17.3	0.098%

This test exposed the need for a new thermal test cell. Modifications to the chuck were made to eliminate the need for the mounting plate and the supporting ring (see Figures 2.17 and 2.18). The thermal expansion coefficient of the silicon wafer, 2.3×10^{-6} /°C [9], will still need to be taken into account, however. In the new jig, the silicon wafer with polyimide membrane is mounted directly. A rubber sheet provides the pressure seal against the wafer. The 1-1/2" hole in the top plate of the jig is machined very accurately and is slightly smaller than the hole in the silicon wafer when etched in the apparatus shown in Figure 2.4. The radius of the membrane is defined by the jig top-plate.
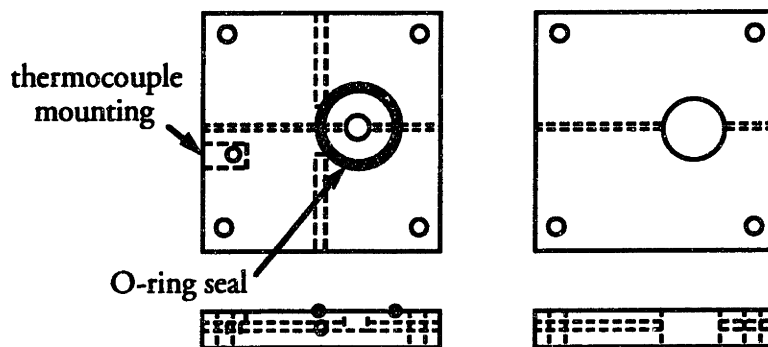
Figure 2.17: Modified load-deflection test cell for temperature testing.
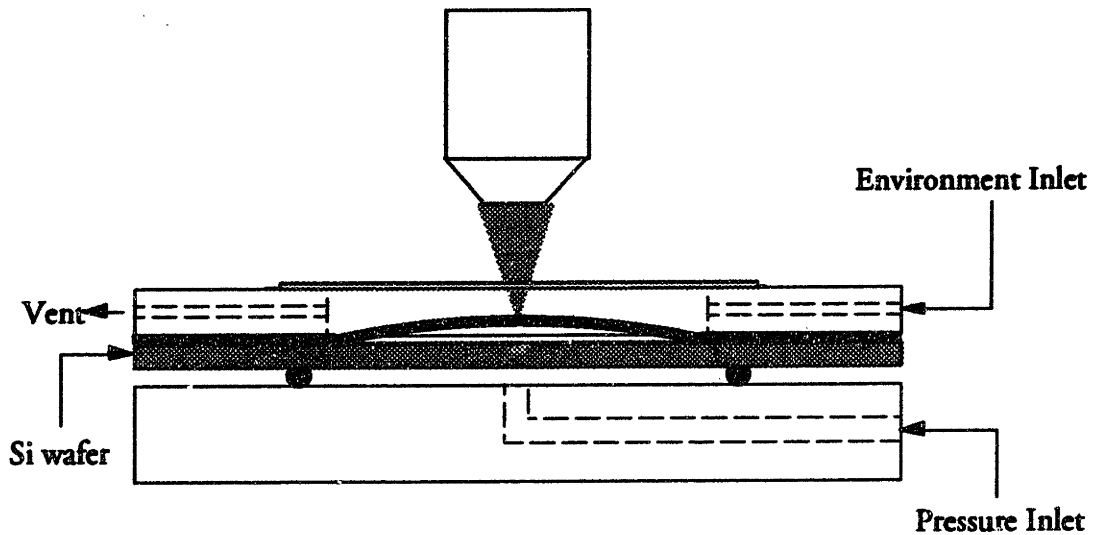
Figure 2.18: Side-view detail of modified load-deflection test cell

Figures 2.19 and 2.20 show measurements made in the new jig on an Hitachi PIQ13 film. When the thermal expansion coefficient is computed, a value of 8.5 x $10^{-6} \pm 4$ x 10^{-6} /° C is found. The silicon expansion coefficient can be accounted for by adding it to this value yielding 1.1 x $10^{-5} \pm 4$ x 10^{-6} /° C. This is smaller than the 2.7 x 10^{-5} °C reported in the literature for PIQ polyimides [9]. Interestingly enough, if the variation in biaxial modulus is ignored, and only the variation in residual stress is accounted for in computing the thermal expansion coefficient, a closer value of 2.5 x $10^{-5} \pm 4$ x 10^{-6} /° C is found. This could indicate that the reported value of thermal expansion is measured with a technique such as wafer curvature that only accounts for changes in the residual stress in the film and not biaxial modulus changes. Alternatively, it is possible that the shift in biaxial modulus measured by the load-deflection technique is an experimental artifact rather than a true softening of the film.
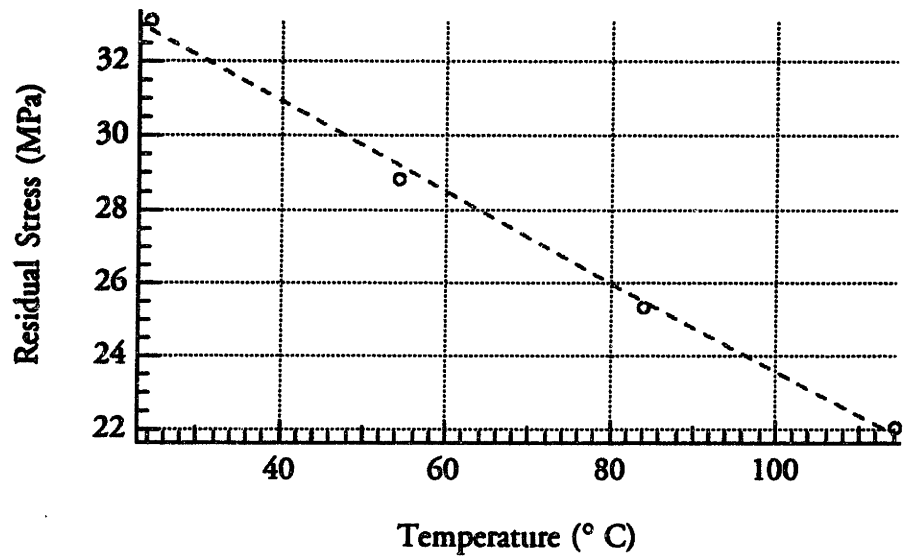
Figure 2.19: Measured residual stress at 0% RH as a function of temperature for Hitachi PIQ13 film.
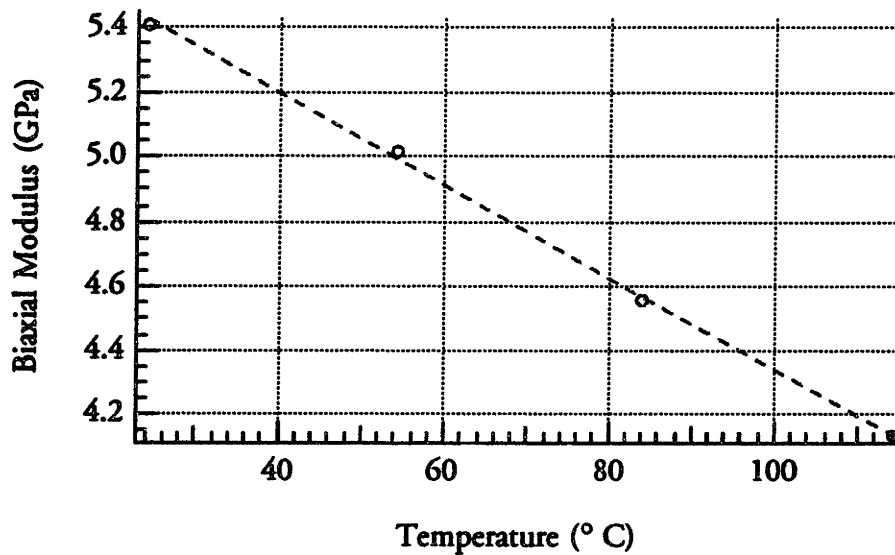
Figure 2.20: Measured biaxial modulus at 0% RH as a function of temperature for Hitachi PIQ13 film.

H. Experimental Results: Viscoelastic Effects

Although these biaxial tests were developed to measure the linear elastic properties of the film, Maseeh has shown that with the construction of circular membranes, the yield and viscoelastic properties can also be extracted by

44

monitoring the time-dependent deformation of the film when it is loaded beyond the yield point [51]. Time referencing was added to the BASIC program controlling the measurement system to facilitate such measurements. Figure 2.21 shows the deflection as a function of time for an Hitachi PIQ13 membrane when the pressure is held at a value much higher than the yield pressure. Although the curve is logarithmic as one might expect, the extraction of the viscoelastic properties of the film is limited by the lack of an appropriate model for analysis of the data.
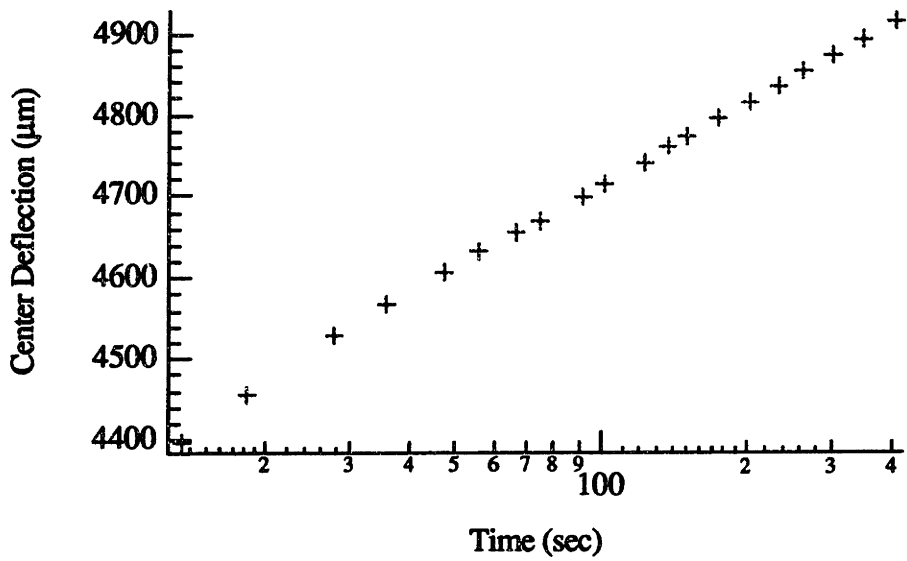
Figure 2.21: Center deflection as a function of time for E923601, a PIQ13 membrane with imbedded aluminum lines. The radius is 19031 μm, and the pressure is constant at 2.65 psi.

Upon release of the pressure, a plastically deformed region in the center of the PIQ13 membrane was observed just as described by Maseeh for DuPont Pyralin® 2525 [51]. The membrane recovery of its original flat appearance occurred after a few minutes to several days depending how far beyond the yield pressure the membrane was loaded. Subsequent measurements of the recovered membrane indicated a decrease in the measured residual stress, and no resolvable

change in biaxial modulus. Similar behavior has was observed for DuPont 2555 and 2556 films as well.

I. Experimental Results: Processing Effects

The suspended-membrane methods were also used to determine the effect of multiple anneal cycles on the mechanical properties of DuPont 2556. This work was done in conjunction with Susan Noe [10]. Multiple 40-minute, 375° C anneal cycles were performed on samples to simulate the multiple cures some layers undergo when fabricating multilevel interconnects. As shown in Figure 2.22, the residual stress is found to increase with subsequent anneal cycles. Unlike the humidity and temperature tests, each point represents measurements conducted on different membranes. Thus the error bars shown in Figure 2.22 are ±10%, the accuracy of the test. The effect of multiple cures is large enough to be resolved even with the large uncertainty, but this clearly illustrates the need for nondestructive testing methods for measuring smaller effects. Susan Noe is pursuing optical methods for this reason [10].
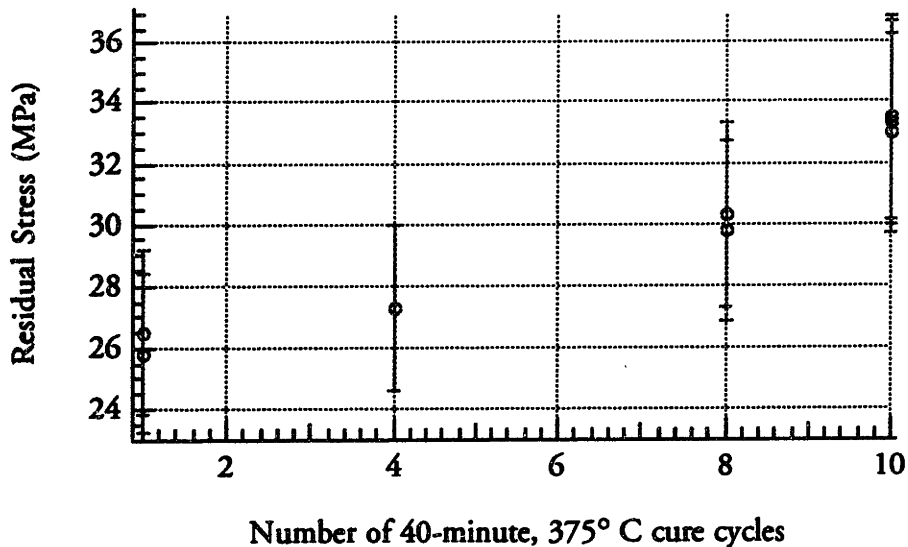
Figure 2.22: Measured residual stress at 0% RH, 20° C as a function of the number of anneal cycles for DuPont 2556 films.
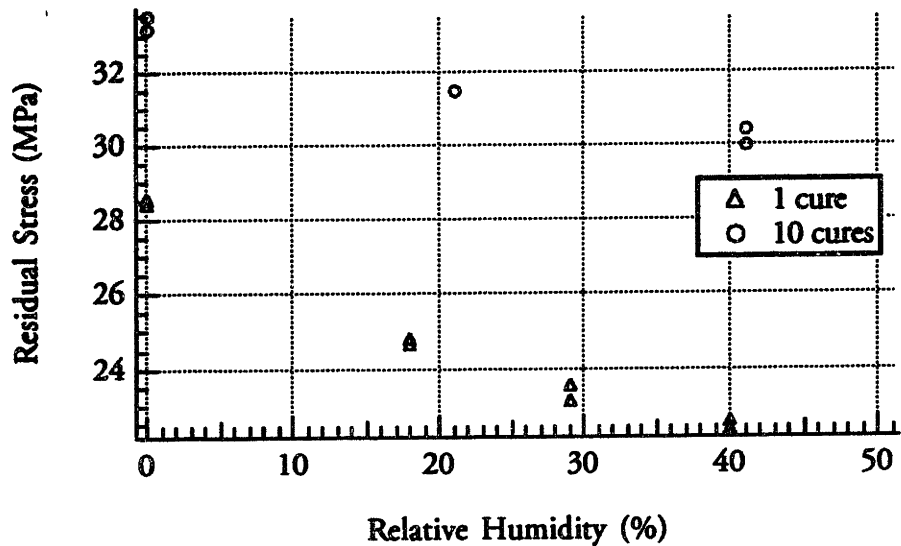
Figure 2.23: Measured residual stress at 20° C as a function of relative humidity and the number of anneal cycles for DuPont 2556 films.
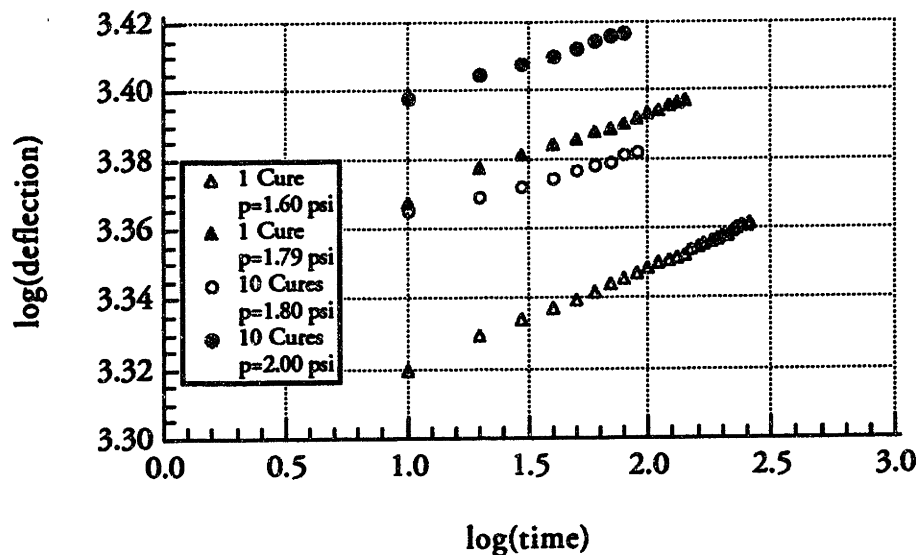
Figure 2.24: Measured center deflection as a function of time and number of anneal cycles when DuPont 2556 films are loaded beyond the elastic limit.

In addition to the increase in residual stress as the number of anneal cycles is increased, a decrease in the coefficient of hygroscopic expansion is also found as shown in Figure 2.23. When the yield pressure was quantitatively measured for the 10-cure and 1-cure samples, the yield pressure is also found to be larger for the 10-cure sample. Shown in Figure 2.24, viscoelastic measurements indicate

that the 10-cure sample also creeps more slowly with the 1-cure sample. This set of experiments unambiguously illustrate that processing variations can have a profound impact on the mechanical properties of polyimide.

J. Limitations of Suspended-Membrane Methods

Two questions remain to be answered about the load/deflection methods. First, what is the ultimate limitation on the accuracy of the methods? Second, what are the final capabilities of the measurement? As a partial answer to the first question, Chapter 6 will compare the results of suspended-membrane and acoustic tests on the same material to check the agreement of the two techniques. The capabilities of the measurement to detect small changes in the residual stress and biaxial modulus due to changes in humidity, temperature, time, and processing have been demonstrated. As noted in the previous sections, however, only large changes can be resolved when multiple samples are compared. Improvements in the accuracy are needed to improve the resolution of these destructive sets of tests.

The primary remaining unanswered source of error is the ability to fabricate accurate membranes. As explained in the previous section, the Poisson ratio measurement error of 30% is almost entirely made up of geometric errors. One possible fabrication technique that may yield more accurate geometries involves the use of dopant selective etchants. Researchers at the University of Michigan [61] have described a double p+ diffusion process and subsequent etching in KOH, which selectively etches lightly doped silicon. The patterning for a circular membrane is shown in Figure 2.25. The thin p+ circular membrane can then be plasma etched after deposition of the polyimide as in [34].

Alternatively, a lightly doped epitaxial layer on top of a heavily doped substrate can serve as an etch stop for a 1:3:8 mixture of $HF:HNO_3: CH_3COOH$ [62]. Membranes can be formed by initially doping through the layer in the

shape of the desired membrane and then etching from the back side using a jig similar to the one described in section C of this chapter. The key to both these proposed fabrication techniques is that the geometry of the membrane is photolithographically determined and can take on any shape.
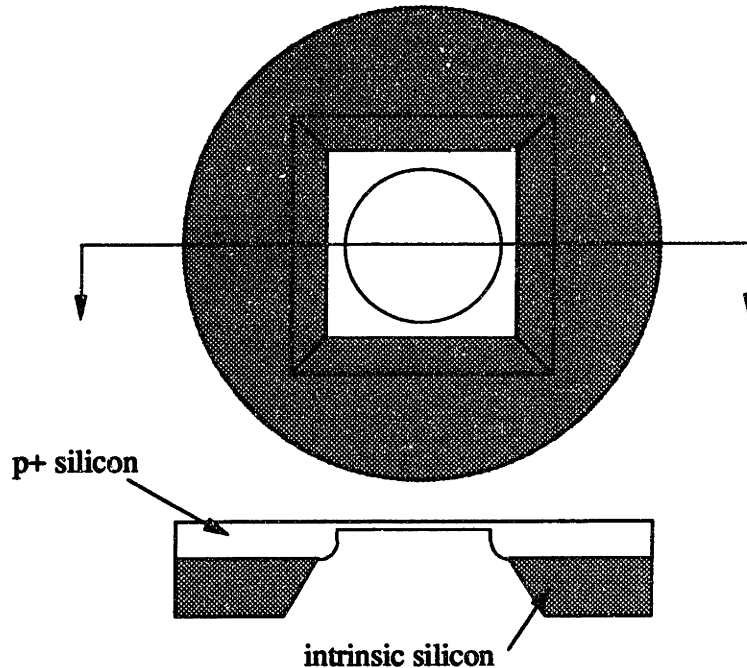
Figure 2.25: Cross section of diffusion defined membrane.

Another potential source of error is mounting stress during testing of the membranes. Since the membranes are mounted on aluminum plates with epoxy, stress can be added to the membrane as a result of the epoxy curing. During the mounting of the plates into the testing jig, additional stress can also be also be transferred to the membrane. To determine if these effects are important, a wafer with a 2556 membrane in it was mounted into the temperature jig described in Section G and the results compared with tests on the film after the Vespel® ring and aluminum plate mounting. To within the 10% measurement error, the results did not indicate any differences.

CHAPTER III: ACOUSTIC METHODS

A. Characteristic Applications of Acoustic Devices

Surface-acoustic-waves (SAW), or Rayleigh waves, are mechanical waves that propagate with most of their energy concentrated within a few wavelengths of the surface of the propagation medium [63, 64]. Typical propagation velocities are on the order of 3000 m/sec.

In sensing applications, the localization of energy at the surface, makes SAW devices very sensitive to small changes in surface properties such as mass density and surface conductivity [24, 63, 64]. In most cases, a thin coating is applied over a surface-acoustic-wave delay line, and mass changes in the film are detected as frequency shifts in an oscillating circuit that has the SAW device in the feedback path [24, 65].

In applying acoustic techniques to the problem of measuring the mechanical properties of thin films, the primary concerns are how the mechanical properties affect the acoustic wave, and how to characterize the acoustic wave. In the following sections of this chapter, the various possibilities and tradeoffs will be explored.

B. Objectives of Acoustic Measurements

The motivation for looking at acoustic techniques is to determine the elastic constants of thin polyimide films. This technique is needed to independently verify the accuracy of the suspended-membrane methods as well as to determine the elastic constants not measurable with the membrane tests. The constants to be measured involve deformations in directions normal to the film surface as well as shear deformations.

There is also a desire, however, to ensure that additional information concerning the swelling behavior of thin polymer films can be acquired. The desired information involves measurement of the weight concentration of water

50

as a function of relative humidity to complete the measurement of the swelling parameter and measurement of the diffusion coefficient. In order to satisfy these needs, any proposed acoustic technique must yield values for the elastic constants and density of a thin film.

These properties must have a reproducible, measurable, and predictable effect on acoustic wave propagation. The following equation, from Farnell [66], is the elastic wave equation for a piezoelectric material.

$$\rho\frac{\delta^2 u_i}{\delta t^2} - c_{ijkl}\frac{\delta^2 u_k}{\delta x_j \delta x_l} - e_{kij}\frac{\delta^2 \phi}{\delta x_j \delta x_k} = 0 \qquad i,j,k,l = 1,2,3$$

$$e_{ikl}\frac{\delta^2 u_k}{\delta x_i \delta x_l} - \varepsilon_{ik}\frac{\delta^2 \phi}{\delta x_i \delta x_k} = 0 \qquad (3.1)$$

where the Einstein summation convention over repeated indices is used [67]. The particle displacement, u_i, and electric potential, ϕ, is related to the density, ρ, the stiffness tensor, c_{ijkl}, the piezoelectric tensor, e_{ijk}, and the dielectric tensor, ε_{ij}. As evident from (3.1) the elastic stiffness and density have a definite impact on wave propagation. Using equation (3.1) and appropriate boundary conditions, it is possible to take measurements of acoustic velocity and deduce the elastic properties that lead to it (see for example [39, 45, 47, 48]).

The rest of this chapter will serve to introduce the basic elements and decisions necessary for designing acoustic transducers. Chapters 4 and 5 will detail the specifics of using acoustic wave propagation as a probe of mass uptake and thin film elastic constants respectively.

C. Preliminary Design Choices

Figure 3.1 presents the basic elements of acoustic measurements. Initially, the primary choice is to determine the form of acoustic wave to be excited and the excitation method. As a thin film probe, surface acoustic waves appear to be

especially appropriate because of the concentration of acoustic energy at the surface of the propagating medium. Lamb waves or other plate modes, propagating on suspended membranes, have also been investigated by White and others [68, 69]], but their higher sensitivity to external influences such as pressure and temperature, and the more difficult fabrication requirements make them less attractive for the task of measuring film properties.

Bulk acoustic waves are usually judged to be inappropriate because the thickness of films are often much less than the acoustic wavelength. Kushibiki [70] and Lee [71], however, describe one possibility in which a compressional acoustic wave from an acoustic microscope is normally incident upon a thin film. The coupling medium between the transducer and the film can either be the substrate that the film is deposited on or a coupling fluid such as water. The phase and amplitude of the reflection coefficient is then measured as a function of frequency. The reflection loss passes through a maximum when the thickness of the film is exactly one quarter of a wavelength. A measurement of the thickness of the film then results in the velocity of the acoustic waves in the film. If the acoustic impedance of the coupling medium is also known, then the impedance of the film can be calculated from the reflection coefficient. Since the acoustic impedance simply depends upon the velocity and the density, such calculations yield a value for the density. Finally, the incorporation of different acoustic modes, ie. shear vs. longitudinal, can yield the shear velocity in the film. Given the shear and the longitudinal velocities as well as the density of the films, one can then attain all the elastic constants of an isotropic film. The disadvantages of this method are that an acoustic microscope is required and that detection of mechanical anisotropy can be difficult because propagation is usually restricted to directions normal to the film surface [72].
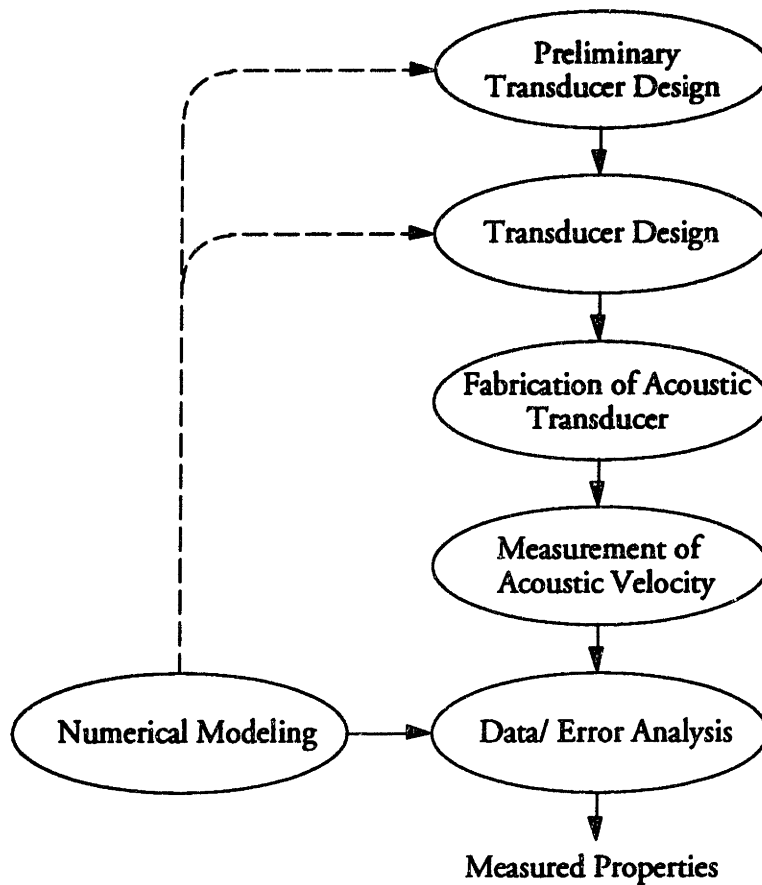
Figure 3.1: Basic elements of acoustic measurements.

Surface acoustic waves were chosen to probe the mechanical properties. The next design choice was to find a means of exciting the appropriate mode and detecting the appropriate characteristic of the wave, usually the wave velocity. A number of different options exist. An acoustic microscope can be used to excite surface waves [22, 73, 74]. Plates of piezoelectric material such as lithium niobate and quartz acting as bulk wave transducers can couple energy into and out of surface wave modes by bonding to the edge [75] or the top [76] of a substrate , coupling through a grating at the surface of the substrate [76], or by controlling the angle of incidence of bulk wave with shaped transducers [76, 77]. Laser pulses can be used to excite and detect acoustic waves [78], or by sensing surface phonons with Brillouin scattering experiments, the problem of acoustic

mode excitation can be eliminated and the mode velocities sensed as optical frequency shifts in a nondestructive optical manner [37, 79-82].

The most common technique for excitation and detection of surface acoustic waves, however, is the use of interdigitated electrodes deposited on a piezoelectric surface [83-85]. Although the other techniques mentioned in the previous paragraph are especially attractive because they do not require that the film be deposited on a piezoelectric substrate, they are all substantially more difficult to carry out without specialized equipment. Interdigitated transducers (IDT), on the other hand, can be fabricated using standard semiconductor fabrication processes [75]. If desired, one of the other excitation/detection schemes can be explored as a means of improving the measurement technique if transduction appears to be a major stumbling block for acoustic techniques.

D. Interdigitated Transducer Design

Ever since 1965, when White and Voltmer originally proposed the use of an interdigitated transducer (IDT) to generate surface acoustic waves on piezoelectric substrates [83], most SAW devices have used IDTs to couple electrical energy into and out of the devices. IDTs consist of periodic strips of metal patterned on the surface of a piezoelectric substrate. Classically the fingers are one quarter wavelength wide, separated by quarter wavelength spaces, and alternately connected to two bus bars. When an AC signal of the appropriate frequency is applied across the bus bars, acoustic waves are generated and propagate outward, normal to the IDT.

In determining the performance of a piezoelectric substrate for use in a SAW device, the primary figure of merit is the piezoelectric coupling coefficient, k^2, which can be computed from the relation $k^2 = 2\Delta v/v$ where Δv is the difference between the Rayleigh wave velocity with and without an infinitesimally thin metal film at the surface to short the electric potential at the surface [86]. Values

54

for k^2 are available in the literature for many materials [63, 75, 87], or numerical simulations can be used to compute k^2 in situations where there may be a dielectric coating over the IDT.

Two-inch diameter by 1-mm thick wafers of ST-cut, X-propagating quartz, which has Euler angles of 0°,132.75°, and 0°, were supplied by Valpey-Fisher of Hopkinton, MA for use as the substrate for the mass sensors. This choice was made because of its wide availability and its zero temperature coefficient of delay [75]. Thus to first order temperature variations do not affect the propagation on ST-cut quartz. The Rayleigh wave velocity is 3158 m/sec with $k^2 = 0.00116$ [87]. Y-cut, Z-propagating lithium niobate was used as the substrate for the elastic stiffness measurements because of its large efficiency as a surface wave transducer. The Rayleigh wave velocity for LiNbO$_3$ is 3488 m/sec with $k^2 = 0.048$ [87].

The wavelength and hence the IDT finger periodicity is computed by taking the ratio of velocity and desired center frequency. A center frequency of 40 MHz was chosen, so the finger periodicity for the ST-quartz substrates is 80 μm. In order to minimize coherent reflections, a split finger geometry was used instead of the classic quarter-wavelength geometry resulting in a finger width and finger spacing of 10 μm [75]. Figure 3.2 shows the split-finger IDT geometry. This is well within our ability to photolithographically pattern with a wet process.

The number of finger pairs N is set to optimize the bandwidth. As N is increased, the bandwidth decreases and the coupling strength increases. As N is decreased, the bandwidth increases, but the conversion loss increases as well. The optimum N [84, 85] can be found from:

$$N = \sqrt{\frac{\pi}{4k^2}}$$

(3.2)

Again using the ST-quartz value of 0.00116 for k^2, the value for N is approximately 30.
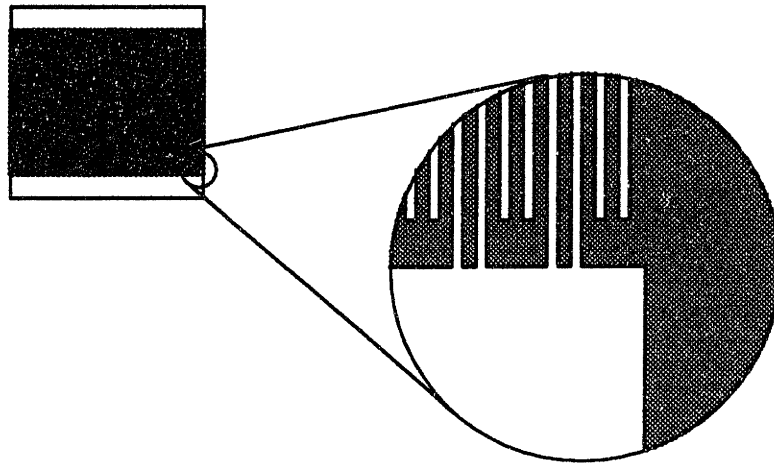
Figure 3.2: Detail of split finger interdigital transducer (IDT) for generation and detection of surface acoustic waves.

The beam width is set by impedance matching concerns. The equivalent circuit of a SAW IDT is composed of a static capacitance and a complex radiation impedance as shown in Figure 3.3 [75].
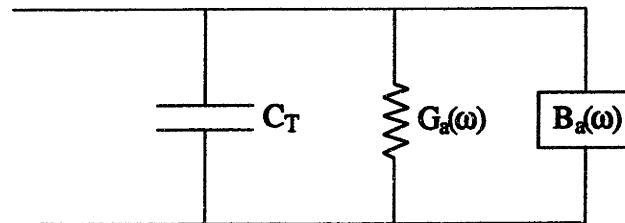
Figure 3.3: Equivalent circuit of IDT.

C_T is the total static capacitance of the IDT and equals NC_s where N is the number of finger pairs, and C_s is the capacitance per finger pair. C_s is approximately $w\varepsilon$, where w is the overlap width of the fingers and ε is the dielectric permittivity of the substrate [63]. $G_a(\omega)$ is the radiation conductance and equals $G_o(\sin\beta/\beta)$ where $G_o=4k^2\omega_oC_sN^2/\pi$, $\beta=N\pi(\omega-\omega_o)/\omega_o$, and ω_o is the center frequency. The radiation susceptance is $B_a(\omega)=G_o(\sin2\beta-2\beta/2\beta^2)$.

56

Following the analysis by Oates [75] the approximation $4k^2N/\pi \ll 1$ is made because k^2 is small, so that at the center frequency the input impedance $Z=1/(G_o+i\omega C_T)$ is approximately $R_o+1/i\omega C_T$ with $R_o=4k^2/\pi\omega_o C_s$. R_o is controlled by k^2 and C_s. Since k^2 is set by the piezoelectric material and the placement of the electrodes, after the materials have been chosen, R_o is adjusted to match a 50Ω impedance line by adjusting the beam width, which controls C_s. The remaining capacitance C_T is be tuned out with a series inductor. The value of the inductor is $1/\omega_o^2 C_T$. Typically for ST-quartz devices the correct beam overlap is 50 wavelengths and for lithium niobate it is 100λ [75]. The inductor is then a few microhenries.

The complete design parameters for the mass sensors and the elastic stiffness test sites will be given in Chapters 4 and 5 respectively.

E. Fabrication Process

The detailed fabrication processes for the two devices are given in Appendix A. The wafers, as supplied by Valpey-Fisher, are cleaned at their location in 70° C trichloroethylene before delivery. Provided they are shipped in suitably clean containers, they usually only require a solvent cleaning with a sequence of rinses in freon, acetone, methanol, and deionized water just before processing begins. If the wafers are stored for months, even in a class 100 clean room, they tend to require an additional cleaning step in 5:1:1 water:hydrogen peroxide:ammonium hydroxide at 80° C for 10 min. The indication of improperly cleaned samples is usually poor adhesion of the aluminum to the substrate. The lithium niobate substrates appear to be particularly prone to this and a 200Å layer of chrome can be evaporated onto the surface to promote adhesion.

The clean wafers were mounted in a Temescal e-beam evaporation system and 1750Å of Al deposited at a rate of 8Å/sec. The IDT electrode pattern was photolithographically replicated in soft-baked photoresist, and the unprotected

metal wet etched to form the IDT. After removal of the photoresist with acetone, adhesion promoter and the polyimide of interest was spun on and soft cured. The exact details of the patterning of the polyimide for the two different devices are discussed in the appropriate following chapters. Typical dimensions of the devices are shown in Figure 3.4.
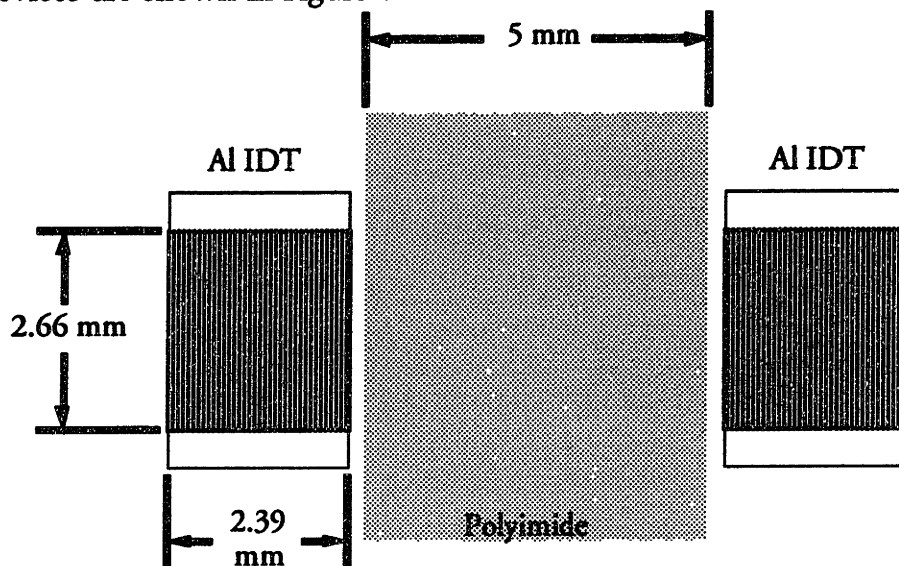
Figure 3.4: Geometry of Mass Uptake SAW sensor.

Upon completion of the SAW device, the wafers were stuck down to an aluminum plate with double-sided tape, and 1-mil gold wires were ultrasonically ball bonded to the IDT bus bars and soldered to .085" diameter, 50Ω, semi-rigid coaxial cable for testing. Typical lengths for the wires were less than 1 cm. B-series tunable inductors purchased from Piconics, Inc. were included at the input and output of the device for impedance matching. Figure 3.5 is a photograph of the completed device ready for testing.
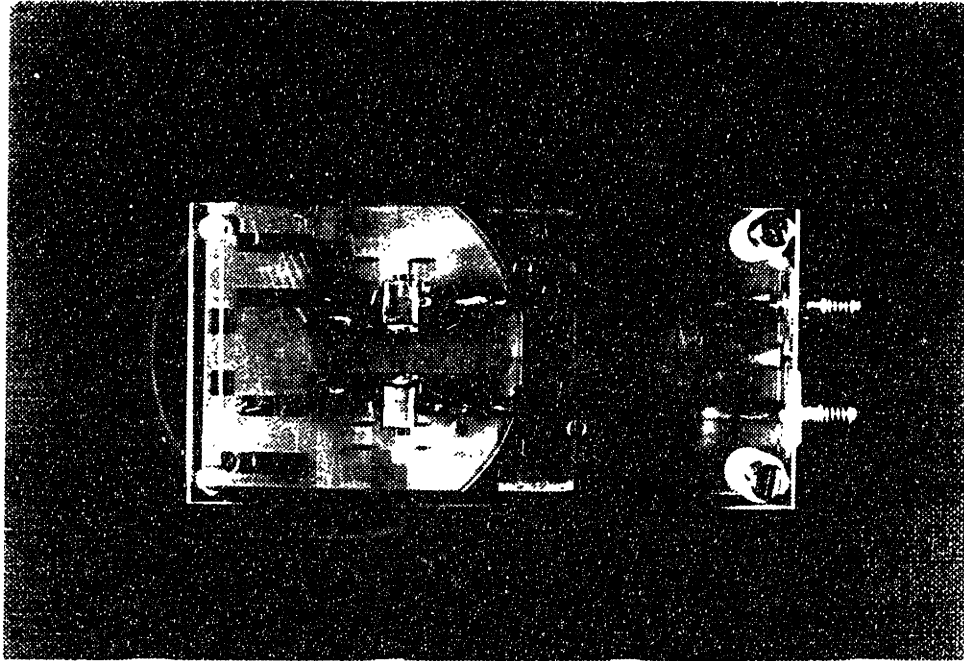
Figure 3.5: Photo of the completed SAW device ready for testing.

F. Verifying Acoustic Wave Propagation

Electrical feedthrough and other effects can lead to coupling between the input and output transducers of a SAW device without any acoustic wave propagation. For this reason it is always prudent to verify the presence of an acoustic wave with one of a few different methods. The easiest method is to apply a pulse of RF to one IDT and observe the signal at the other IDT as a function of time and frequency. A system for doing this is shown in Figures 3.6 and 3.7. The HP8753C Network Analyzer, operated in CW mode, acts as the frequency source. When acoustic transmission of the energy is present, three characteristics will be observed. A typical oscilloscope traces are shown in Figures 3.8 and 3.9. If acoustic transmission occurs, the delay from the electrical feedthrough pulse to the transmitted pulse is on the order of several microseconds. This is a clear sign of acoustic propagation because the high

propagation speed of electromagnetic waves precludes electrical delays of microseconds without several hundred meters of cable.
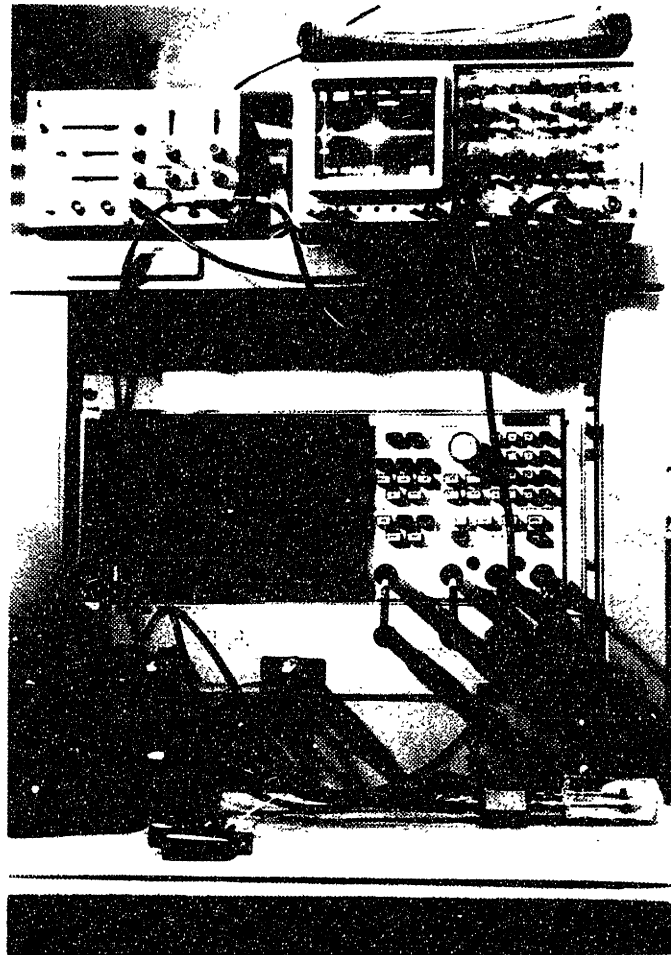
Figure 3.6: Photo of the pulse-echo system for verifying acoustic propagation.

HP8753C Network Analyzer

HP8012B Pulse Generator   Tektronix 2440 Oscilloscope

Sync

Pulse

CW mode

Watkins Johnson S1

WJ 6200-503
Amplifier
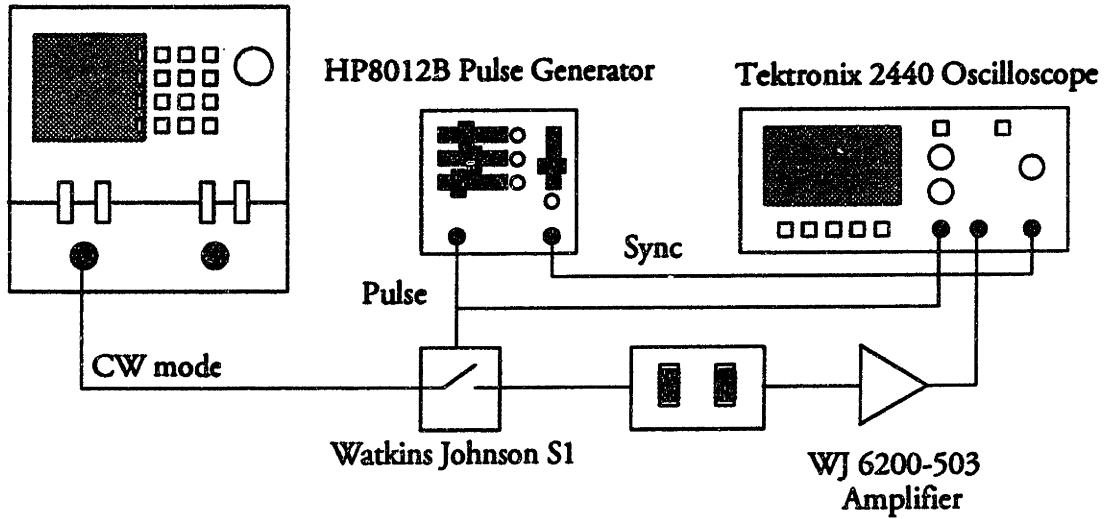
Figure 3.7: Pulse-echo system for verifying acoustic propagation.

CH1 100mVΩ M00 A   1μs -4.69mV? EXT1
CH2 200mVΩ

CH1gnd

CH2gnd

CLIP
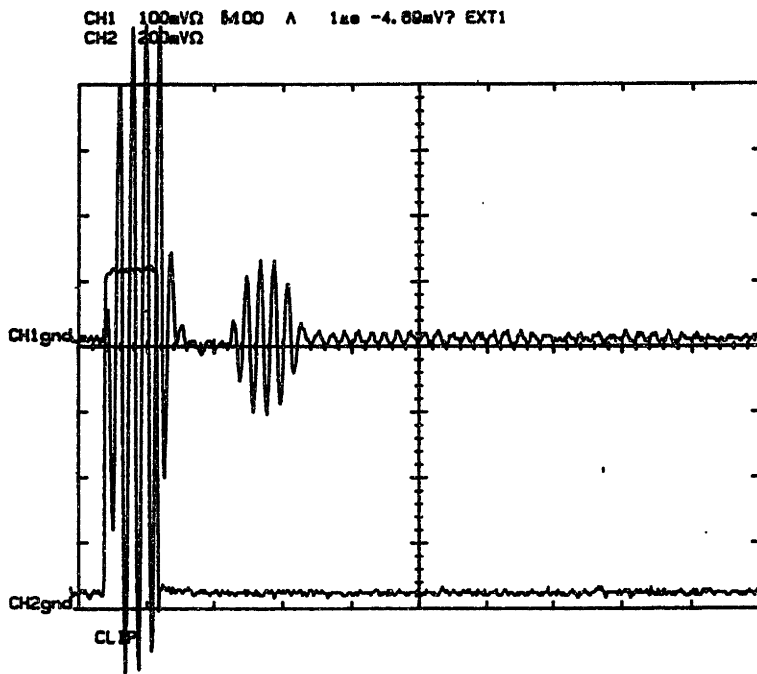
Figure 3.8: Oscilloscope trace showing acoustic propagation.
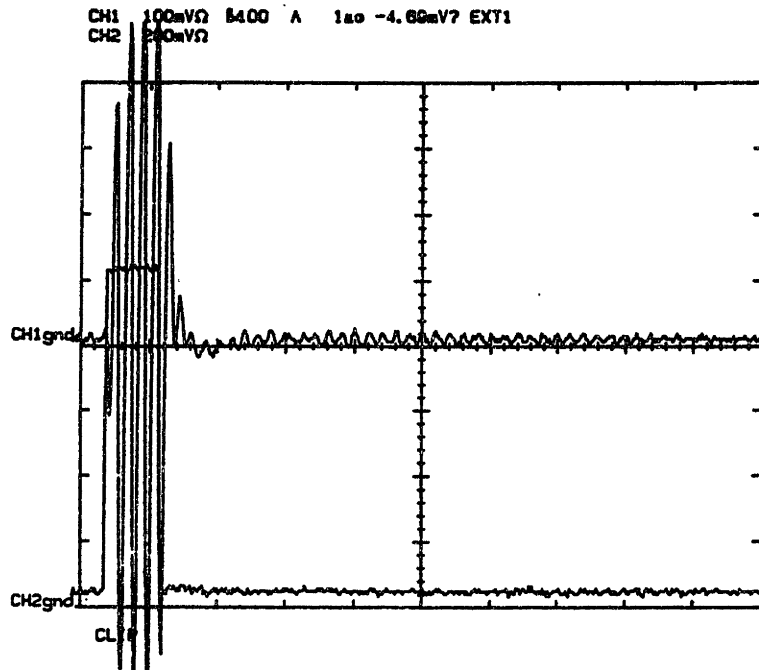
Figure 3.9: Oscilloscope trace showing no acoustic propagation.

The second characteristic is if the frequency is tuned slightly away, the transmitted pulse should disappear due to the limited bandwidth of the IDT. Finally, the transmitted pulse should also disappear when a small drop of water is put in the propagation path. This is because the normal component of the particle motion in Rayleigh waves launches compressional waves in the water that makes the surface wave propagation very lossy.

After verifying acoustic propagation, the acoustic measurements can continue with measurements of the appropriate acoustic characteristic, either insertion loss or propagation velocity. The next two chapters will detail the specific aspects of acoustic measurement needed to detect mass uptake and thin-film elastic stiffness.

CHAPTER IV: ACOUSTIC METHODS FOR MASS SENSING

A. Readout of Surface Acoustic Wave Devices for Sensing Applications

When the film overcoat on a SAW delay line is thin relative to an acoustic wavelength and the Rayleigh velocity of the film is significantly lower than that of the substrate, Wohltjen [24, 65] and Auld [64] found perturbation theory can be used to find that the effect of an overcoating film is simply a mass loading effect given by equation (4.1).

$$\frac{\Delta v_R}{v_R} = \kappa(k_1 + k_2)fh\Delta\rho \qquad (4.1)$$

where v_R is the substrate Rayleigh wave velocity; Δv_R is the change in velocity due to the change in density; f is the frequency; $\Delta\rho$ is the mass density change; h is the film thickness; κ is the fraction of the total delay path, from IDT center to IDT center, that is covered by the swelling film; and k_1 and k_2 are substrate sensitivity constants that can be found in [64, 87]. For X-propagating, ST-cut quartz $k_1 = -8.9267 \times 10^{-8}$ m²-sec/kg and $k_2 = -3.8622 \times 10^{-8}$ m²-sec/kg.

Both of the conditions can be met with polymer overcoats, so changes in the $h\Delta\rho$ of a thin polymer film due to moisture uptake should be measurable as changes in acoustic velocity. The changes in thickness as the polymer swells are small [10] compared to the density changes, so all changes are attributed to density variation. Thus ignoring thickness effects and inverting (4.1), the change in density caused by swelling is:

$$\Delta\rho = \frac{\Delta v_R}{v_R} \frac{1}{\kappa(k_1 + k_2)fh} \qquad (4.2)$$
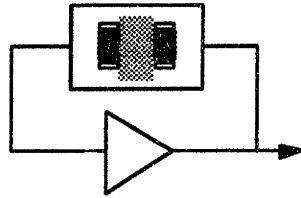
WJ A24
Amplifier

Figure 4.1: Oscillator circuit for monitoring velocity variations due to mass density changes.

Because only changes in velocity need to be monitored, rather than the absolute value of the velocity, an oscillator with the SAW delay line in its feedback path is usually used to monitor the velocity changes as shifts in the frequency of the oscillator. Figure 4.1 shows the oscillator circuit used. In such a configuration, the oscillation frequency is governed by two conditions: the total gain around the feedback loop at that frequency is greater than or equal to unity, and the total phase at that frequency around the loop is an integral multiple of 2π. Within the bandwidth of the SAW delay line then, the oscillation frequency is determined by:

$$\frac{2\pi f}{v_R} L + \phi_e = 2\pi N \qquad (4.3)$$

where N is any integer, ϕ_e is the electrical delay present in the feedback loop, and L is the IDT center-to-center distance. ϕ_e is usually ignored because it is much smaller than the acoustic delay and because it is essentially constant within the bandpass of the device. Taking derivatives of both sides of 4.3 yields the desired result:

$$\frac{\Delta f}{f} = \frac{\Delta v_R}{v_R} \qquad (4.4)$$

As another alternative for monitoring the velocity changes is to use an HP8753C Network Analyzer to measure the gain and phase of the S_{12} network transmission parameter. By setting a marker on the 8753C to track the zero

64

phase point, effectively the same information as in the oscillator circuit can be attained. In addition, however, the insertion loss through the device can also be monitored. Figure 4.2 shows a typical trace from the network analyzer. Real time data, which is useful for diffusion coefficient measurements, can also be read out from the network analyzer with a simple BASIC program running on an IBM PC/AT. The computer program is listed in Appendix B.
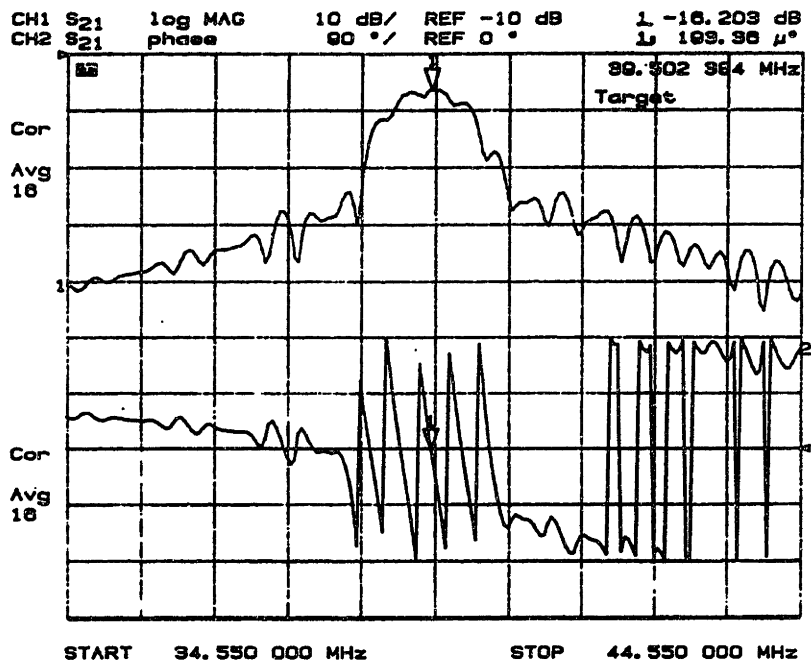
Figure 4.2: Gain and phase of S_{21} parameter for Quartz SAW mass sensor.

B. Fabrication Issues

The design and fabrication of the IDT for the SAW mass sensor was done according to Chapter 3. The IDT design parameters were calculated without consideration of the thin polyimide overlayer. The parameters for the sensor are tabulated in Table VIII.

TABLE VIII
Parameters for SAW mass sensor IDT.

Parameter	Value
Substrate	ST-quartz, x-prop
Polyimide	DuPont PI2555
Center frequency	40 MHz
Number of finger pairs	30
IDT design	split finger
finger width/spacing	10 μm
finger overlap	2.5 mm
IDT center-center spacing	7.38 mm
Polyimide coated length	4.81 mm
Polyimide thickness	2.25 μm
Tuning Inductor	B682-61-00
	(4.53-6.8 μH)

In order to pattern the thin polyimide over the SAW delay line as in Figure 3.4, a wet etch process outlined in Appendix A was used. First, adhesion promoter in a mixture of 95 ml of methanol, 5 ml of water, and two drops of DuPont VM-651 adhesion promoter was mixed 24 hours prior to deposition of the polyimide and stored at room temperature. After completion of the patterning of the aluminum IDT, the adhesion promoter was spun onto the quartz wafers at 3000 rpm for approximately 10 seconds. A single coat of DuPont Pyralin® 2555 polyimide was then poured onto the wafer, spread at 500 rpm for 5 seconds and spun at 3000 rpm for 60 seconds. The coated wafer was then baked in an exhausted Blue-M oven at 120° C for 10 minutes before more photoresist was deposited and exposed. The photoresist developer used to remove the exposed photoresist also removed the underlying polyimide. After removing the photoresist in acetone, the polyimide was cured at 400° C for 90 minutes. This resulted in a polyimide thickness of 2.25 μm as measured with a Dektak profilometer.

C. Measurement of Diffusion Coefficient

Using the humidity control system described in Chapter 2, Figure 2.11 and a network analyzer the zero-phase frequency can be monitored as a function of

time, so the mass response of polyimide to a step change in humidity could be monitored. The data are graphed in Figure 4.3. In this case the sample was first dryed in a bell jar with desiccant for 24 hours and then blanketed in dry air while the measurement was set up. Using a computer to sample the zero-phase frequency at 100 msec intervals, the dry air was then abruptly removed and the dry-to-wet transition thus recorded. After equilibration at room humidity, the wet-to-dry transition was measured by abruptly blanketing the device in dry air.

Using a Fickian diffusion law, and assuming one dimensional diffusion through the thickness of the film, the equation for the frequency as a function of time is [88]:

$$\phi(t) = \phi_f + (\phi_i - \phi_f) \sum_{n=0}^{\infty} \frac{8\exp\left(\frac{D(2n+1)^2\pi^2 t}{4h^2}\right)}{\pi^2(2n+1)^2} \tag{4.5}$$

where ϕ_f and ϕ_i are the final and initial phases, h is the film thickness, and D is the diffusion constant.
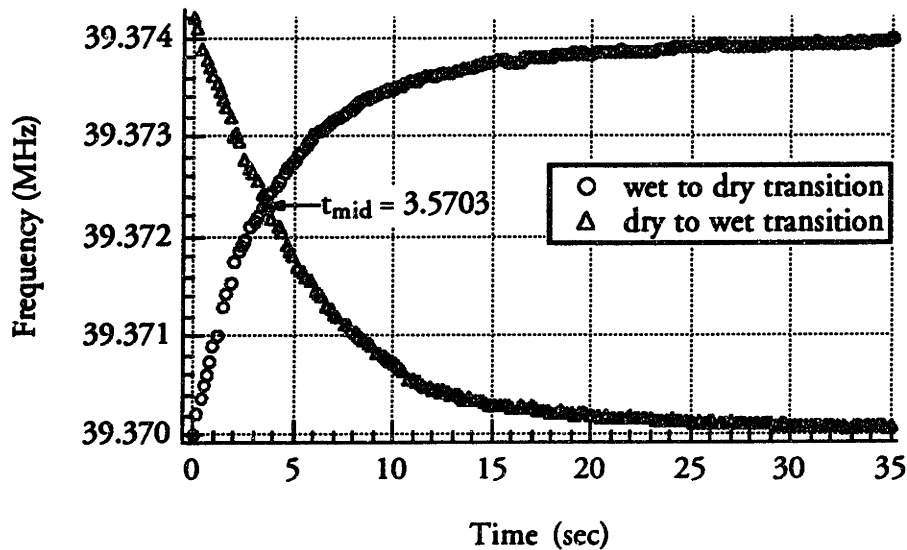
Figure 4.3: Response of polyimide coated SAW delay line to abrupt changes in humidity. Polyimide thickness is 2.25 μm.

Following the analysis by Denton [58], the half way point of the transient is reached when $\sqrt{Dt/h^2}$=0.44. From measurements of the film thickness and the time to the midpoint of the transient, the diffusion constant can be extracted. From Figure 4.3, t_{mid} is 3.57 seconds, which indicates a value for D of 2.7×10^{-9} cm^2/sec. This compares favorably to the 4.5×10^{-9} cm^2/sec value found by Denton [58] using capacitive measurements. The discrepancy appears to be due to the long tail in the transient behavior. Rather than a single diffusion coefficient, the data are better described by two coefficients. Such a slow diffusion process would be consistent with the long equilibration times found necessary for the load-deflection tests in Section F, Chapter 2.

D. Measurement of Mass Uptake
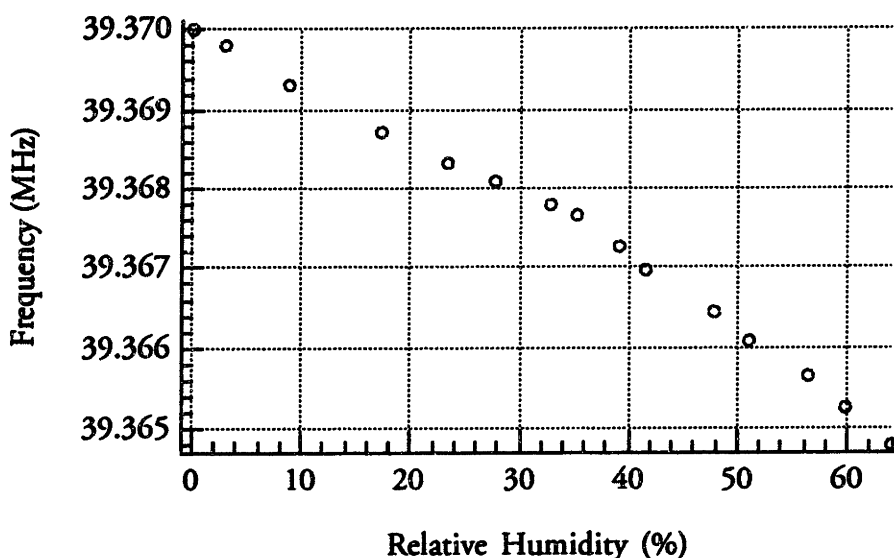
Figure 4.4: Zero-phase frequency as a function of relative humidity at 21° C.

Using a network analyzer to track the zero transmitted phase point as a function of relative humidity, Figures 4.4 and 4.5 were recorded. The mass uptake of the DuPont 2555 polyimide at a given relative humidity can then be calculated from equations (4.2) and (4.4). Conversion of the data results in the

graph shown in Figure 4.6. The rate of mass uptake per % RH is 0.02% / %RH which agrees well with published values [57, 59].
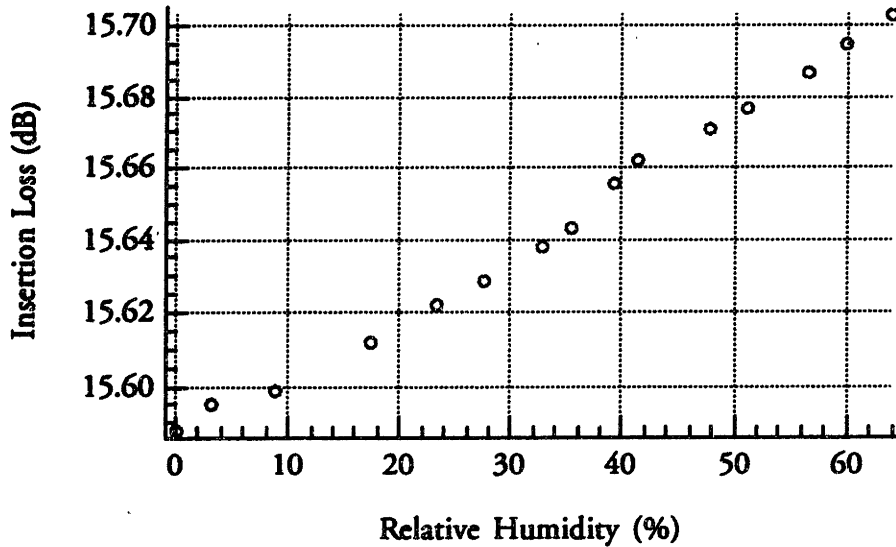
Figure 4.5: Zero-phase insertion loss as a function of relative humidity at 21° C.
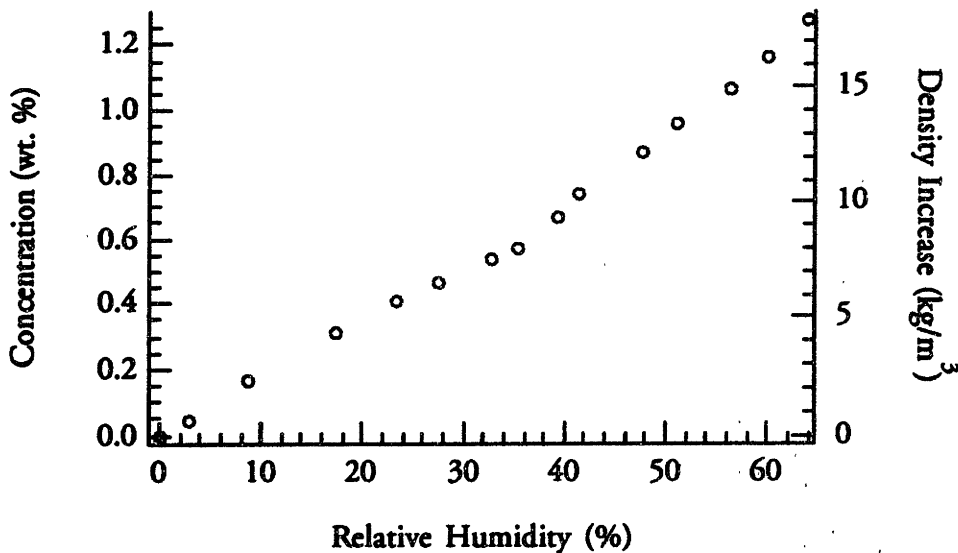
Figure 4.6: Mass uptake as a function of humidity for DuPont PI 2555.

It is interesting to note that there is a clear change in slope of the frequency versus humidity curve at 35% RH and a corresponding increase in insertion loss. While a portion of this has been attributed to peaking in the flow rate of the air

exiting the humidity control system at 35% RH, it cannot be completely assigned to a flow dependence as explained in Section C, Chapter 7. The remaining effect appears to indicate that some change in the way moisture is being taken up occurs at an RH of 35% and a frequency of 39.3675 MHz.

This result was not expected, although the change in slope has been seen before by Brace in 1988 [89]. The slight increase in loss indicates there might be some relaxation process occurring at that particular combination of humidity and frequency [90].

The existence of a sub-glass transition in PMDA-ODA polyimide has been documented in the literature [60]. Using dynamic mechanical tests at a frequency of 576 Hz, Bernier and Kline in 1968 found a relaxation peak occurring near 230 K that they attributed to water molecules present in the polyimide. They theorized that below 230 K the water molecules are predominantly held by hydrogen bonds; above that temperature, they are unbonded. They report an activation energy for the process of 11.4 kcal/mole. Evidence of nonuniform water bonding has also been seen in nylon [91].

If the activation energy for PMDA-ODA is assumed to apply for the BTDA-ODA/MPDA polyimide studied in this thesis, time-temperature superposition can be used to translate the RF data in our experiments to the 576 Hz that Bernier used. The equation for the shift factor log a_T is [5]:

$$\log a_T = \frac{\Delta H}{R}\left[\frac{1}{T_2} - \frac{1}{T_1}\right] \qquad (4.6)$$

where R is the universal gas constant = 1.986×10^{-3} kcal/mol$\bullet$K, ΔH is the activation energy, and T_1 and T_2 are the two temperatures. Using 576 Hz and 39.3675 MHz to compute the shift factor yields a value of 11.13. By (4.6), the temperature of the sub-glass transition is thus 187 K. Although it is quite far

below the 230 K measured by Bernier, this could be considered a reasonable value given the different materials being investigated.

CHAPTER V: ACOUSTIC METHODS FOR MEASURING THIN-FILM ELASTIC STIFFNESS

A. Evidence of Anisotropy in Polyimide Films

In all the previous chapters, the polyimide films have been assumed to be mechanically isotropic. X-ray diffraction [92, 93] and optical waveguiding [94] experiments have revealed anisotropy in polyimide films. In this chapter, the acoustic methods are modified in order to measure the true elastic constants of the anisotropic film.

Because the polyimide films are spun-cast, there is no in-plane ordering in the film. This has been confirmed optically [94]. Thus for these spun-cast films, the most general symmetry state is transverse isotropic, for which there are five independent elastic constants instead of the two needed for an isotropic film [67].

In order to measure all five elastic constants of the film a new measurement method must be developed. At the present time, there are a number of techniques for determining some of these constants. Among them are the suspended-membrane methods described in Chapter 2 and uniaxial Instron tests [26] for in-plane properties. Acoustic microscope [72] techniques have been proven useful for measuring properties normal to the film surface. In most cases, however, measurements of different constants require construction of separate samples and hence are limited in their sensitivity due to the compounding of the inaccuracies of the individual tests and the possibility of slight variations from sample to sample.

Surface acoustic wave methods, on the other hand, are not destructive. Furthermore, since particle motion in a surface wave can involve both compressive and shear deformation in and out of the surface [64], a measurement technique using surface acoustic waves should be capable of

measuring all five constants on a single sample of material. The question is what minimum number of modes is necessary to completely characterize spun-cast polymer films.

Using surface-acoustic-wave-simulation software available from McGill University in Montreal [66, 95] and described in the next section, numerical experiments were conducted to determine the sensitivity of Rayleigh-like modes in a two layer system to the five elastic constants of the coating: c_{11}, c_{33}, c_{13}, c_{44}, and c_{66}. Only the in-plane shear modulus, c_{66}, of the film was found to not influence the propagation of these modes. This is consistent with the understanding that particle motion in Rayleigh-like modes is strictly in the plane formed by the surface normal and the wave vector, also known as the sagittal plane.

In a way similar to the use of TE and TM optical modes to measure birefringence in a film, however, it has been speculated [48] that different acoustic modes can be used to increase the sensitivity to c_{66}. In the Love mode, deformation is purely shear normal to the sagittal plane [66] and sensitivity is only to the shear moduli, c_{44} and c_{66}. Thus by measuring the propagation of Love modes in addition to the Rayleigh-like modes, the in-plane shear modulus should be measurable. It should be noted that Love modes propagate in two-layer systems only when the Rayleigh-wave velocity of the film is lower than that of the substrate. Again using the simulation software, the predicted SAW velocity in polyimide is as much as a factor of three smaller than the velocity in quartz or lithium niobate, so either substrate should be suitable for use in measuring the properties of polyimide.

B. Surface-Acoustic-Wave Simulation Software

When the film overlayer is thin relative to the acoustic wavelength, perturbation theory can be used to solve for the effect on acoustic wave

propagation. Equation (4.1) is the result. The primary difference, however, between the design of the SAW sensor and the design of a mechanical probe is the thickness of the film. For the sensor, there was a requirement that the film thickness be very much smaller than the acoustic wavelength and equation (4.1) holds. In order to have sensitivity to the elastic constants of the film, however, the thickness of the film must be comparable to the wavelength and analytical models of the wave propagation do not exist.

Qualitatively, the addition of a film on top of a surface-acoustic-wave delay line makes the wave propagation dispersive. The exact shape of the dispersion curve depends upon the elastic properties of both the film and the substrate as well as the thickness and density of the film [66, 96]. Assuming that the substrate is well characterized, a measurement of the velocity dispersion can be related to the elastic constants of the film when the experimental data are fitted to calculated dispersion curves. By controlling the mode of propagation, sensitivity to the different elastic constants of the film can be achieved.

Measurements of surface-acoustic-wave dispersion have been shown to provide accurate and complete elastic information about many types of thin films. This procedure, measuring the surface-acoustic-wave-velocity dispersion caused by the presence of a thin film at the surface, has been utilized by several research groups around the world to characterize films of molybdenum, aluminum, silicon monoxide, and many others [38, 45, 47, 48].

Numerical models are used to solve for the acoustic velocity dispersion. For this thesis, a program provided by Prof. E. Adler at McGill University was used to solve the multilayer acoustic problem [66]. Other programs and methods of computing the dispersion, however, are also available [96, 97]. The McGill program uses the wave equation as given in (3.1), the assumed form of the solutions, $u_j = a_j \exp(ikbz) \exp[ik(x-vt)]$, and the boundary conditions to form a

matrix of equations whose determinant must be zero for all propagating waves. The free parameter is the velocity, so the program finds the phase velocity which minimizes the boundary determinant given an velocity search range, operating frequency, film thickness, and material parameters.

C. IDT Design

This simulation program was used for two purposes: design of the SAW devices and computation of the mechanical properties from experimental dispersion data. In designing the devices, the primary concerns were finding the approximate phase velocity and hence the wavelength at the desired center frequency and finding the piezoelectric coupling constant k^2. Both these constants are needed to design the IDTs as explained in Chapter 3.

To find the phase velocity, an input file containing the substrate elastic constants, the approximate film constants, the center frequency, the film thickness and an approximate range that the velocity is expected to be in is input into the program. The input file format is given in Appendix B. This is a rather straight forward use of the program. To find k^2, the velocity is found with and without a thin metal layer between the substrate and the film [86]. The value of k^2 is then $2\Delta v/v$.

Once the coupling constant is found, the design of the SAW device is exactly the same as in Chapter 3. Since the coupling constant is reduced by the coating, the bandwidth of the devices is much narrower than for the normal SAW devices. For the lithium niobate devices, four different center frequencies of 35, 40, 45, and 50 MHz were chosen to yield at least four points on the dispersion curve. The remaining design parameters are given in Table IX.

Design of the Love devices is also similar to that carried out in Chapter 3. Lardat, et al. have shown that normal IDTs can be used to excite Love waves on quartz provided the sagittal plane is perpendicular to the X-axis [98]. ST-cut

quartz was used as the substrate, with propagation perpendicular to the X-axis. The design parameters for the Love devices are given in Table X.

TABLE IX
Parameters for Rayleigh-SAW IDTs.

Parameter	35 MHz	40 MHz	45 MHz	50 MHz
substrate	Y-cut,Z-prop LiNbO$_3$	Y-cut,Z-prop LiNbO$_3$	Y-cut,Z-prop LiNbO$_3$	Y-cut,Z-prop LiNbO$_3$
k^2	4.59E-4	2.19E-3	1.18E-2	3.65E-3
# of finger pairs	41	19	8	14
split finger?	Y	Y	N	N
finger width/spacing	8.1 μm	6.2 μm	8.7 μm	5.8 μm
finger overlap	1 mm	1mm	2.4 mm	0.67 mm
IDT center-center spacing	7.6406 mm	5.93 mm	5.261 mm	5.3132 mm
Tuning Inductor	1.13 μH	1.89 μH	1.44 μH	2.33 μH

TABLE X
Parameters for Love-SAW IDTs.

Parameter	22 MHz	24 MHz	26 MHz	28 MHz	30 MHz
substrate	ST-cut, y-prop Quartz	ST-cut, y-prop Quartz	ST-cut, y-prop Quartz	ST-cut, y-prop Quartz	ST-cut, y-prop Quartz
k^2	3.8E-3	1.75E-3	6.48E-4	3.11E-4	1.8E-4
# of finger pairs	14	21	35	50	66
split finger?	Y	Y	Y	Y	Y
finger width/spacing	21 μm	13.6 μm	9.4 μm	7.4 μm	6.2 μm
finger overlap	20 mm	8.3 mm	2.9 mm	1.3 mm	1 mm
IDT center-center spacing	7.31 mm	7.2576 mm	7.6132 mm	7.9452 mm	8.2612 mm
Tuning Inductor	4.2 μH	5.6 μH	8.5 μH	11.4 μH	14 μH

D. Software for Finding Elastic Constants from Experimental Velocities

To compute the mechanical properties from experimental dispersion data, the simulation software was called from a C program in which the elastic constants of the film are varied to minimize the squared difference between the experimental and simulated phase velocities. Direction set (Powell's) methods

76

are used to determine how the constants are varied to find the minimum (the C code for this is given in [99]). A listing of the routines necessary for setting up the search and for calling the simulation code is given in Appendix B. Figure 5.1 gives the organization of the program. The fitting program is called *velfit.c* whereas the simulation code is *trssaw.f.* The input file *sawfit.dat* contains the initial guesses of the film properties, the initial search directions, and the experimental velocities measured. The file *saw.scf* is the template for the input file to the simulation program. It contains the search ranges, the substrate material constants, and the film properties not being fitted such as thickness and density.

Using the template, the fitting program writes another file, *cinput*, containing the search values of the elastic constants. The simulation program writes the list of simulated velocities and the associated boundary condition determinant for each velocity to the file *outfile*. The boundary condition determinant value, if greater than 10^{-4}, indicates that the velocity did not converge properly and that the associated velocity is suspect. This usually occurs when the search range was not wide enough to capture the correct value.

The fitting program reads in the simulated velocities, computes the squared error against the measured values, and adds the search step information to the file *track.fit.* The next search step is then computed and the process repeated until the error is minimized. After the minimization is finished, the program then toggles the individual elastic constants by 1% to complete a two-level factorial design experimental grid [100, 101] and writes the result to *factor.ana.* The results can then be analyzed to determine the sensitivity of the velocities to each of the elastic constants as explained later in this chapter.
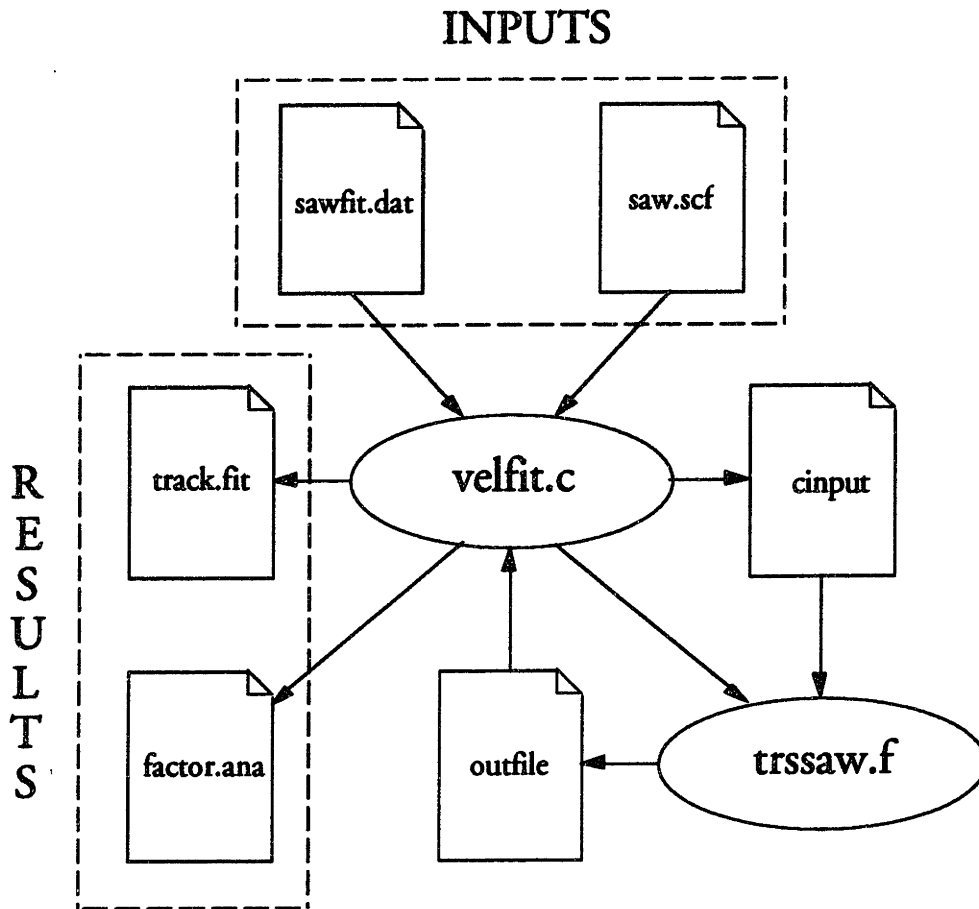
Figure 5.1: Organization of computer program for calculating elastic constants from dispersion data.

Certain subtleties in how the elastic constants are searched for helps the program in finding the best fit. First, the velocity search ranges are initially set to the experimental velocities ± 50 m/sec. If the boundary condition determinants fail to converge to less than 10^{-4} then the ranges can be increased as necessary, being cautious to avoid making the range encompass two modes.

Second, the shear moduli are searched for alone using only the Love mode velocities initially. For two shear moduli and three velocities, this takes approximately 2 CPU minutes on a Cray-2 to complete. Taking the values from the Love modes as fixed, the remaining constants are searched for using only the Rayleigh-like modes. For three constants and five velocities, this second search takes about 11 Cray-2 minutes. The entire complement of five constants are

then searched for using both the Rayleigh and the Love modes. This final step requires 24 Cray-2 minutes. Times on a Sun-4 are approximately 150 times longer.

Finally, the order in which the constants are searched for is set by the sensitivity of the velocity to the constant. The most influential constants should be fit first; the least effective, last. The order for two constant, isotropic, searches is c_{44} and then c_{11} with $c_{12} = c_{11} - 2^*c_{44}$. The order for five constant, transverse isotropic, searches is c_{13}, c_{11}, c_{33}, c_{66}, and then c_{44} with $c_{12} = c_{11} - 2^*c_{66}$.

E. Sensitivity Calculations

2: c_{11}= 10.21 GPa   4: c_{11}= 10.31 GPa
   c_{44}= 1.20 GPa c_{44}= 1.20 GPa
   v = 2258.8551 m/sec   v = 2259.2319 m/sec

1: c_{11}= 10.21 GPa   3: c_{11}= 10.31 GPa
   c_{44}= 1.19 GPa c_{44}= 1.19 GPa
   v = 2248.2051 m/sec   v = 2248.5744 m/sec
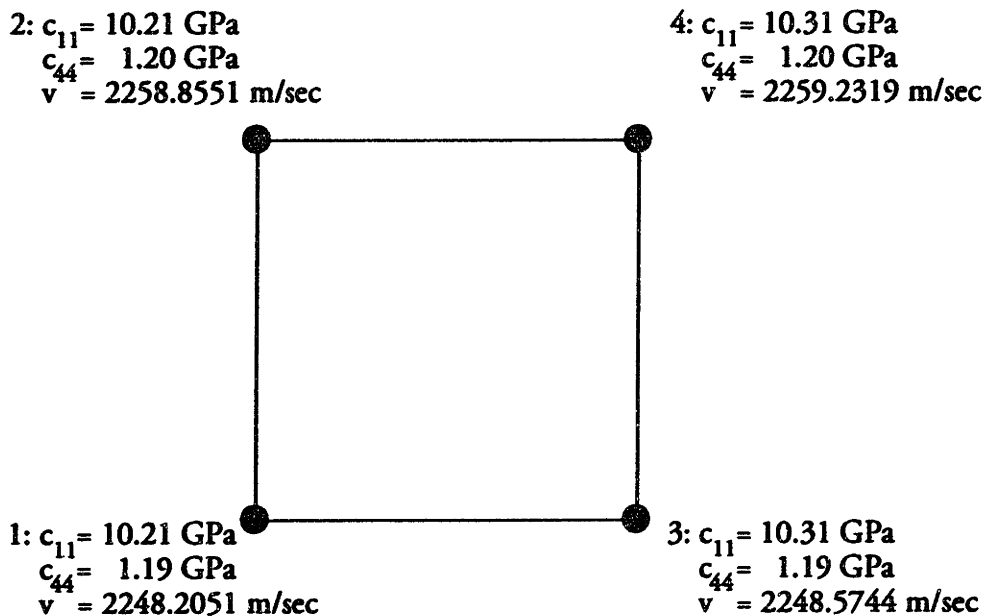
Figure 5.2: Grid of simulated velocities for factorial analysis of the sensitivity of phase velocity to the elastic constants c_{11} and c_{44}.

Because there is no analytical relationship between the elastic constants and the phase velocity, computation of the uncertainty in the fitted values is difficult. By conducting a full two-level factorial analysis [100, 101] on data generated by the simulation program, however, the uncertainty can be estimated. As an example, a portion of the data from the sensitivity analysis of a two-constant fit is

shown in Figure 5.2. At each of the four points, the elastic constants are used in the simulation program to find the phase velocity.

Point 1 is always the simulated velocity given the fit values of c_{11} and c_{44}. In this case, the fit values of the elastic constants are 10.21 and 1.19 GPa for c_{44} and c_{11} respectively. Point 4 is the simulated velocity for elastic constants that are 1% larger than the fit values. The values of c_{11} and c_{44} are 10.31 and 1.20 GPa respectively. Points 2 and 3 are computed using the shown values of the elastic constants to complete the grid.

The derivative $\delta v/\delta c_{44}$ can then be estimated from the data in Figure 5.2 by:

$$\frac{\delta v}{\delta c_{44}} \approx \frac{1}{2}\left[\frac{v(2) - v(1)}{c_{44}(2) - c_{44}(1)} + \frac{v(4) - v(3)}{c_{44}(4) - c_{44}(3)}\right] = 895 \text{ m/sec/GPa} \qquad (5.1)$$

and the derivative $\delta v/\delta c_{11}$ by:

$$\frac{\delta v}{\delta c_{11}} \approx \frac{1}{2}\left[\frac{v(3) - v(1)}{c_{11}(3) - c_{11}(1)} + \frac{v(4) - v(2)}{c_{11}(4) - c_{11}(2)}\right] = 3.65 \text{ m/sec/GPa} \qquad (5.2)$$

In this case, in which there are only two fit parameters, the formulas for the derivatives are relatively simple. For five fit parameters, however, the number of points in the grid is 2^5, or 32. Yate's algorithm [100] provides a simple way of computing the derivatives for this more complex case.

Typically, as an estimate of the error in the measurement of the velocity the squared error between simulated and measured velocities is divided by the number of degrees of freedom, (n-2), where n is the number of velocities and 2 is the number of fit parameters. For the experimental tests described in this chapter, however, n is typically 8, and the number of degrees of freedom is rather small at 6. When five elastic constants are fit, the number of degrees of freedom decreases to 3. The small number of degrees of freedom causes the estimate of the error in the velocity measurement to be unrealistically pessimistic. In some

cases this estimate is as large as ±35%. As a more realistic estimate of the uncertainty in velocity, a value of ±10% was used.

Dividing this error by the derivatives found above results in an estimate of the uncertainty in the elastic constants: ±0.25 GPa for c_{44} and ±61.6 GPa for c_{11}. Using only this velocity for the fit would indicate an uncertainty of 21% in c_{44} and ∞ in c_{66}. Fortunately, the other modes have different sensitivities and the real uncertainty in the elastic constants is between the lowest and the most common uncertainty level for all the velocities.

One flaw in this computation is that the uncertainty is really an absolute worst case analysis because that is the amount of variation needed in that single parameter to account for all the error in velocity. In actuality, the error is distributed across all the fit parameters.

F. Device Fabrication

Because of the larger film thickness in these devices, the patterning of the polyimide could no longer be done with the photoresist developer alone as it could in the mass sensor case. In order to make contact cuts through the polyimide to the IDTs, the fabrication process had to be modified to include a metal mask and a plasma etching step. The full process is given in Appendix B.

The fabrication process is identical up to the spinning of the polyimide. Instead of a single coat of polyimide spun at 3000 rpm, however, the approximately 10-μm thick film is deposited in three coatings, individually spun at 2000 rpm for 60 seconds and softbaked for 30 min at 160° C. Rather than immediately patterning the partially imidized polyimide, the polyimide is fully cured at this point. 1000Å of aluminum is then evaporated on top of that to act as the hard mask for plasma etching. Holes are opened in the aluminum layer with a photolithographic step combined with wet etching and removal of the photoresist in acetone. The unprotected polyimide is then etched with a Plasma

Technology Plasmalab RIE system. The etch was completed in approximately 20 minutes when a pure oxygen flow of 21 sccm, a pressure of 97 mtorr, and 225 watts of power were used.

After completion of the etch, some remaining scum appeared to be left on the surface that could not be etched with the oxygen plasma. The scum could be removed, however, with a gentle scrubbing with cotton swabs and ammonia soap. The presence of this scum appeared to be related to the oxygen flow rate, becoming less noticeable at flow values approaching 75 sccm.

Figure 5.3: Photo of completed SAW wafers. Rayleigh-wave, lithium niobate wafer is on the right. Love-wave, quartz wafer is on left..

Next, photoresist was spun on the wafers and patterned to protect the aluminum contacts exposed with the removal of the polyimide. The aluminum hard mask was then stripped in a wet etch, and the photoresist removed in acetone to complete the wafers. Figure 5.3 is a photograph of the completed wafers. The input and output IDTs at a specific center frequency are then wire-bonded and the wafers packaged as in Chapter 3. Testing of other devices on the

same wafer requires the appropriate wire-bonding and repackaging of the wafer. Figures 5.4 and 5.5 show the packaged wafers.
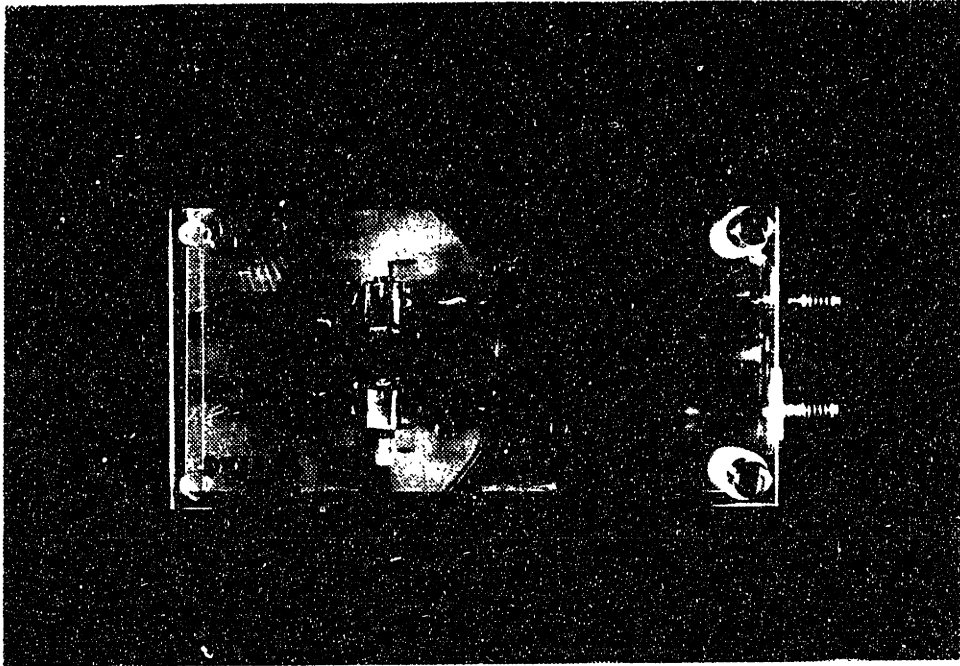
Figure 5.4: Photo of packaged quartz SAW device.
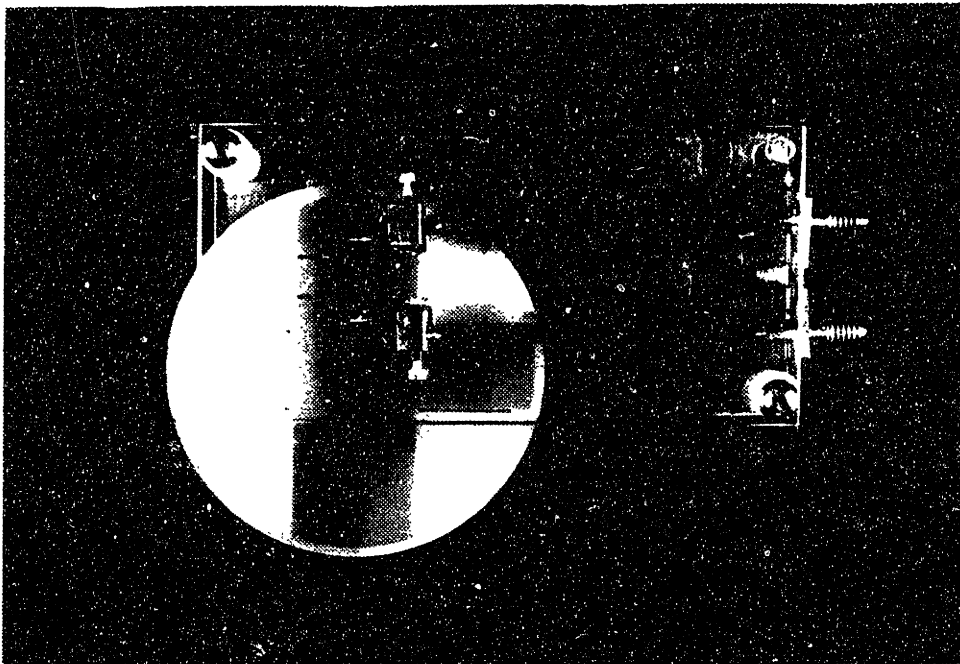
Figure 5.5: Photo of packaged lithium niobate SAW device.

G. Experimental Results

By monitoring the transmitted pulse using the system shown in Figure 3.7, frequencies at which acoustic propagation occurred were noted. Multiplication of the IDT wavelength by the frequency gives a value for the phase velocity [102]. The results for a SAW device with 9.85 μm of PI2555 on it are given in Table XI. Because of the large insertion loss of the devices, this was the only means of reliably finding the phase velocity of the acoustic modes. It is estimated that the error in locating the center frequency was ±5%, leading to a ±5% uncertainty in phase velocity.

TABLE XI
Measured acoustic velocities for 9.85 μm of PI2555 on YZ-LiNbO$_3$.

Device	λ (μm)	Thickness (λ)	Center freq. (MHz)	Phase velocity (m/sec)	Fit?
35 MHz	64.8	.152	19.4	1260	-
	64.8	.152	33.0	2138	R
	64.8	.152	51.2	3318	R
40 MHz	49.6	.1986	32.4	1607	L
	49.6	.1986	43.5	2158	R
	49.6	.1986	71.6	3551	-
45 MHz	34.8	.283	34.0	1183	L
	34.8	.283	38.9	1353	R
50 MHz	23.2	.4246	45.7	1060	L
	23.2	.4246	51.5	1196	R
	23.2	.4246	52.5	1217	-

In order to shorten the amount of computer time necessary, not all the velocities were used in the fit program. The modes with velocities over about 3400 m/sec correspond to plate modes and were removed. The 1260 m/sec mode at 35 MHz was found to be unrealistic and believed to be due either to a noisy pulse generator causing excitation of modes even when the RF signal from the network analyzer was not set at an appropriate center frequency or coincidental tuning of the IDTs to modes that should not be excited.

Although only Rayleigh waves should be excitable and detectable with an IDT when propagation is on YZ-lithium niobate [98], certain modes in Table XI are labeled Love modes. Evidence exists that says a thin film can transform SAW waves on lithium niobate into Love waves [103]. In addition, trial searches for elastic constants when the modes were assumed to be Rayleigh waves led to unphysical results. The lower velocity modes for each transducer are thus labeled Love waves with an L in the *Fit?* column. The Rayleigh waves are labeled with an R, and the unused velocities with a -.

Because Love wave propagation was possible using just the lithium niobate wafers, the quartz Love devices were redundant. Since they represent a separate sample of polyimide, the properties are not guaranteed to be identical to those of the polyimide deposited on the lithium niobate wafers. For this reason, the quartz devices were used only in Chapter 7, acting as a check of the shear moduli found from the lithium niobate data.

The appropriate phase velocities in Table XI were input into the fitting program, *velfit.c*, and the search conducted according to the previous section with two fitting constants, c_{11} and c_{44}. The other constants were computed from these two by assuming mechanical isotropy in the film. Their formulas are:

$$c_{22} = c_{33} = c_{11} \qquad (5.3a)$$

$$c_{55} = c_{66} = c_{44} \qquad (5.3b)$$

$$c_{12} = c_{13} = c_{23} = c_{11} - 2c_{66} \qquad (5.3c)$$

where the stiffness tensor has been written in reduced index form according to Nye [67]. The result was a value of 10.2 GPa for c_{11} and a value of 1.19 GPa for c_{44}. The sensitivity analysis indicated uncertainties of $\pm 10\%$ and $\pm 20\%$ respectively. The uncertainties are discouraging, but as stated previously, they represent absolute worst case computations. Errors in the velocity measurement

are also larger than can be achieved; other researchers have cited velocity measurements to better than 0.1% [48].

By plugging the values for c_{11} and c_{44} into the simulation program and computing the dispersion curves, Figure 5.6 can be generated. Although many of the velocities appear to be very close to the simulated curves, it is clear that a few of the measured velocities appear to be quite far off.
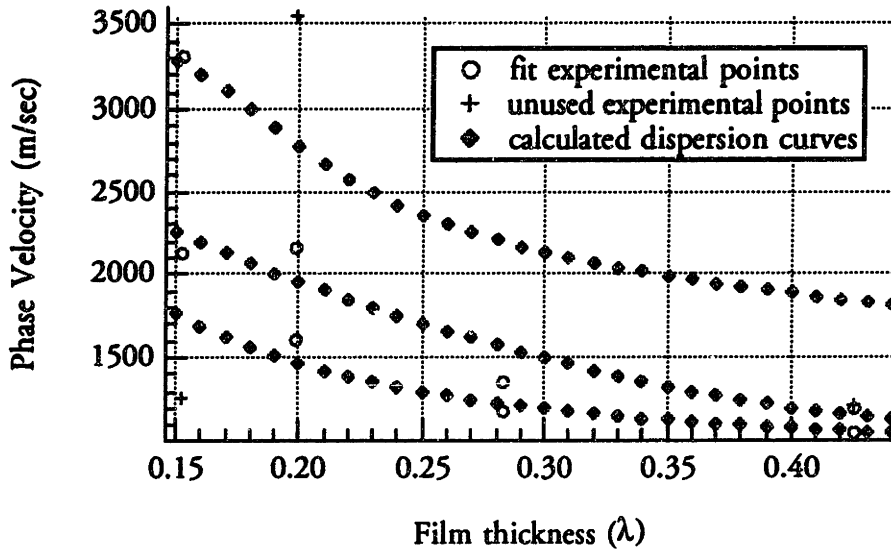
Figure 5.6: Experimental data and simulated dispersion curves generated from the two fitted elastic constants.

When the values of Table XI were used to find values for the five elastic constants, c_{11}, c_{33}, c_{13}, c_{44}, and c_{66}, the values found were:

$$c_{11} = c_{22} = 11.4 \text{ GPa} \pm 12\% \qquad (5.4a)$$

$$c_{13} = c_{23} = 9.2 \text{ GPa} \pm 8\% \qquad (5.4b)$$

$$c_{33} = 10.9 \text{ GPa} \pm 15\% \qquad (5.4c)$$

$$c_{44} = c_{55} = 1.5 \text{ GPa} \pm 35\% \qquad (5.4d)$$

$$c_{66} = 1.0 \text{ GPa} \pm 40\% \qquad (5.4e)$$

$$c_{12} = c_{11} - 2c_{66} \qquad (5.4f)$$

Plugging these five fitted values into the simulator yields the dispersion curves in Figure 5.7. Note that the fit does not appear to be too much better than in

Figure 5.6 where only two fitted constants were used. This implies that for realistic values of elastic constants, the shape of the dispersion curves cannot be made arbitrary which indicates a certain amount of insensitivity of the acoustic propagation to the elastic constants in the film. This, of course, is confirmed by the uncertainty calculations.
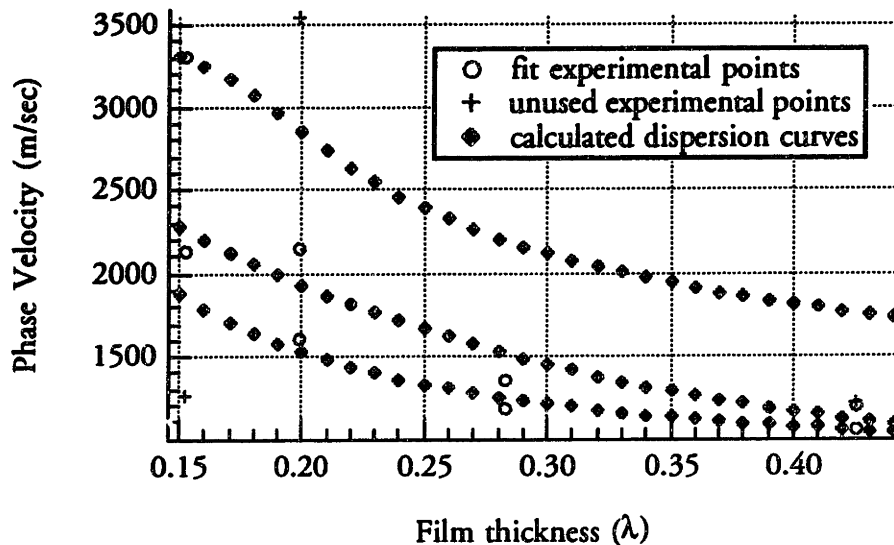
Figure 5.7: Experimental data and simulated dispersion curves generated from the five fitted elastic constants.

H. Limitations of Acoustic Methods

The large uncertainty in the extracted values of the elastic constants is discouraging. The primary problem, however, appears to be the inability to extract the acoustic velocities to better than 10%. With denser and more accurate data, the errors can be cut dramatically, as witnessed by the fact that simulated dispersion curves input into the velfit fitting program always yield the correct values of elastic constants to within 1%. Possible methods of increasing the accuracy of the velocity measurements include going to a phase-sensitive velocity measurement scheme [104], other novel velocity measurement schemes [105], using Brillouin scattering [37, 79-82], and possibly just designing better IDTs at much more closely spaced frequencies.

With the denser and more accurate velocities, the amount of computer time required to conduct the search for the best-fit elastic constants should also decrease. For measurements accurate to within a few m/sec, or 0.1%, the need for redundancy in the data is reduced, so fewer velocities need to be simulated during the process of simulating. In addition, a novel method of doing the fitting, which can speed computations by several orders of magnitude, can then be implemented. This method removes the need to simulate the velocities for each set of trial elastic constants, a task that takes 5 CPU minutes on a Sun-4. Instead, the measured velocities are directly input into the boundary condition determinant (BCD) and a value representing the closeness of the velocity to the propagating velocity is found. Figure 5.8 is a graph of the BCD as a function of velocity, clearly showing the value of three propagation velocities. By directly minimizing the BCD as a function of the elastic constants, the need to simulate the acoustic propagation at each search point is avoided. The BCD evaluation clearly takes a fraction of the time of the full simulation because the simulation program internally uses the BCD as the function minimized when a propagation velocity is found.

In addition to these two concerns, it should be noted that there are three other limitations to the techniques as they are described in this thesis. This applies to not only the acoustic methods described in this chapter, but also those described in Chapters 4 for measuring diffusion constants, and mass uptake during swelling. The first of these is that by choosing to use IDTs to excite and detect surface acoustic waves an implicit decision to use only piezoelectric substrates has been made. Since our initial desire was to measure the properties of polyimide films, and we knew that the substrate could influence those properties, an unknown amount of error is introduced due to our assumption that at least the elastic constants of the film do not vary with the substrate material.

88
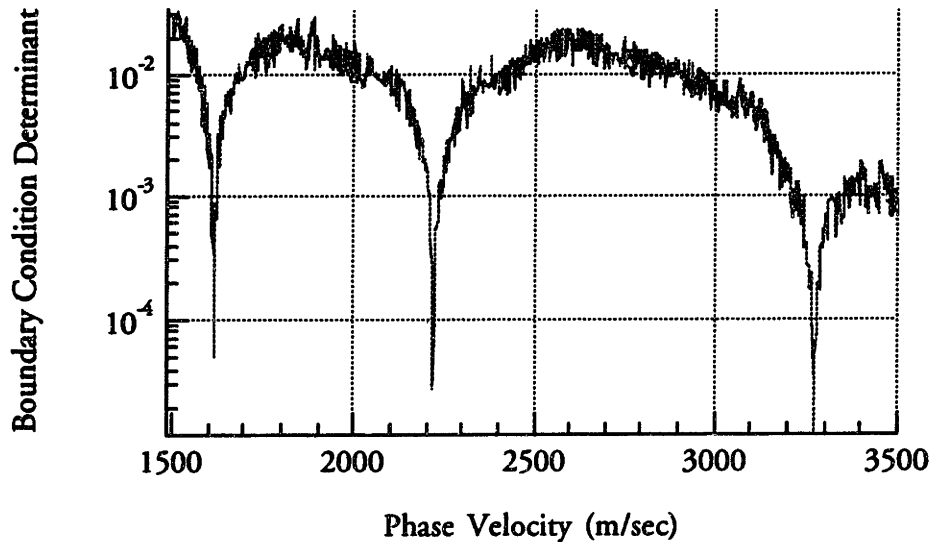
Figure 5.8: Calculated boundary condition determinant as a function of phase velocity, demonstrating three propagation velocities.

This limitation can be avoided by doing the same analysis but with a different transduction mechanism. The use of Brillouin scattering has been proven very effective in determining the dispersion of many modes in multilayer systems [37, 79-82]. Since it requires no active excitation of the acoustic modes, such a technique could be applicable to almost any multilayer measurement scheme. Bonded transducers [75, 76], can also be used to excite and detect surface acoustic waves on non-piezoelectric materials. Another alternative is to abandon the acoustic dispersion methods outlined here in favor of the acoustic microscopy techniques [22, 70, 71, 73, 106].

The second limitation to the method is that residual stress in the film is not accounted for in the modeling of the acoustic propagation. This would also tend to aggravate the problem of different substrates, but even with a single substrate the accuracy with which the elastic constants are determined is limited by whether or not stress is accounted for. Some researchers have looked into modeling the effect of strain on acoustic wave propagation for use as strain

sensors [107, 108]. In a very simplistic sense, the effect is accounted for in the wave equation of (3.1) with a set of effective elastic constants c_{ijkl}', in which certain constants are stiffened or softened by the stress. For polyimide deposited on silicon, the residual stress is roughly 30 MPa from suspended-membrane tests. As measured above, the elastic constants of polyimide are at least on the order of 1 GPa, so the stress correction is on the order of 3%. Although further refinement of the method would ideally involve correction of this error, it was not deemed necessary to redo the modeling to account for such a small effect, especially considering the large measurement errors already present.

The final limitation to these and any acoustic methods is that the measurements are inherently dynamic tests and subject to acoustic losses. The modeling software allows for real elastic constants only, so lossless propagation is assumed. There are techniques with which the propagation loss can be measured as a function of frequency, but again, evidence suggests that the loss in polyimide for frequencies less than 50 MHz can be neglected [109]. Also of concern, because polyimide is the material of interest, is that the elastic constant determined at 50 MHz may or may not be equivalent to the static mechanical stiffness. Because it is a polymer, it is subject to the rules of time-temperature superposition. For experiments conducted near the glass transition temperature of the polymer, the difference between tests done on a time scale of seconds versus tests on a nanosecond scale would be very dramatic. It is assumed that the test are done sufficiently far below the T_g of the polyimide (> 200° C below) that the effect of the difference in time scale can be neglected.

CHAPTER VI: COMBINED RESULTS OF MEMBRANE AND ACOUSTIC TESTS

A. Purpose of Investigating Two Independent Measurement Methods

This thesis studies two independent measurement methods: load-deflection of suspended membranes and surface-acoustic-wave velocity measurement rather than just either of them alone for three reasons. First, it allows confirmation of the accuracy of the measurements because measurement of the same material should yield identical results if both methods are accurate. Second, it allows measurement of more complex effects such as swelling which may involve ratios of a number of different measureable parameters. Finally, it offers the luxury of at least two viewpoints when trying to explain unexpected behavior.

B. Verification of Suspended-Membrane Results

In order to directly compare the results of the suspended-membrane tests with the acoustic results, which are given as elastic stiffness values, the elastic constants must be converted into the modulus values measured by the membrane tests. The relationship between modulus and elastic stiffness can is described by:

$$s_{ij} \, c_{jk} = \delta_{ik} \quad \text{or} \quad s = c^{-1} \tag{6.1a}$$

$$E_{11} = \frac{1}{s_{11}} \tag{6.1b}$$

$$E_{33} = \frac{1}{s_{33}} \tag{6.1c}$$

$$v_{12} = -\frac{s_{12}}{s_{11}} \tag{6.1d}$$

$$v_{13} = -\frac{s_{13}}{s_{11}} \tag{6.1e}$$

$$v_{31} = -\frac{s_{13}}{s_{33}}$$ (6.1f)

where E_{11} is the in-plane Young's modulus; E_{33} is the Young's modulus normal to the plane; v_{12} is the in-plane Poisson ratio; v_{13} is the Poisson ratio normal to the plane in response to in-plane deformations; v_{31} is the in-plane Poisson ratio in response to out-of-plane deformations; s_{ij} is the compliance tensor; c_{ij} is the stiffness tensor; and δ_{ij} is equal to 1 when i=j and 0 otherwise.

Converting the results from Chapter 5, the values of modulus and Poisson ratio given in Table XII are found. The data agrees with the Young's modulus of 3.2 GPa and Poisson ratio of 0.42 found from uniaxial and biaxial measurements on 2525 [44], which is a less dilute form of 2555. Computing the biaxial modulus, $E/(1-v)$, from the data yields a value of 6.0 GPa in the isotropic case and 5.1 GPa for the in-plane biaxial modulus in the transverse-isotropic case. These agree with the suspended-membrane value of 6.1 GPa found in Chapter 2 to well within the uncertainty of the measurements.

The error bars on the computed values of modulus and Poisson ratio when using the acoustic data were estimated to be ±20% in modulus and ±60% in Poisson ratio. As in Chapter 5, these values were estimated using factorial analysis of the sensitivity of the numerical fit to velocity uncertainties of 10%, when E and v are used as the fitting constants rather than c_{11} and c_{44}.

TABLE XII
Values of modulus and Poisson ratio computed from
results of acoustic tests.

Symmetry assumed	c_{ij}	s_{ij}	Modulus or Poisson ratio
isotropic	c_{11} = 10.2 GPa c_{44} = 1.19 GPa	s_{11} = 0.292 GPa^{-1} s_{44} = 0.837 GPa^{-1}	E = 3.42 GPa v = 0.43
transverse isotropic	c_{11} = 11.4 GPa c_{33} = 10.9 GPa c_{13} = 9.23 GPa c_{44} = 1.49 GPa c_{66} = 1.05 GPa	s_{11} = 0.337 GPa^{-1} s_{33} = 0.373 GPa^{-1} s_{13} = -0.166 GPa^{-1} s_{44} = 0.672 GPa^{-1} s_{66} = 0.956 GPa^{-1}	E_{11} = 2.97 GPa E_{33} = 2.68 GPa v_{12} = 0.42 v_{13} = 0.49 v_{31} = 0.45

Comparison of the results with those published by Smirnova for some of the elastic compliances found from rheovibron and torsion tests of PMDA-ODA polyimide [110] also show reasonable agreement. Smirnova finds: $s_{11} = 0.31$ GPa^{-1}, $s_{44} = 1.00$ GPa^{-1}, and $s_{66} = 0.82$ GPa^{-1}.

C. Polymer Swelling

It is well known that polymers swell as they equilibrate with their surrounding medium, even when that surrounding medium is just humid air [5]. From the process engineer's viewpoint, swelling is an unwanted effect that can cause difficulty in both defining small features in the polyimide as well as masking large sections of polyimide during high-temperature processing.

Swelling is quantified by a constant known as the swelling parameter. Simply stated, the swelling parameter is the amount of strain per weight percent of solvent or:

$$S = \frac{\varepsilon}{C_o} \qquad (6.2)$$

where S is the swelling parameter, C_o is the concentration, and ε is the strain. It is measured as the ratio of two quantities: the change in strain with changes in concentration of the solvent in the surrounding environment, and the change in weight concentration in the film as a function of the concentration in the surrounding environment. Since load-deflection techniques measure both the residual stress and the biaxial modulus (to within a function of the Poisson ratio) of the film, the residual strain as a function of the surrounding environment can be measured. The value found in Chapter 2 for PI2555 was 0.0021% strain/%RH. The weight concentration as a function of RH was measured with the SAW mass sensor. The value from Chapter 4 is 0.019% / %RH. Therefore, using equation (6.2) the swelling parameter for PI2555 is 0.11% strain/wt. % water. This value is slightly smaller than the 0.31% strain/wt. % water for

vacuum-dried epoxy measured by Berry with a bending-cantilever method [111], but is nevertheless reasonable given ule very different materials being compared.

Although measurements of the mass uptake were not made with the other materials, values can be found in the literature for Hitachi PIQ and PIQL100 polyimides. They are 0.023% / %RH and 0.013% / %RH respectively [59]. Using the measured coefficient of hygroscopic expansions of 0.0014% strain/%RH and 0.00025% strain/%RH respectively, the swelling parameters for PIQ and PIQL100 are found to be 0.06% strain/wt. % water and 0.02% strain/wt. % water.

D. Moisture Controlled Sub-Glass Transition
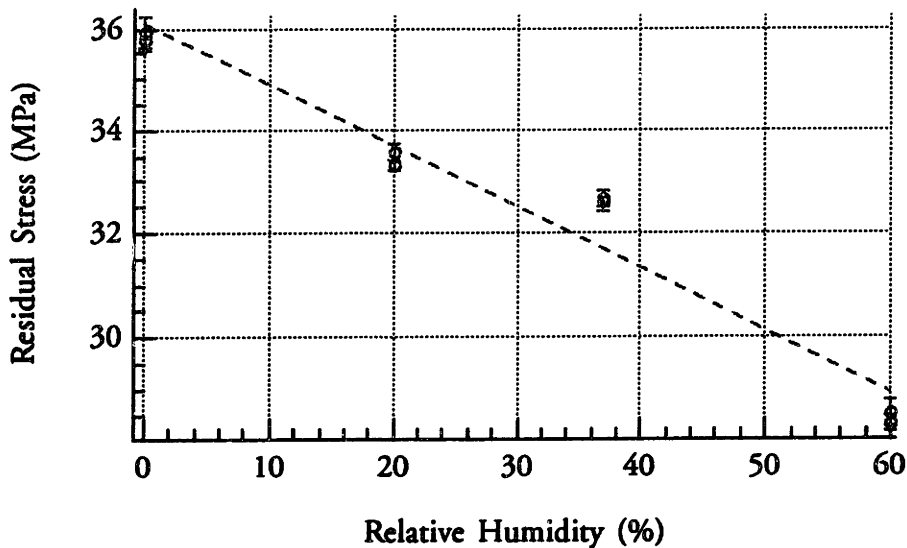
Figure 6.1: Measured residual stress at 20° C as a function of relative humidity for Hitachi PIQ13 film.

As noted in Chapter 4, the data from the SAW mass sensor suggests that a change in the manner in which water is taken up in polyimide seems to occur near 35% RH, 21° C, and 39.3675 MHz. Looking back to Chapter 2, the residual stress curve measured by load-deflection methods for Hitachi PIQ13, given in Figure 6.1, also seems to undergo a change in slope near 35% RH. The fact that

the load-deflection test is a static loading test in contrast to the dynamic acoustic tests seems to suggest that the water is taken into the polyimide in a haphazard way, but rather in a staged manner. Certain sites appear to fill first and a second-order thermodynamic transition occurs at a certain concentration. Optical birefringence data as a function of relative humidity [10] also appears to exhibit this effect.

CHAPTER VII: RESULTS OF TESTS ON DUPONT PI2555

A. Fabrication Procedure

As a demonstration of the capabilities of the methods described in the previous chapters, both the suspended-membrane and the acoustic tests were conducted on a single batch of Dupont PI2555 polyimide films. From Chapter 2 it is clear that the desired properties are known to vary with process conditions, so all samples were fabricated from the same lot of material and subject to the same processing conditions. The fabrication processes as described in Chapters 2-6 and Appendix B were followed. DuPont VM-651 Adhesion Promoter from Lot J705789, manufactured on 8/22/90, was mixed and applied to all wafers before spinning on three coats of DuPont Pyralin PI2555 from Lot J695781, manufactured on 9/10/90 to yield a 10 μm thick film. Because the mass sensor requires a thin film of polyimide to avoid undesired sensitivity to the film's elastic properties, one ST-quartz wafer was coated with only one coat of polyimide spun at 5000 rpm for 60 seconds instead of the 2000 rpm that the other wafers were underwent. The resulting thickness was 1.55 μm. To permit the wet-patterning of the polyimide for the mass sensor wafer, the softbake was done at 120° C for 15 min. The first softbake for the multicoated samples were also done at 120° C for 15 min for consistency. Subsequent softbake cycles for the multicoated wafers were done at 160° C for 30 min. After patterning of the mass sensor wafer and completion of the three coats of material on the other wafers, the entire batch of wafers were loaded under nitrogen flow into a Black Max quartz tube and cured at 400° C for 90 min. Subsequent patterning of the remaining acoustic wafers and the fabrication of the suspended membrane sites proceeded exactly as described in Appendix B and Chapter 2.

96

B. Experimental Results: Suspended-Membrane: Humidity

A small change was made in the procedure for doing the tests. Instead of an unregulated flow of air across the top and bottom of the membrane, the flow was restricted to 0.5 scfh across the top and 1.75 scfh across the bottom. This was done to remove flow dependent shifts in the measurements. Figures 7.1 and 7.2 show the data.

As stated in Chapter 4, evidence that the moisture is taken up in different ways at different concentrations is still present. In fact, the slight initial increase in biaxial modulus could be due to hydrogen bonding of the small amounts of water present at low levels of humidity [91]. Table XIII lists the properties extracted from the data. The properties agree with those found in Chapter 2 to within 20%.
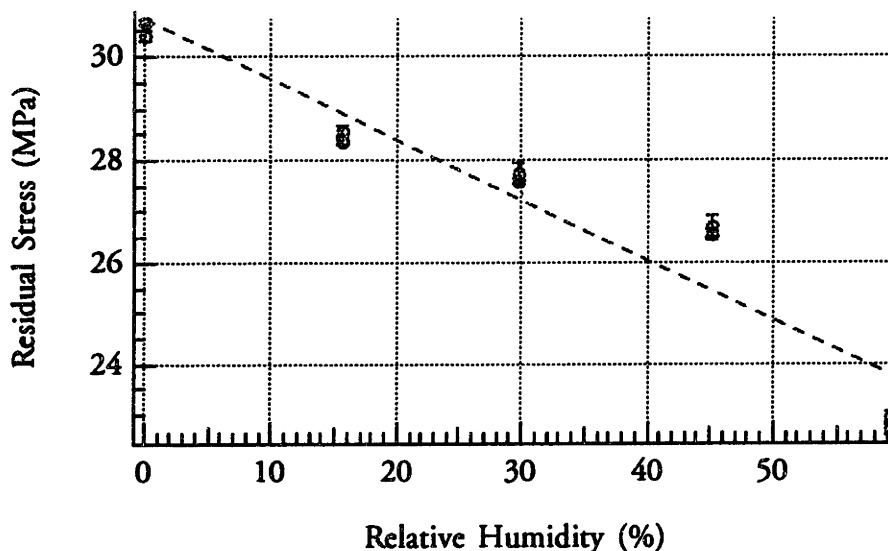
Figure 7.1: Measured residual stress at 20° C as a function of relative humidity for DuPont PI2555 film.
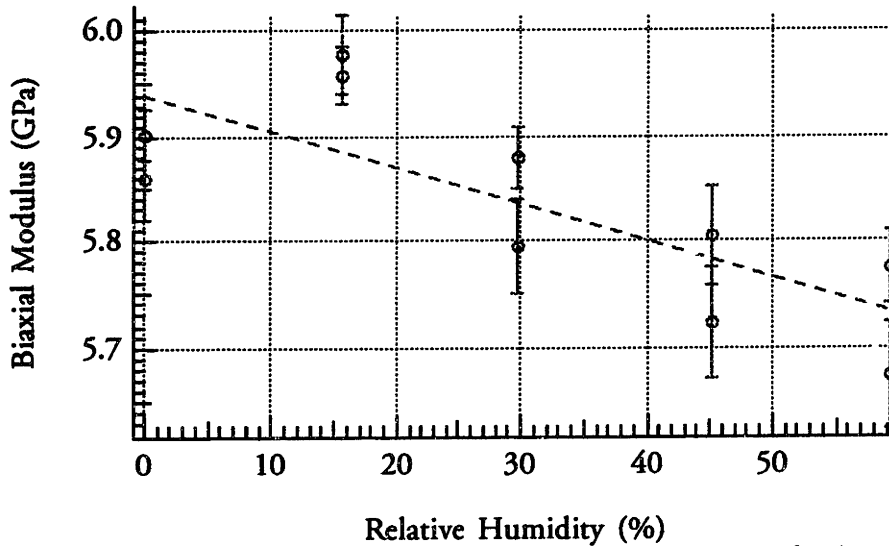
Figure 7.2: Measured biaxial modulus at 20° C as a function of relative humidity for DuPont PI2555 film.

TABLE XIII:
Mechanical Properties for DuPont 2555 Found from Suspended-Membrane Measurements.

Property	Value
Residual Stress (MPa) at 0% RH	30.7±1
Biaxial Modulus (GPa) at 0% RH	5.94±0.08
Residual Strain (%) at 0% RH	0.52±0.02
Variation in Stress with RH (kPa/%RH)	-117±29
Variation in Modulus with RH (MPa/%RH)	-3.5±2.3
Variation in Strain with RH (%/%RH)	-0.0017±0.0006

C. Experimental Results: Acoustic Mass

As in the suspended-membrane case, a regulated flow of 5.0 scfh directed at the surface of the SAW mass uptake sensor was used throughout the measurements. This was done to remove flow dependent shifts in the measurements. Figures 7.3-7.6 show the data. Table XIV summarizes the properties found. The data are within 20% of the values found in Chapter 4.
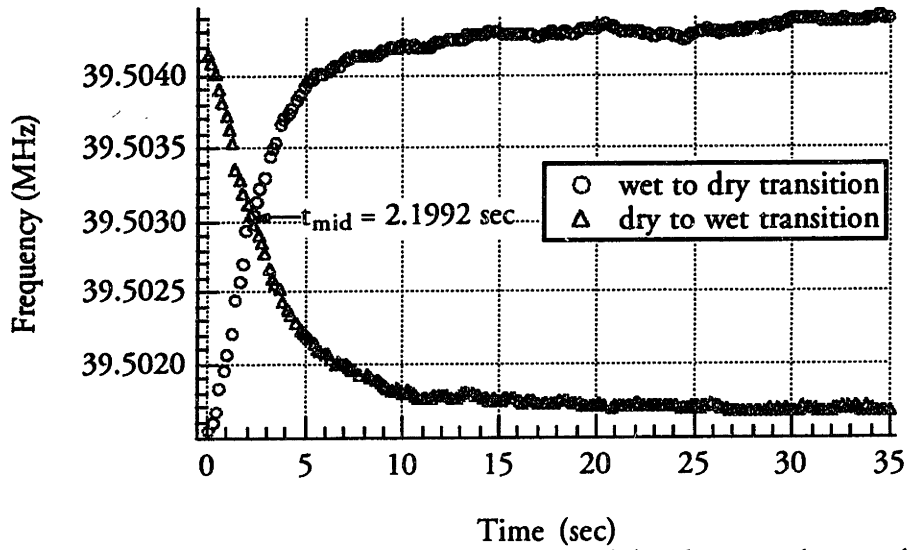
Figure 7.3: Response of polyimide coated SAW delay line to abrupt changes in humidity. Polyimide thickness is 1.55 μm.
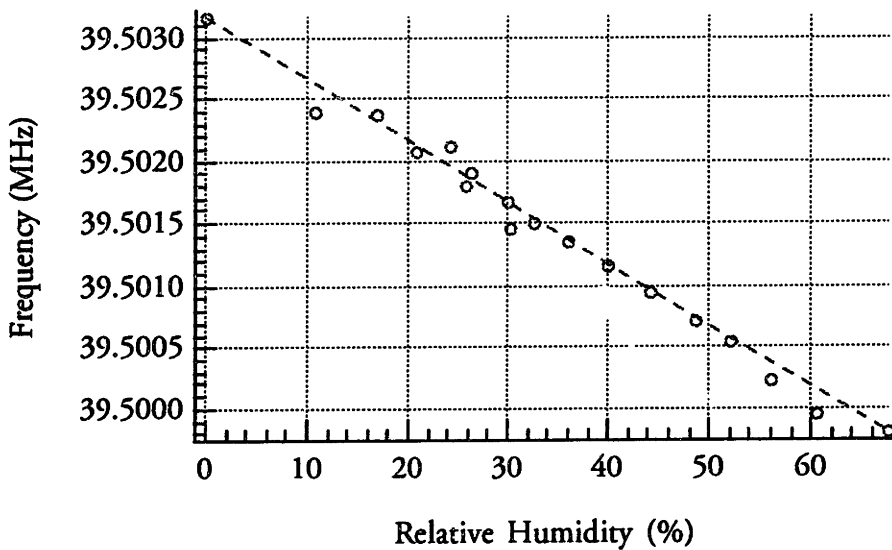
Figure 7.4: Zero-phase frequency as a function of relative humidity at 20° C.
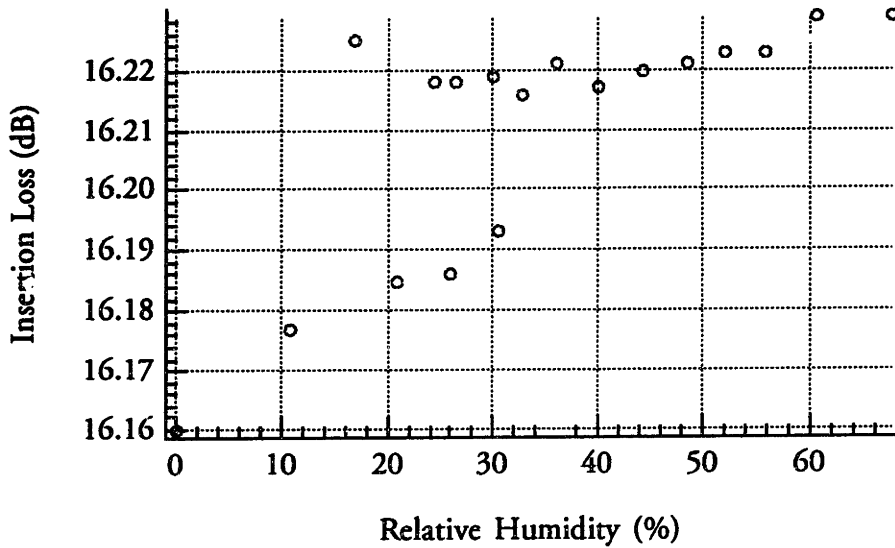
Figure 7.5: Zero-phase insertion loss as a function of relative humidity at 20° C.
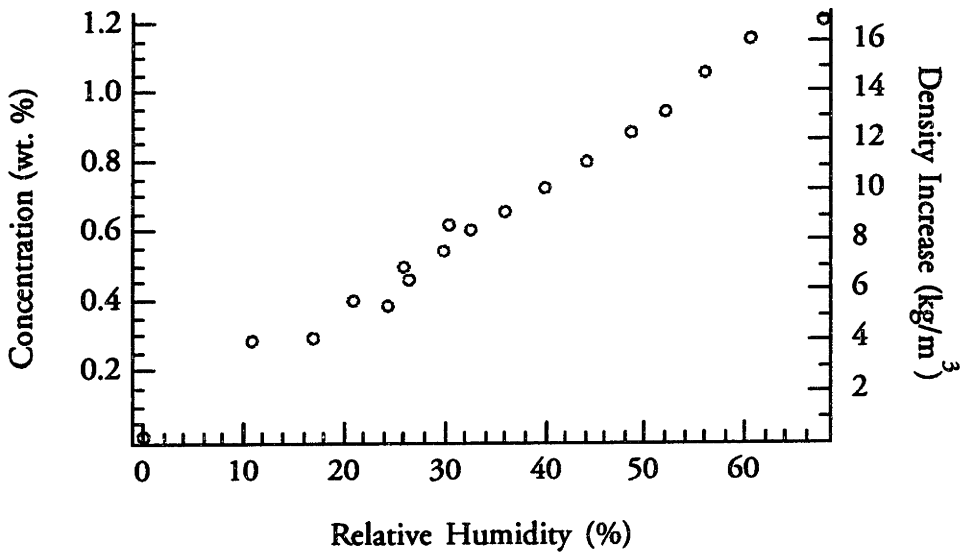
Figure 7.6: Mass uptake as a function of humidity for DuPont PI 2555.

TABLE XIV:
Mechanical Properties for DuPont 2555 Found from Acoustic Mass Uptake
Measurements.

Property	Value
Diffusion coefficient (cm²/sec)	2.1×10^{-9}
Mass uptake with humidity (%/%RH)	0.018
Swelling Parameter (% strain/wt.%)	0.09

100

One interesting feature of the data to note is that the change in slope at 35% in the mass uptake versus humidity plot seems to have disappeared. This has been attributed to the regulation of the flow. When the flow was unregulated, the humidity control system led to increasing flow rates from 0% to 35% RH and decreasing flow rates thereafter. The change in slope observed in Chapter 4 was partially a flow induced effect. Considering the same humidity control system was used for all tests, this peaking in the unregulated flow could have led to all the changes in properties occurring at 35% RH. Changes in slope, however, are observed in the regulated-flow suspended-membrane tests. In addition, even with the flow regulated the insertion loss of the SAW sensor, shown in Figure 7.5, also exhibits an abrupt increase at 35%. The noise in the measurement, which leads to the double-valued appearance of the data between 15-35% RH, however, makes interpretation difficult. Further investigation is warranted.

D. Experimental Results: Acoustic Elastic Constants

In addition to the acoustic tests described in Chapter 5 of this thesis, optical tests were also done on this batch of 2555 films to confirm anisotropy in the film. Using a Metricon PC-2000 measurement system to measure the polyimide adhered to the surrounding silicon after fabrication of the suspended membrane, the thickness was found to be 9.3 μm and refractive indices, n_{TM} and n_{TE}, 1.6784 and 1.6935 respectively. A full description of this optical measurement can be found in [10, 112].

In conducting the acoustic elastic-constant measurements, the only changes in procedure from Chapter 5 were the measurement of the quartz Love devices and careful control of the humidity at which the tests were done. The samples were dried in a bell jar with desiccant, and the samples tested under a flow of dry nitrogen. The experimental results are tabulated in Tables XV and XVI.

101

TABLE XV
Measured acoustic velocities for 10.02 μm of PI2555 on YZ-LiNbO$_3$.

Device	λ (μm)	Thickness (λ)	Center freq. (MHz)	Phase velocity (m/sec)	Fit?
35 MHz	64.8	.1547	25.7	1667	L
	64.8	.1547	50.7	3288	R
40 MHz	49.6	.202	34.4	1705	-
	49.6	.202	40.9	2029	R
	49.6	.202	71.8	3561	-
45 MHz	34.8	.288	32.8	1142	L
	34.8	.288	42.9	1493	R
	34.8	.288	50.2	1745	-
	34.8	.288	68.6	2387	R
	34.8	.288	80.6	2803	-
	34.8	.288	94.5	3290	-
50 MHz	23.2	.432	38.7	897	-
	23.2	.432	44.4	1031	L
	23.2	.432	50.3	1166	R
	23.2	.432	155	3606	-

TABLE XVI
Measured acoustic velocities for 9.9 μm of PI2555 on STY-Quartz.

Device	λ (μm)	Thickness (λ)	Center freq. (MHz)	Phase velocity (m/sec)	Fit?
22 MHz	168	.0589	24.6	4129	L
	168	.0589	32.1	5394	-
24 MHz	109	.091	21.3	2313	L
	109	.091	22.6	2462	-
26 MHz	75.2	.132	22.0	1654	L
28 MHz	59.2	.167	33.7	1992	L

The elastic constants found from the lithium niobate data are given in Table XVII. The uncertainties are approximately the same as in Chapter 5, so they are not listed in the table. Figures 7.7 and 7.8 show the fitted dispersion curves. When the quartz Love data is used to calculate the shear moduli c_{44} and c_{66}, values of 1.36 GPa and 0.9 GPa respectively. Figure 7.9 shows the calculated

102

dispersion curves using these values as well as those found from the lithium niobate data. The effect of the large uncertainty in velocity, estimated to be ±10% for the quartz data, can be seen.

Comparing the results in Table XVII with those in Chapter 6, Table XIII shows good agreement between the isotropic values of the elastic constants, but poor agreement for the transverse-isotropic constants. Although the fabrication processes and the experimental conditions of the two samples were slightly different, the large uncertainty in the values of the constants makes it impossible to conclusively say that the materials are actually as different as the elastic measurements appear to indicate. Instead, the data appear to indicate that the uncertainties are indeed as large as estimated in Chapter 5.

TABLE XVII
Values of elastic constants, moduli, and Poisson ratio computed from results of acoustic tests.

Symmetry assumed	c_{ij}	s_{ij}	Modulus or Poisson ratio
isotropic	c_{11} = 11.7 GPa c_{44} = 1.13 GPa	s_{11} = 0.306 GPa^{-1} s_{44} = 0.885 GPa^{-1}	E = 3.27 GPa v = 0.45
transverse isotropic	c_{11} = 11.8 GPa c_{33} = 11.6 GPa c_{13} = 9.14 GPa c_{44} = 1.06 GPa c_{66} = 0.99 GPa	s_{11} = 0.322 GPa^{-1} s_{33} = 0.257 GPa^{-1} s_{13} = -0.109 GPa^{-1} s_{44} = 0.946 GPa^{-1} s_{66} = 1.010 GPa^{-1}	E_{11} = 3.11 GPa E_{33} = 3.89 GPa v_{12} = 0.57 v_{13} = 0.34 v_{31} = 0.42
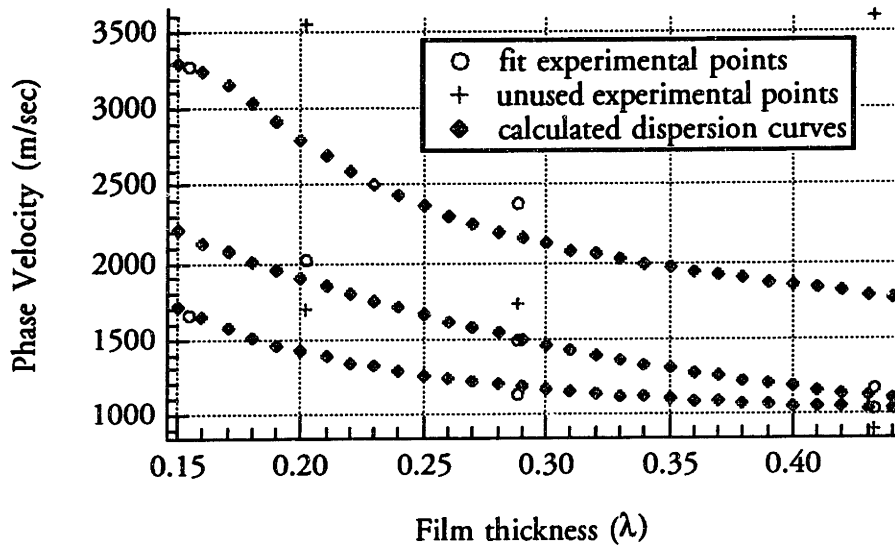
Figure 7.7: Experimental data and simulated dispersion curves generated from the two fitted elastic constants.
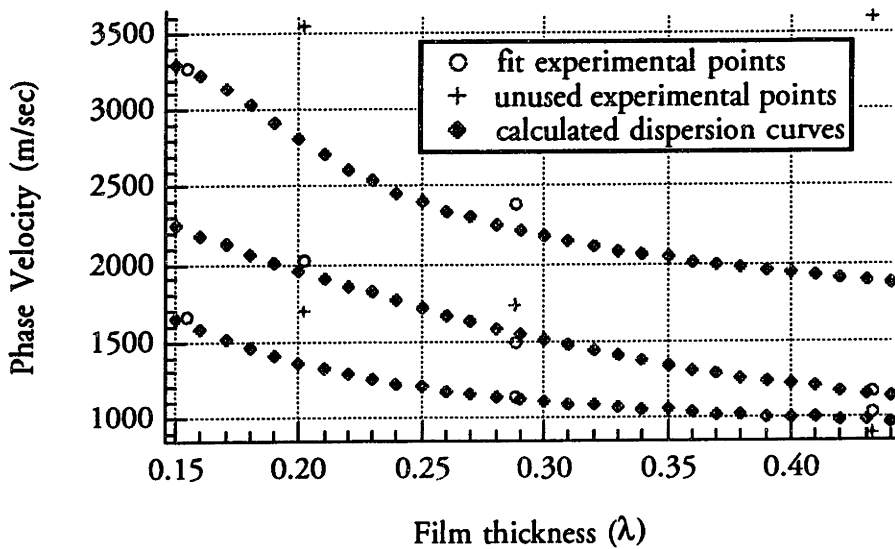
Figure 7.8: Experimental data and simulated dispersion curves generated from the five fitted elastic constants.
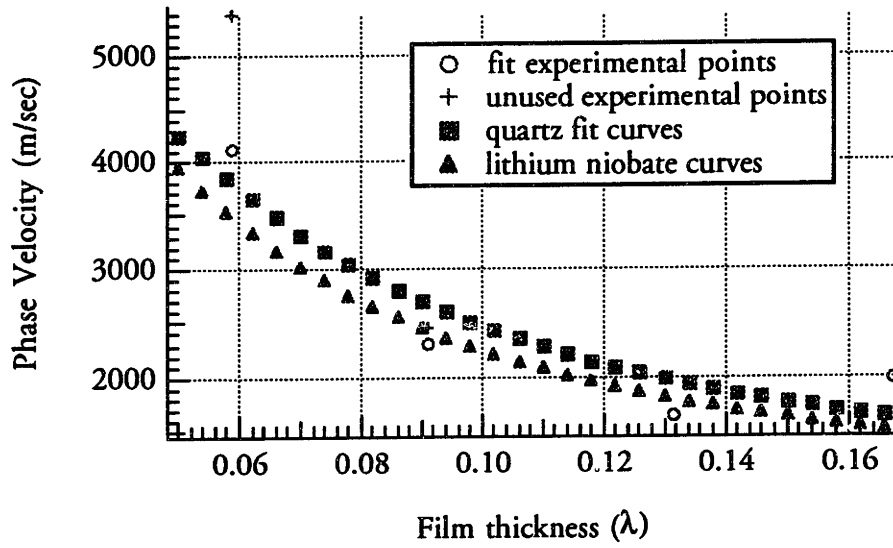
Figure 7.9: Experimental data and simulated dispersion curves generated from the two fitted shear moduli.

CHAPTER VIII: SUMMARY AND CONCLUSIONS

Two measurement techniques have been described in this thesis. Although neither test is new, improvements to each have been made to give them new capabilities. A summary of the properties measured in this thesis is given in Table XVIII. Modifications in the modeling, fabrication, testing, and data analysis portions of the suspended-membrane methods have improved the accuracy and reproducibility of the measurements. With the improved reproducibility and added experimental control, measurement of the effects of humidity, temperature, time, and processing on both the residual stress and the biaxial modulus is demonstrated.

Application of acoustic methods provides information about diffusion constants and mass uptake that, when combined with the new load-deflection results, completes the characterization of the swelling properties. Furthermore, some indications that acoustic tests may be used to detect and measure sub-glass transitions in glassy-state polymer films have been found. Acoustic tests also serve to independently verify the accuracy of the suspended-membrane methods. Finally, with the addition of Love mode propagation to the list of studied acoustic modes, complete determination of the stiffness matrix, and thus the mechanical anisotropy, of thin coatings becomes possible.

The application of both these methods to the determination of the mechanical properties of Dupont PI2555 polyimide is used as an example of the effectiveness of the two techniques. Even though the methods were modified specifically for measuring polyimide and the effect of humidity on its properties, they are not limited to this material by any means. The same methods have already been applied to materials ranging from silicon nitride to car paint. Using only slightly modified measurement equipment, the swelling properties resulting from solvents other than water can also be measured straightforwardly.

TABLE XVIII
Summary of Measured Mechanical Properties.

Method	Property	DuPont 2555	DuPont 2556	10 cure DuPont 2556	DuPont 2611	Hitachi PIQ13	Hitachi PIQL100
S	Residual Stress (MPa) at 0% RH	35.2±0.4 30.7±1.0	28.1±0.9	33.3±0.6	34.8±0.7	36.1±1	11.5±0.4
U	Biaxial Modulus (GPa) at 0% RH	6.08±0.04 5.94±0.08	6.40±0.04	5.54±0.1	14.4±0.1	6.17±0.06	17.7±0.1
S	Residual Strain (%) at 0% RH	0.58±0.01 0.52±0.02	0.44±0.009	0.60±0.01	0.24±0.006	0.59±0.02	0.065 ±0.003
P E N	Variation of Stress with Humidity (kPa/%RH)	-130±18 -117±29	-150±33	-83±16	-120±26	-120±26	-47±12
D E D	Variation of Modulus with Humidity (MPa/%RH)	-3.5±2.3	-8.0 ± 3.3	-----	-5.5 ± 2.8	-6.2 ± 1.5	-7.3 ± 2.9
M E M B R	Variation of Strain with Humidity (%/%RH)	-0.0021 ± 0.0004 -0.0017± 0.0006	-0.0019 ± 0.0003	-0.0015 ± 0.0003	-0.00054 ± 0.0002	-0.0014 ± 0.0006	-0.00025 ± 0.00008
A N E	Thermal Expansion (/°C)					1.1×10^{-5}	
	Plastic Deformation?	Y	Y	Slower/ Higher Yield σ		Y	

107

TABLE XVIII(cont.):
Summary of Measured Mechanical Properties

Method	Property	DuPont 2555
A C O U S T I C	Diffusion Coefficient (cm^2/sec)	2.7×10^{-9} 2.1×10^{-9}
	Mass Uptake (%/%RH)	0.020 0.018
	isotropic c_{11} (GPa)	10.2 11.7
	isotropic c_{44} (GPa)	1.19 1.13
	transverse isotropic c_{11} (GPa)	11.4 11.8
	transverse isotropic c_{33} (GPa)	10.9 11.6
	transverse isotropic c_{13} (GPa)	9.2 9.14
	transverse isotropic c_{44} (GPa)	1.5 1.06
	transverse isotropic c_{66} (GPa)	1.0 0.99
Both	Swelling Parameter (% strain/wt.%)	0.11 0.09

Areas of future work are also identified. Further enhancements to the accuracy and utility of load\deflection methods will almost certainly rely on advancements in the process of fabricating accurate suspended membranes. The modification of the acoustic models to account for strain effects as well as acoustic loss are necessary to improve the accuracy of the acoustic methods. More complete, more accurate, and possibly different methods of measuring the acoustic wave dispersion are also needed in order to reduce the measurement error in the properties of films as well as to investigate films deposited on nonpiezoelectric substrates. A new, faster method of analyzing the acoustic data is also presented.

REFERENCES

[1]   Lupinski, J.H. and R.S. Moore, ed. *Polymeric Materials for Electronics Packaging and Interconnection.* ACS Symposium Series, ed. M.J. Comstock. 1989, American Chemical Society: Washington, D. C.

[2]   Tummala, R.A. and E.J. Rymaszewski, *Microelectronics Packaging Handbook.* ed. A.G. Klopfenstein. 1989, New York: Van Nostrand Reinhold.

[3]   Bowden, M.J. and S.R. Turner, ed. *Polymers for High Technology.* ACS Symposium Series, ed. M.J. Comstock. 1987, American Chemical Society: Washington, D. C.

[4]   Wilson, A.M., *Use of Polyimides in VLSI Fabrication,* in *Polyimides: synthesis, characterization, and applications,* K.L. Mittal, Editor. 1984, Plenum Press: New York. p. 715-733.

[5]   Ward, I.M., *Mechanical Properties of Solid Polymers.* 2 ed. 1983, New York: John Wiley & Sons.

[6]   Sroog, C.E., *et al., Aromatic Polypyromellitimides from Aromatic Polyamic Acids.* Journal of Polymer Science: Part A, 1965. 3: p. 1373-1390.

[7]   Sroog, C.E., *Polyimides.* Macromolecular Reviews, 1976. 11: p. 161-208.

[8]   Hiemenz, P.C., *Polymer Chemistry.* 1984, New York: Marcel Dekker, Inc.

[9]   Wilson, A.M., *Polyimide Insulators for Multilevel Interconnections.* Thin Solid Films, 1981. 83: p. 145-163.

[10]   Noe, S.C., J.Y. Pan, and S.D. Senturia. *Optical Waveguiding as a Method for Characterizing the Effect of Extended Cure and Moisture on Polyimide Films.* in *ANTEC.* 1991. Montreal: Society of Plastics Engineers.

[11]   Anderson, G.P., S.J. Bennett, and K.L. DeVries, *Analysis and Testing of Adhesive Bonds.* 1977, New York: Academic Press.

[12]   Mittal, K.L., *Adhesion Measurement of Thin Films.* Electrocomponent Science and Technology, 1976. 3: p. 21-42.

[13]   Hinkley, J.A., *A Blister Test for Adhesion of Polymer Films to SiO_2.* Journal of Adhesion, 1983. 16: p. 115-126.

[14]   Allen, M.G. and S.D. Senturia, *Application of the Island Blister Test for Thin Film Adhesion Measurement.* Journal of Adhesion, 1989. 29: p. 219-231.

[15]   Galipeau, D.W., *et al. The Study of Polyimide Films and Adhesion Using a Surface Acoustic Wave Sensor.* in *Ultrasonics Symposium.* 1990. Honolulu, HI: IEEE.

[16]   Lean, E.G. and C.G. Powell, *Nondestructive Testing of Thin Films by Harmonic Generation of Dispersive Rayleigh Waves.* Applied Physics Letters, 1971. 19(9): p. 356-359.

[17]   Moses, S. and R.K. Witt, *Evaluation of Adhesion by Ultrasonic Vibrations.* Industrial and Engineering Chemistry, 1949. 41: p. 2334-2338.

[18]   Knollman, G.C. and J.J. Hartog, *Shear modulus gradients in adhesive interfaces as determined by means of ultrasonic Rayleigh waves (II).* Journal of Applied Physics, 1982. 53(8): p. 5514-5517.

[19]   Knollman, G.C. and J.J. Hartog, *Shear modulus gradients in adhesive interfaces as determined by means of ultrasonic Rayleigh waves.* Journal of Applied Physics, 1982. 53(3): p. 1516-1524.

[20]   Behrndt, K.H., *Film-Thickness and Deposition-Rate Monitoring Devices and Techniques for Producing Films of Uniform Thickness,* in *Physics of Thin Films,* G. Hass and R.E. Thun, Editor. 1966, Academic Press: New York. p. 1-59.

[21]   Adams, A.C., D.P. Schinke, and C.D. Capio, *An Evaluation of the Prism Coupler for Measuring the Thickness and Refractive Index of Dielectric Films on Silicon Substrates.* Journal of the Electrochemical Society, 1979. 126(9): p. 1539-1543.

[22]   Weglein, R.D., *SAW dispersion and film-thickness measurement by acoustic microscopy.* Applied Physics Letters, 1979. 35(3): p. 215-217.

[23]   Schmidt, M.A. and R.T. Howe, *Silicon Resonant Microsensors.* Ceramic Engineering and Science Proceedings, 1987. 8(9-10): p. 1019-1034.

[24]   Wohltjen, H. and R. Dessy, *Surface Acoustic Wave Probe for Chemical Analysis. I. Introduction and Instrument Description.* Analytical Chemistry, 1979. 51(9): p. 1458-1464.

[25]   Glang, R., R.A. Holmwood, and R.L. Rosenfeld, *Determination of Stress in Films on Single Crystalline Silicon Substrates.* The Review of Scientific Instruments, 1965. 36(1): p. 7-10.

[26]   Maden, M.A. and R.J. Farris. *Determination of Elastic Constants and Biaxial Stresses in Thin Polymer Films.* in *ANTEC.* 1991. Montreal: Society of Plastics Engineers.

[27]   Bromley, E.I., et al., *A technique for the determination of stress in thin films.* Journal of Vacuum Science Technology B, 1983. 1(4): p. 1364-1366.

[28]   Beams, J.W., *Mechanical Properties of Thin Films of Gold and Silver,* in *Structure and Properties of Thin Films,* C.A. Neugebauer, J.B. Newkirk, andD.A. Vermilyea, Editor. 1959, Wiley: New York. p. 183-192.

[29]   Meeks, S.W., et al. *Residual Stress Mapping with a Scanning Phase-Measuring Acoustic Microscope.* in *Ultrasonics Symposium.* 1989. IEEE.

[30]   Campbell, D.S., *Mechanical Properties of Thin Films,* in *Handbook of Thin Film Technology,* L.I. Maissel and R. Glang, Editor. 1970, McGraw-Hill Book Company: New York. p. 12.3-12.50.

[31]   Hardwick, D.A., *The Mechanical Properties of Thin Films: A Review*. Thin Solid Films, 1987. 154: p. 109-124.

[32]   Hoffman, R.W., *The Mechanical Properties of Thin Condensed Films*, in *Physics of Thin Films*, G. Hass and R.E. Thun, Editor. 1966, Academic Press: New York. p. 211-273.

[33]   Mehregany, M., M.G. Allen, and S.D. Senturia. *The Use of Micromachined Structures for the Measurement of Mechanical Properties and Adhesion of Thin Films*. in *Solid State Sensors Workshop*. 1986. Hilton Head, SC: IEEE.

[34]   Allen, M.G., et al., *Microfabricated structures for the in situ measurement of residual stress, Young's modulus, and ultimate strain of thin films*. Applied Physics Letters, 1987. 51(4): p. 241-243.

[35]   Maseeh, F., et al. *Calibrated Measurements of Elastic Limit, Modulus, and the Residual Stress of Thin Films Using Micromachined Suspended Structures*. in *IEEE Solid-State Sensor and Actuator Workshop*. 1988. Hilton Head, S. C.: IEEE.

[36]   Crean, G.M., A. Golanski, and J.C. Oberlin, *Effective elastic constants of thin-film tungsten-silicide from surface acoustic wave analysis*. Applied Physics Letters, 1987. 50(2): p. 74-76.

[37]   Bell, J.A., et al., *Elastic constants of, and Stonely waves in, molybdenum films measured by Brillouin scattering*. Applied Physics Letters, 1988. 52(8): p. 610-612.

[38]   Jelks, E.C. and R.S. Wagers. *Elastic Constants of Electron-Beam-Deposited Thin Films of Molybdenum and Aluminum on $LiNbO_3$*. in *Ultrasonics Symposium*. 1983. IEEE.

[39]   Tsubouchi, K., K. Sugai, and N. Mikoshiba. *AlN Material Constants Evaluation and SAW Properties on AlN/Al_2O_3 and AlN/Si*. in *Ultrasonics Symposium*. 1981. IEEE.

[40]   Vinci, R.P. and J.C. Braveman. *Mechanical Testing of Thin Films*. in *International Conference on Solid-State Sensors and Actuators*. 1991. San Francisco, CA: IEEE.

[41]   Motorola, Semiconductor Products Sector, personal communication.

[42]   Lin, P. and S.D. Senturia. *The In-Situ Measurement of Biaxial Modulus and Residual Stress of Multi-Layer Polymeric Thin Films*. in *Materials Research Society Spring Meeting*. 1990. San Francisco.

[43]   Pan, J.Y., et al. *Verification of FEM Analysis of Load-Deflection Methods for Measuring the Mechanical Properties of Thin Films*. in *IEEE Solid-State Sensor and Actuator Workshop*. 1990. Hilton Head, S. C.: IEEE.

[44]   Maseeh, F. and S.D. Senturia, *Elastic Properties of Thin Polyimide Films*, in *Polyimides: Materials, Chemistry and Characterization*, C. Feger, M.M. Khojasteh, and J.E. McGrath, Editor. 1989, Elsevier Science Publishers B. V.: Amsterdam. p. 575-584.

[45]   Wagers, R.S. PVF_2 Elastic Constants Evaluation. in Ultrasonics Symposium. 1984. IEEE.

[46]   Carlotti, G., et al., Acoustic investigation of the elastic properties of ZnO films. Applied Physics Letters, 1987. 51(23): p. 1889-1991.

[47]   Hickernell, F.S. and R.S. Wagers. The Acoustic Wave Properties of Thin Film Niobium Pentoxide. in Ultrasonics Symposium. 1984. IEEE.

[48]   Frohlich, H.J. and H. Stab, Evaluation of the Elastic Constants of SiO Thin Films from SAW Propagation Measurements. Acta Physica Slovaka, 1987. 37(4): p. 223-229.

[49]   Tittmann, B.R., et al., Determination of Physical Property Gradients from Measured Surface Wave Dispersion. IEEE Transactions on Ultrasonics, Ferroelectrics, and Frequency Control, 1987. UFFC-34(5): p. 500-507.

[50]   Wohltjen, H. and R. Dessy, Surface Acoustic Wave Probes for Chemical Analysis. III. Thermomechanical Polymer Analyzer. Analytical Chemistry, 1979. 51(9): p. 1470-1475.

[51]   Maseeh, F. and S.D. Senturia. Viscoelasticity and Creep Recovery of Polyimide Thin Films. in IEEE Solid-State Sensor and Actuator Workshop. 1990. Hilton Head, S. C.: IEEE.

[52]   Pan, J.Y. and S.D. Senturia. Suspended-Membrane Methods for Determining the Effects of Humidity on the Mechanical Properties of Thin Polymer Films. in ANTEC. 1991. Montreal: Society of Plastics Engineers.

[53]   Tabata, O., et al. Mechanical Property Measurements of Thin Films Using Load-Deflection of Composite Rectangular Membrane. in Micro Electro Mechanical Systems: An Investigation of Micro Structures, Sensors, Actuators, Machines, and Robots. 1989. Salt Lake City, UT: IEEE.

[54]   Allen, M.G., Measurement of Adhesion and Mechanical Properties of Thin Films Using Microfabricated Structures. 1989, Massachusetts Institute of Technology.

[55]   Lin, P., The In-Situ Measurement of Mechanical Properties of Multi-Layer Coatings. 1990, Massachusetts Institute of Technology.

[56]   Robbins, H. and B. Schwartz, Chemical Etching of Silicon. Journal of the Electrochemical Society, 1960. 107(2): p. 108-111.

[57]   Denton, D.D., J.B. Camou, and S.D. Senturia. Effects of Moisture Uptake on the Dielectric Permittivity of Polyimide Films. in Int'l Symp. on Moisture and Humidity. 1985. Washington, D. C.

[58]   Denton, D.D., et al., Moisture Diffusion in Polyimide Films in Integrated Circuits. Journal of Electronic Materials, 1985. 14(2): p. 119-136.

[59]   Numata, S., et al., Chemical Structures and Properties of Low Thermal Expansion Polyimides, in Recent Advances in Polyimide Science and Technology, W.D. Weber

112

and M.R. Gupta, Editor. 1987, Mid-Hudson Chapter of the Society of Plastics Engineers, Inc.: Poughkeepsie, NY. p. 164-173.

[60] Bernier, G.A. and D.E. Kline, *Dynamic Mechanical Behavior of a Polyimide.* Journal of Applied Polymer Science, 1968. 12: p. 593-604.

[61] Suzuki, K. *A 1024-element high-performance silicon tactile imager.* in *IEDM.* 1988. IEEE.

[62] Muraoka, H. and T. Ohhashi, , in *Semiconductor Silicon,* H. Huff and R. Burgess, Editor. 1973, Princeton, NJ. p. 327.

[63] Kino, G.S., *Acoustic Waves: Devices, Imaging, & Analog Signal Processing.* Prentice-Hall Signal Processing Series, ed. A.V. Oppenheim. 1987, Englewood Cliffs, NJ: Prentice-Hall, Inc.

[64] Auld, B.A., *Acoustic Fields and Waves in Solids.* 2 ed. Vol. II. 1990, Malabar, FL: Robert E. Krieger Publishing Company.

[65] Wohltjen, H., *Mechanism of Operation and Design Considerations for Surface Acoustic Wave Device Vapour Sensors.* Sensors and Actuators, 1984. 5: p. 307-325.

[66] Farnell, G.W. and E.L. Adler, *Elastic Wave Propagation in Thin Layers,* in *Physical Acoustics,* W.P. Mason and R.N. Thurston, Editor. 1972, Academic Press: New York. p. 35-127.

[67] Nye, J.F., *Physical Properties of Crystals.* 1957, London: Oxford University Press.

[68] White, R.M., *et al.,* *Plate-Mode Ultrasonic Oscillator Sensors.* IEEE Transactions on Ultrasonics, Ferroelectrics, and Frequency Control, 1987. UFFC-34(2): p. 162-171.

[69] Wenzel, S.W., *A Multisensor Employing an Ultrasonic Lamb-Wave Oscillator.* IEEE Transactions on Electron Devices, 1988. 35(6): p. 735-743.

[70] Kushibiki, J., H. Maehara, and N. Chubachi, *Measurements of acoustic properties for thin films.* Journal of Applied Physics, 1982. 53(8): p. 5509-5513.

[71] Lee, C.C., C.S. Tsai, and X. Cheng, *Complete Characterization of Thin- and Thick-Film Materials Using Wideband Reflection Acoustic Microscopy.* IEEE Transactions on Sonics and Ultrasonics, 1985. SU-32(2): p. 248-258.

[72] Ledbetter, H. and M. Lei. *Elastic Constants of Fiber-Reinforced Composites: A Fresh Measurement Approach.* in *Ultrasonics Symposium.* 1990. Honolulu, HI: IEEE.

[73] Robbins, W.P. and R.K. Mueller, *Thin-Film Characterization Using a Scanning Laser Acoustic Microscope With Surface Acoustic Waves.* IEEE Transactions on Ultrasonics, Ferroelectrics, and Frequency Control, 1988. 35(4): p. 477-483.

113

[74] Liang, K., *et al. Surface Wave Velocity Measurements at 50 Megahertz*. in *Ultrasonics Symposium*. 1982. IEEE.

[75] Oates, D.E., *Surface Acoustic Wave Devices*, in *VLSI Electronics: Microstructure Science*. 1985, Academic Press: New York. p. 289-336.

[76] White, R.M., *Surface Elastic Waves*. Proceedings of the IEEE, 1970. 58(8): p. 1238-1277.

[77] Latuszek, A. *A New Method of SAW Generation on the Surface of Arbitrary Solid Materials*. in *Ultrasonics Symposium*. 1986. IEEE.

[78] Lin, H.-N., R.J. Stoner, and H.J. Maris. *Ultrasonic Experiments at Ultra-High Frequency with Picosecond Time-Resolution*. in *Ultrasonics Symposium*. 1990. Honolulu, HI: IEEE.

[79] Bell, J.A., *et al.*, *Elastic constants of Mo/Ta superlattices measured by Brillouin scattering*. Physical Review B, 1987. 35(8): p. 4127-4130.

[80] Carlotti, G., *et al. Brillouin Scattering from Surface Phonons in ZnO Films*. in *Ultrasonics Symposium*. 1989. Montreal: IEEE.

[81] Rowell, N.L. and G.I. Stegeman, *Brilloin Scattering from Surface Phonons in Thin Films*. Physical Review Letters, 1978. 41(14): p. 970-973.

[82] Rowell, N.L. and G.I. Stegeman. *Measurement of Elastic Properties and Surface Wave Parameters in Thin Films*. in *Ultrasonics Symposium*. 1978. IEEE.

[83] White, R.M. and F.W. Voltmer, *Direct piezoelectric coupling to surface elastic waves*. Applied Physics Letters, 1965. 7: p. 314-316.

[84] Smith, W.R., *Analysis of interdigital surface wave transducers by use of an equivalent circuit model*. IEEE Transactions on Microwave Theory and Techniques, 1969. MTT-17(11): p. 856-864.

[85] Smith, W.R., *et al.*, *Design of Surface Wave Delay Lines with Interdigital Transducers*. IEEE Transactions on Microwave Theory and Techniques, 1969. MTT-17(11): p. 865-873.

[86] Smith, W.R., *Coupling Efficiency Estimates for Acoustic Surface Wave Excitation with Piezoelectric Film Overlays*. Journal of Applied Physics, 1971. 42(7): p. 3016-3018.

[87] Slobodnik, A.J., Jr., E.D. Conway, and R.T. Delmonico, *Microwave Acoustics Handbook Volume 1A: Surface Wave Velocities*. 1973, Air Force Cambridge Research Laboratories.

[88] Crank, J., *The Mathematics of Diffusion*. 1956, Oxford: Clarendon Press.

[89] Brace, J.G., T.S. Sanfelippo, and S.G. Joshi, *A Study of Polymer/Water Interactions Using Surface Acoustic Waves*. Sensors and Actuators, 1988. 14: p. 47-68.

[90]   Martin, S.J. and G.C. Frye, *Surface Acoustic Wave Response to Changes in Viscoelastic Film Properties.* Applied Physics Letters, 1990. 57(18): p. 1867-1869.

[91]   Deopura, B.L., A.K. Sengupta, and A. Verma, *Effect of moisture on physical properties of nylon.* Polymer Communications, 1983. 24: p. 287-288.

[92]   Takahashi, N., D.Y. Yoon, and W. Parrish, *Molecular Order in Condensed States of Semiflexible Poly(amic acid) and Polyimide.* Macromolecules, 1984. 17(12): p. 2583-2588.

[93]   Russell, T.P., H. Gugger, and J.D. Swalen, *In-Plane Orientation of Polyimide.* Journal of Polymer Science: Polymer Physics Edition, 1983. 21: p. 1745-1756.

[94]   Prest, W.M., Jr. and D.J. Luca, *The origin of the optical anisotropy of solvent cast polymeric films.* Journal of Applied Physics, 1979. 50(10): p. 6067-6071.

[95]   Adler, E.L., et al. *Interactive PC software for SAW propagation in anisotropic multilayers.* in *Ultrasonics Symposium.* 1988. Chicago, IL: IEEE.

[96]   Tiersten, H.F., *Elastic Surface Waves Guided by Thin Films.* Journal of Applied Physics, 1969. 40(2): p. 770-789.

[97]   Jones, W.R., W.R. Smith, and D. Perry, *Numerical Computation of Acoustic Surface Waves in Layered Piezoelectric Media-Computer Program Descriptions.* 1971, Hughes Aircraft Company.

[98]   Lardat, C., C. Maerfeld, and P. Tournois, *Theory and Performance of Acoustical Dispersive Surface Wave Delay Lines.* Proceedings of the IEEE, 1971. 59(3): p. 355-368.

[99]   Press, W.H., et al., *Numerical Recipes in C: The Art of Scientific Computing.* 1988, Cambridge: Cambridge University Press.

[100]   Box, G.E.P., W.G. Hunter, and J.S. Hunter, *Statistics for Experimenters.* 1978, New York: John Wiley & Sons.

[101]   Montgomery, D.C., *Design and Analysis of Experiments.* 2 ed. 1984, New York: John Wiley & Sons.

[102]   Hickernell, F.S., *The Acoustic Properties of Oxide Films and Their Application to Acoustic Surface Wave Devices.* Journal of Solid State Chemistry, 1975. 12: p. 225-231.

[103]   Shimizu, H., Y. Suzuki, and T. Kanda. *Love-Type-SAW Resonator of Small Size with Very Low Capacitance Ratio and Its Application to VCO.* in *Ultrasonics Symposium.* 1990. Honolulu, HI: IEEE.

[104]   Toulouse, J. *A Modified Version of the Phase Sensitive Technique for Measurements of Absolute Sound Velocity in Solids.* in *Ultrasonics Symposium.* 1987. Denver, CO: IEEE.

[105] Zhao, Z., *et al.*, *A Novel Technique to Measure the Group Velocity of Sound in Dispersive Media.* IEEE Transactions on Ultrasonics, Ferroelectrics, and Frequency Control, 1989. 36(5): p. 481-484.

[106] Tsukahara, Y., K. Ohira, and N. Nakaso. *An Ultrasonic Micro-Spectrometer for the Evaluation of Elastic Properties with Microscopic Resolution.* in *Ultrasonics Symposium.* 1990. Honolulu, HI: IEEE.

[107] Nalamwar, A.L. and M. Epstein, *Effects of Applied Strain in ZnO Thin-Film SAW Devices.* IEEE Transactions on Sonics and Ultrasonics, 1976. SU-23(3): p. 144-147.

[108] Nalamwar, A.L. and M. Epstein, *Surface acoustic waves in strained media.* Journal of Applied Physics, 1976. 47(1): p. 43-48.

[109] Johnsen, C.A., *et al. Polyimide as an Acoustic Absorber for High Frequency SAW Applications.* in *Ultrasonics Symposium.* 1988. Chicago, IL: IEEE.

[110] Smirnova, V.E. and M.I. Bessonov, *Mechanical and Optical Anisotropy of Oriented Polyimide Films,* in *Polyimides: Materials, Chemistry, and Characterization,* C. Feger, M.M. Khojasteh, and J.E. McGrath, Editor. 1989, Elsevier Science Publishers B. V.: Amsterdam. p. 563-574.

[111] Berry, B.S. and W.C. Pritchet, *Bending-cantilever method for the study of moisture swelling in polymers.* IBM Journal of Research and Development, 1984. 28(6): p. 662-667.

[112] Tien, P.K., R. Ulrich, and R.J. Martin, *Modes of Propagating Light Waves in Thin Deposited Semiconductor Films.* Applied Physics Letters, 1969. 14(9): p. 291-294.

APPENDIX A: DETAILED FABRICATION SEQUENCE

A. Mass-Uptake SAW Devices

Mass-uptake SAW devices were fabricated in the Technology Research Laboratory, a class 100 clean room facility in the Microsystems Technology Laboratories. Two-inch diameter by 1-mm thick wafers of ST-cut, X-propagating quartz, which has Euler angles of $0°, 132.75°$, and $0°$, were supplied by Valpey-Fisher of Hopkinton, MA for use as the substrate for the devices. The wafers, as supplied by Valpey-Fisher, are cleaned at their location in $70°$ C trichloroethylene before delivery. Provided they are shipped in suitably clean containers, they usually only require a solvent cleaning with a sequence of rinses in freon, acetone, methanol, and deionized water just before processing begins. If the wafers are stored for months, even in a class 100 clean room, they tend to require an additional cleaning step in 5:1:1 water:hydrogen peroxide:ammonium hydroxide at $80°$ C for 10 min. The remainder of the fabrication sequence is given on the next page in Table XIX.

B. Elastic-Constant-Measurement SAW Devices

Elastic-constant-measurement SAW devices were also fabricated in the Technology Research Laboratory. Two-inch diameter by 1-mm thick wafers of ST-cut, Y-propagating quartz were used as substrates for the Love devices. Two-inch diameter by 0.5-mm thick wafers of Y-cut, Z-propagating lithium niobate were used as substrates for the Rayleigh devices. A cleaning sequence identical to that given in Section A was used. The remainder of the fabrication sequence is given in Table XX.

117

TABLE XIX:
Fabrication Sequence for Mass-Uptake SAW Devices.
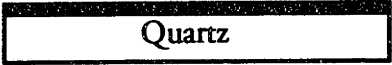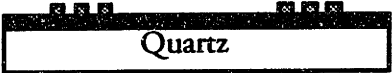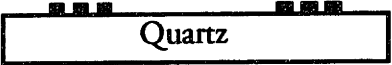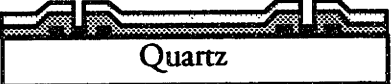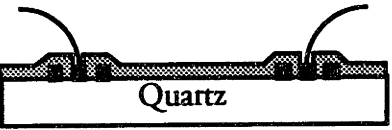
Step Description	Side-View Diagram
E-beam Deposition 1750Å Al @ 8 Å/sec	Quartz
Photolith Interdigital Transducer Soft bake photoresist only Mask 1 (align to flat)	Quartz
Wet etch Al PAN etch 20 sec @ 100Å/sec, 50° C	Quartz
Resist removal Acetone	Quartz
Polyimide deposition and b-cure Adhesion Promoter, 5 sec @ 5000 rpm 5sec @ 700 rpm/60 sec @ 5000 rpm b-cure, 15 min at 120° C for 2 μm	Quartz
Photolith contact via Soft bake photoresist only Mask 2 (Align to Mask 1 pattern)	Quartz
Resist removal Acetone	Quartz
PI anneal 400° C for 90 min in nitrogen	Quartz
Package Au wire bond	Quartz

118

TABLE XX:
Fabrication Sequence for Elastic-Constant-Measurement SAW Devices.
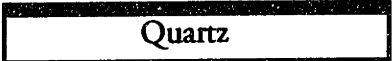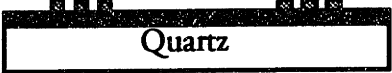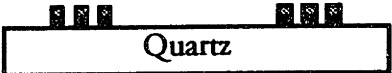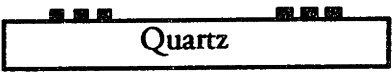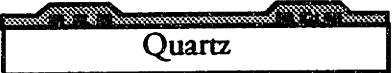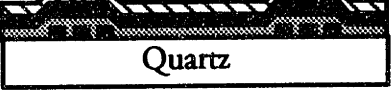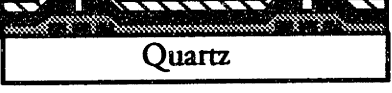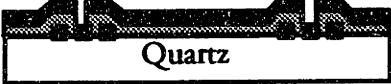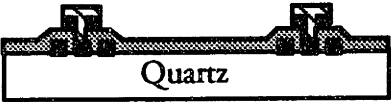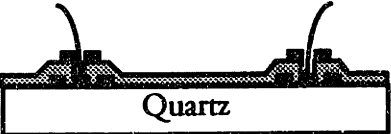
Step Description	Side-View Diagram
E-beam Al Deposition 1750 Å @ 8 Å/sec	Quartz
Photolith Interdigital Transducer Soft bake photoresist only Mask 1 (Align to flat)	Quartz
Wet etch Al PAN etch 20 sec @ 100Å/sec, 50° C	Quartz
Resist removal Acetone Soak	Quartz
PI deposition and cure Adhesion Promoter, 5 sec @ 5000 rpm 5sec @ 700 RPM/60 sec @ 2000 RPM b-cure: 1st coat: 15 min at 120° C 　　　　2nd coat: 30 min at 160°C anneal: 90 min at 400° C	Quartz
E-beam Deposition 1000 Å Al @ 8 Å/sec	Quartz
Photolith contact mask Soft bake photoresist only Mask 2 (Align to Mask 1 pattern)	Quartz
Wet etch Al PAN etch 20 sec @ 100Å/sec, 50° C	Quartz
Resist removal Acetone Soak	Quartz

119

TABLE XX (cont.):
Fabrication Sequence for Elastic-Constant-Measurement SAW Devices.

Step Description	Side-View Diagram
Open contacts through PI Plasma-Therm RIE 20 min, 225W, 100 mtorr, 21 sccm O_2	Quartz
Photolith reverse contact mask Soft bake photoresist only Mask 3 (Align to Mask 2 pattern)	Quartz
Wet etch Al PAN etch 10 sec @ 100Å/sec, 50° C	Quartz
Resist removal Acetone Soak	Quartz
Package Au wire bond	Quartz

APPENDIX B: COMPUTER PROGRAM SOURCE CODE

A. Load-Deflection Data-Acquisition and Analysis Program

As shown in Figure 2.13 and explained in Chapter 2, the program *footld.bas* was written to acquire, store, print, and analyze the pressure and deflection data from a suspended-membrane experiment. The program is written in BASIC to run on an IBM PC/AT personal computer and communicates with the pressure sensor through a multimeter and an IEEE-488 interface and with the z-axis micrometer through a serial interface box. The complete listing of the program follows.

The first half of the program implements a simple user-interface driven by the computer's function keys. Information on the shape of the membrane, its radius, its thickness, its estimated Poisson ratio, the pressure sensor's voltage-pressure calibration, the temperature, humidity, and time of the experiment are input and stored for use in analyzing the data. The acquisition of the data occurs in the few lines of code between lines 1520-1720.

The final half of the program analyzes the acquired data and prints the computed biaxial modulus, residual stress, pressure offset, and the uncertainties in each. A matrix approach [100] is used to least-squares fit the data to the equation:

$$p = b_0 d + b_1 d^3 + p_0 \tag{B.1}$$

where p is the pressure, d the deflection, and b_0, b_1, and p_0 are the fitted constants.

When the pressure deflection pairs, (d_i, p_i) are written in the matrix equation form $y = Ab$:

$$\begin{bmatrix} p_1 \\ p_2 \\ p_3 \\ . \\ . \\ . \\ p_n \end{bmatrix} = \begin{bmatrix} 1 & d_1 & d_1^3 \\ 1 & d_2 & d_2^3 \\ 1 & d_3 & d_3^3 \\ . & . & . \\ . & . & . \\ . & . & . \\ 1 & d_n & d_n^3 \end{bmatrix} \begin{bmatrix} p_o \\ b_o \\ b_1 \end{bmatrix} \qquad (B.2)$$

The solution can be found from the matrix equation:

$$b = [A^TA]^{-1}A^Ty \qquad (B.3)$$

The variance-covariance matrix can be computed as:

$$V_b = [A^TA]^{-1}\sigma^2 \qquad (B.4)$$

where the variance in each experimental observation, σ^2, can be estimated as $S_R/(n-3)$ with S_R being the sum of the squares of the residuals and n being the number of pressure-deflection pairs measured. The standard error of the fit parameters are then found on the diagonal of the variance-covariance matrix.

To compute the 95% confidence intervals for the fit parameters, the standard errors are multiplied by a factor equal to the 0.025 probability point of the t distribution with (n-3) degrees of freedom [100]. A lookup table in the program provides the appropriate factor, which is usually between 2.0 and 3.0 for most experiments.

When the confidence interval for the pressure offset, p_o, is less than the best-fit value for the offset, the computed pressure offset, biaxial modulus, residual stress, and the confidence intervals for each are printed and the program halted. When the confidence interval for the pressure offset is greater than the computed offset, the offset is judged to be statistically insignificant and the data fit to the new equation:

$$p = b_0d + b_1d^3 \qquad (B.5)$$

before the values for biaxial modulus, residual stress, and uncertainty are printed.

```
10   CLEAR ,60000! : IBINIT1=60000! : IBINIT2=IBINIT1+3 : BLOAD
     "bib.m",IBINIT1
20   CALL
     IBINIT1(IBFIND,IBTRG,IBCLR,IBPCT,IBSIC,IBLOC,IBPPC,IBBNA,IBONL,IB
     RSC,IBSRE,IBRSV,IBPAD,IBSAD,IBIST,IBDMA,IBEOS,IBTMO,IBEOT,IBRDF
     ,IBWRTF,IBTRAP,IBDEV,IBLN)
30   CALL
     IBINIT2(IBGTS,IBCAC,IBWAIT,IBPOKE,IBWRT,IBWRTA,IBCMD,IBCMDA,
     IBRD,IBRDA,IBSTOP,IBRPP,IBRSP,IBDIAG,IBXTRC,IBRDI,IBWRTI,IBRDIA,
     IBWRTIA,IBSTA%,IBERR%,IBCNT%)
40   DIM  D(100),P(100),T(100),A(4,4),B(4),AI(4,4),VI(100),TS(50)
50   OPEN "COM1:1200,N,8,1,CS,DS" AS #1
60   UDNAME$ = "DVM"
70   CALL IBFIND  (UDNAME$,DVM%)
80   CALL IBCLR(DVM%)
90   V% = 1 : CALL IBSRE (DVM%,V%)
100  KEY(1) ON:KEY(2) ON:KEY(3) ON:KEY(4) ON:KEY(5) ON:KEY(6) ON
110  KEY(7) ON:KEY(8) ON:KEY(9) ON:KEY(10) ON:KEY(11) ON:KEY(14) ON
120  ON KEY (1) GOSUB 2620
130  ON KEY (2) GOSUB 2820
140  ON KEY (3) GOSUB 2790
150  ON KEY (4) GOSUB 3370
160  ON KEY (5) GOSUB 2850
170  ON KEY (6) GOSUB 2880
180  ON KEY (7) GOSUB 2910
190  ON KEY (8) GOSUB 3630
200  ON KEY (9) GOSUB 3180
210  ON KEY(10) GOSUB 1730
220  ON KEY(11) GOSUB 2550
230  ON KEY(14) GOSUB 3690
231  TS(1)=12.706:TS(2)=4.303:TS(3)=3.182:TS(4)=2.776:TS(5)=2.571:TS(6)=2.
     447
232  TS(7)=2.365:TS(8)=2.306:TS(9)=2.262:TS(10)=2.228:TS(11)=2.201:TS(12)
     =2.179
233  TS(13)=2.16:TS(14)=2.145:TS(15)=2.131:TS(16)=2.12:TS(17)=2.11:TS(18)
     =2.101
234  TS(19)=2.093:TS(20)=2.086:TS(21)=2.08:TS(22)=2.074:TS(23)=2.069:TS(2
     4)=2.064
235  TS(25)=2.06:TS(26)=2.056:TS(27)=2.052:TS(28)=2.048:TS(29)=2.045:TS(3
     0)=2.042
236  FOR I = 31 TO 50
237  TS(I) = 2.042
238  NEXT I
240  CLS
250  OPEN "RR.DEF" FOR INPUT AS #2
260  INPUT #2,NAM$,ID$,DAT$,P0,P1,P2,TEM,HUM,A,T,C1,C2,PR
270  FILEN$ = ""
280  CLOSE #2
290  IF NAM$ = "Ed" THEN GOTO 350
300  IF NAM$ = "Dan" THEN GOTO 330
```

```
310 PATH$ = "c:\jpan\lddata\"
320 GOTO 360
330 PATH$ = "c:\dans\"
340 GOTO 360
350 PATH$ = "c:\edm\"
360 CLS
370 FLAG2 = 1
380 GOSUB 2630
390 CLS
400 FLAG2 = 0
410 INPUT "Do you wish to reevaluate old data";RESP$
420 IF RESP$ <> "Y" AND RESP$ <> "y" AND RESP$ <> "N" AND RESP$ <>
    "n" THEN GOTO 410
430 IF RESP$ = "N" OR RESP$ = "n" THEN GOTO 690
440 CLS
450 INPUT "What filename is the data stored under";FILEN$
460 OPEN PATH$+FILEN$ FOR INPUT AS #2
470 INPUT #2,NAM$
480 INPUT #2,NAM$,DAT$,ID$
490 INPUT #2,TYP$,A,T,PR
500 INPUT #2,HUM,TEM,P0,P1,P2
510 I=0
520 INPUT #2,D(I),VI(I),P(I),T(I)
530 IF EOF(2) THEN 560
540 I=I+1
550 GOTO 520
560 CLOSE #2
561 FOR COUNT = 0 TO I
562 P(COUNT) = P0+P1*VI(COUNT)+P2*VI(COUNT)*VI(COUNT)
563 P(COUNT) = P(COUNT)*14.696/760
564 NEXT COUNT
570 IF TYP$ = "CIRCLE" THEN GOTO 620
580 IF TYP$ = "SQUARE" THEN GOTO 650
590 C1 = 2
600 C2 = 1.33/(1 + PR)
610 GOTO 670
620 C1 = 4
630 C2 = 8*(.957-(.208*PR))/3
640 GOTO 670
650 C1 = 3.41
660 C2 = 1.37*(1.446-(.427*PR))
670 FLAG2 = 1
680 GOTO 990
690 CLS
700 TFACT = -1 : TREF = 0
710 PRINT "***** Remember to set power supply to 8 volts *****"
720 PRINT
730 PRINT "F1: Measurement made by ";NAM$
740 PRINT "F2: Date of measurement: ";DAT$
750 PRINT "F3: Sample ID: ";ID$
760 PRINT "F4: Calibration curve: P(torr) = ";P0;"+";P1;"* V +";P2;"* V^2"
770 PRINT "F5: Temperature:";TEM;"degrees Celsius"
780 PRINT "F6: Relative humidity:";HUM;"%"
790 IF C1 = 4 THEN GOTO 850
```

124

```
800 IF C1 = 3.41 THEN GOTO 830
810 PRINT "F7: Rect memb with half width of";A;"microns and t of";T;"microns"
820 GOTO 860
830 PRINT "F7: Square memb with half width of";A;"microns and t
    of";T;"microns"
840 GOTO 860
850 PRINT "F7: Circ memb with radius of";A;"microns and t of";T;"microns"
860 PRINT "F8: Poisson Ratio:";PR
870 IF FILEN$ = "" THEN GOTO 900
880 PRINT "F9: Data stored under filename ";PATH$ + FILEN$
890 GOTO 910
900 PRINT "F9: Data not being stored"
910 PRINT:PRINT:PRINT:PRINT:PRINT
920 PRINT "Hit any key to start measurement"
930 RESP$ = INKEY$: IF RESP$ = "" THEN GOTO 930
940 IF FILEN$ <> "" OR FLAG2 = 1 THEN GOTO 990
950 LOCATE 20,1
960 INPUT "Are you sure you want to proceed without storing data";RESP$
970 IF RESP$ <> "Y" AND RESP$ <> "y" AND RESP$ <> "N" AND RESP$ <>
    "n" THEN GOTO 960
980 IF RESP$ = "N" OR RESP$ = "n" THEN GOTO 690
990 IF FILEN$ = "" OR FLAG2 = 1 THEN 1010
1000 OPEN PATH$ + FILEN$ FOR OUTPUT AS #2
1010 LPRINT "Measurement made by ";NAM$
1020 LPRINT "Date of measurement: ";DAT$
1030 LPRINT "Sample ID: ";ID$
1040 IF C1 = 4 THEN GOTO 1100
1050 IF C1 = 3.41 THEN GOTO 1080
1060 LPRINT "Rectangular membrane with half width of";A;"microns and
    thickness of";T;"microns"
1070 GOTO 1110
1080 LPRINT "Square membrane with half width of";A;"microns and thickness
    of";T;"microns"
1090 GOTO 1110
1100 LPRINT "Circular membrane with radius of";A;"microns and thickness
    of";T;"microns"
1110 LPRINT "Relative humidity:";HUM;"%"
1120 LPRINT "Temperature:";TEM;"degrees Celsius"
1130 LPRINT "Calibration curve used:"
1140 LPRINT "        P(torr) = ";P0;"+";P1;"* V +";P2;"* V^2"
1150 LPRINT "Poisson Ratio:";PR
1160 IF FILEN$ = "" THEN GOTO 1190
1170 LPRINT "Data stored under filename ";PATH$ + FILEN$
1180 GOTO 1200
1190 LPRINT "Data not being stored"
1200 LPRINT
1210 LPRINT "D (um)    ";"V (volts)    ";"P (psi)      ";"Time (sec)"
1220 LPRINT
1230 IF FLAG2 = 0 THEN GOTO 1290
1240 FOR COUNT = 0 TO I
1250 LPRINT USING "####      #.#####      ##.#####
    ######.##";D(COUNT),VI(COUNT),P(COUNT),T(COUNT)
1260 NEXT COUNT
1270 I = I + 1
```

```
1280 GOSUB 1730
1290 CLS
1300 PRINT "Press foot pedal to take point (F10 to end measurement)"
1310 PRINT
1320 PRINT "        ";"D (um)    ";"V (volts)    ";"P (psi)      ";"Time (sec)"
1330 PRINT
1340 IF FILEN$ = "" THEN GOTO 1450
1350 PRINT #2,"D ";"V ";"P";"T"
1360 PRINT #2,NAM$;",";DAT$;",";ID$
1370 IF C1 = 4 THEN GOTO 1430
1380 IF C1 = 3.41 THEN GOTO 1410
1390 PRINT #2,"RECTANGULAR,";A;T;PR
1400 GOTO 1440
1410 PRINT #2,"SQUARE,";A;T;PR
1420 GOTO 1440
1430 PRINT #2,"CIRCLE,";A;T;PR
1440 PRINT #2,HUM;TEM;P0;P1;P2
1450 I = 0
1460 OPEN "RR.DEF" FOR OUTPUT AS #3
1470 PRINT #3,NAM$;",";ID$;",";DAT$
1480 PRINT #3,P0;P1;P2
1490 PRINT #3,TEM;HUM;A;T;C1;C2;PR
1500 CLOSE #3
1510 M = 4
1520 IF M = 24 THEN M = 4
1530 LOCATE M,16
1540 VALUE$ = SPACE$(16)
1550 IF EOF(1) THEN GOTO 1550
1560 LINE INPUT #1,DEFLECT$
1570 CALL IBRD (DVM%,VALUE$)
1580 T(I) = (TIMER-TREF)*TFACT
1590 DEFLECT$ = RIGHT$(DEFLECT$,9)
1600 D(I) = VAL(DEFLECT$)
1610 D(I) = D(I)*1000
1620 M = M + 1
1630 V=VAL(VALUE$)
1640 P = P0 + P1*V + P2*V^2
1650 P(I) = (P*14.696)/760
1660 LPRINT USING "####      #.#####      ##.#####
     ######.##";D(I),V,P(I),T(I)
1670 LOCATE M-1,1
1680 PRINT USING "##      ####      #.#####      ##.####
     ######.##";I+1,D(I),V,P(I),T(I)
1690 IF FILEN$ = "" THEN GOTO 1710
1700 PRINT #2,D(I);V;P(I);T(I)
1710 I = I + 1
1720 GOTO 1520
1730 CLS
1740 A(2,2) = 0
1750 A(3,3) = 0
1760 A(2,3) = 0
1770 A(1,3) = 0
1780 A(1,2) = 0
1790 B(1) = 0
```

```
1800 B(2) = 0
1810 B(3) = 0
1820 N = I - 1
1830 FOR I = 0 TO N
1840 A(2,2) = A(2,2) + D(I)^2
1850 A(3,3) = A(3,3) + D(I)^6
1860 A(2,3) = A(2,3) + D(I)^4
1870 A(1,3) = A(1,3) + D(I)^3
1880 A(1,2) = A(1,2) + D(I)
1890 B(1) = B(1) + P(I)*6894.75479#
1900 B(2) = B(2) + P(I)*D(I)*6894.75479#
1910 B(3) = B(3) + P(I)*D(I)^3*6894.75479#
1920 NEXT I
1930 A(3,2) = A(2,3)
1940 A(3,1) = A(1,3)
1950 A(2,1) = A(1,2)
1960 A(1,1) = N + 1
1970 DETA = A(1,1)*A(2,2)*A(3,3) - A(1,1)*A(2,3)*A(3,2)
1980 DETA = DETA + A(1,2)*A(2,3)*A(3,1) - A(1,2)*A(2,1)*A(3,3)
1990 DETA = DETA + A(1,3)*A(2,1)*A(3,2) - A(1,3)*A(2,2)*A(3,1)
2000 AI(1,1) = A(2,2)*A(3,3) - A(3,2)*A(2,3)
2010 AI(1,2) = A(1,3)*A(3,2) - A(1,2)*A(3,3)
2020 AI(1,3) = A(1,2)*A(2,3) - A(2,2)*A(1,3)
2030 AI(2,1) = A(3,1)*A(2,3) - A(2,1)*A(3,3)
2040 AI(2,2) = A(1,1)*A(3,3) - A(3,1)*A(1,3)
2050 AI(2,3) = A(2,1)*A(1,3) - A(1,1)*A(2,3)
2060 AI(3,1) = A(2,1)*A(3,2) - A(3,1)*A(2,2)
2070 AI(3,2) = A(1,2)*A(3,1) - A(1,1)*A(3,2)
2080 AI(3,3) = A(1,1)*A(2,2) - A(2,1)*A(1,2)
2090 AI(1,1) = AI(1,1)/DETA
2100 AI(1,2) = AI(1,2)/DETA
2110 AI(1,3) = AI(1,3)/DETA
2120 AI(2,1) = AI(2,1)/DETA
2130 AI(2,2) = AI(2,2)/DETA
2140 AI(2,3) = AI(2,3)/DETA
2150 AI(3,1) = AI(3,1)/DETA
2160 AI(3,2) = AI(3,2)/DETA
2170 AI(3,3) = AI(3,3)/DETA
2180 CONSTANT = 0
2190 A1 = 0
2200 A3 = 0
2210 FOR I = 1 TO 3
2220 CONSTANT = CONSTANT + B(I)*AI(1,I)
2230 A1 = A1 + B(I)*AI(2,I)
2240 A3 = A3 + B(I)*AI(3,I)
2250 NEXT I
2270 R=0
2280 FOR I = 0 TO N
2290 K=(P(I) - (CONSTANT/6894.75479#))-A1*D(I)/6894.75479#-
    A3*D(I)*D(I)*D(I)/6894.75479#
2300 R=R+K*K
2320 NEXT I
2321 R = R/(N-2)
2322 FOR I = 1 TO 3
```

```
2323 AI(I,I) = AI(I,I)*R
2324 AI(I,I) = SQR(AI(I,I))
2325 IF N > 50 THEN TSTAT = TS(50): GOTO 2339
2326 TSTAT = TS(N - 2)
2339 AI(I,I) = AI(I,I)*TSTAT
2340 NEXT I
2350 STRESS = A1*A^2/(C1*T):SERROR = AI(2,2)*6894.75479#*A^2/(C1*T)
2360 MODULUS = A3*A^4/(C2*T):MERROR =
     AI(3,3)*6894.75479#*A^4/(C2*T)
2361 IF AI(1,1) > ABS(CONSTANT/6894.75479#) THEN GOTO 2450
2370 PRINT "OFFSET: ";CONSTANT/6894.75479#;" psi +/- ";AI(1,1);" psi"
2380 PRINT "RESIDUAL STRESS: ";STRESS/1000000!;" MPa +/-
     ";SERROR/1000000!;" MPa"
2390 PRINT "BIAXIAL MODULUS: ";MODULUS/1000000000#;" GPa +/-
     ";MERROR/1000000000#;" GPa"
2410 LPRINT
2420 LPRINT "OFFSET: ";CONSTANT/6894.75479#;" psi +/- ";AI(1,1);" psi"
2430 LPRINT "RESIDUAL STRESS: ";STRESS/1000000!;" MPa +/-
     ";SERROR/1000000!;" MPa"
2440 LPRINT "BIAXIAL MODULUS: ";MODULUS/1000000000#;" GPa +/-
     ";MERROR/1000000000#;" GPa"
2441 IF AI(1,1) < ABS(CONSTANT/6894.75479#) THEN GOTO 2460
2450 GOSUB 9010
2460 IF FILEN$ <> "" THEN CLOSE #2
2470 PRINT
2480 PRINT "Hit any key to continue"
2490 RESP$ = INKEY$: IF RESP$ = "" THEN GOTO 2490
2500 FILEN$ = ""
2510 IF FLAG2 = 1 THEN RETURN 390
2520 CLOSE #3
2530 IF FILEN$ <> "" THEN CLOSE #2
2540 RETURN 690
2550 CLOSE
2560 END
2570 RESUME 3350
2580 DELAY = 0
2590 DELAY = DELAY + 1
2600 IF DELAY < 50 THEN GOTO 2590
2610 RETURN
2620 LOCATE 20,1
2630 PRINT "Are you Jeff, Ed, or Dan (If none of these, see Jeff before
     proceeding)"
2640 PRINT
2650 INPUT "(j, e, or d)";RESP$
2660 IF RESP$ <> "j" AND RESP$ <> "J" AND RESP$ <> "e" AND RESP$ <> "E"
     AND RESP$ <> "d" AND RESP$ <> "D" THEN GOTO 2550
2670 IF RESP$ = "e" OR RESP$ = "E" THEN GOTO 2750
2680 IF RESP$ = "d" OR RESP$ = "D" THEN GOTO 2720
2690 NAM$ = "Jeff"
2700 PATH$ = "c:\jpan\lddata\"
2710 GOTO 2770
2720 NAM$ = "Dan"
2730 PATH$ = "c:\dans\"
2740 GOTO 2770
```

128

```
2750 NAM$ = "Ed"
2760 PATH$ = "c:\edm\"
2770 IF FLAG2 = 1 THEN RETURN 390
2780 RETURN 690
2790 LOCATE 20,1
2800 INPUT "What is the sample ID";ID$
2810 RETURN 690
2820 LOCATE 20,1
2830 INPUT "What is the date";DAT$
2840 RETURN 690
2850 LOCATE 20,1
2860 INPUT "What is the temperature";TEM
2870 RETURN 690
2880 LOCATE 20,1
2890 INPUT "What is the relative humidity";HUM
2900 RETURN 690
2910 LOCATE 20,1
2920 PRINT "Is the membrane rectangular, square, or circular"
2930 PRINT
2940 INPUT "(r, s, or c)";RESP$
2950 IF RESP$ <> "s" AND RESP$ <> "S" AND RESP$ <> "r" AND RESP$ <> "c"
     AND RESP$ <> "R" AND RESP$ <> "C" THEN GOTO 2940
2960 IF RESP$ = "c" OR RESP$ = "C" THEN GOTO 3040
2970 IF RESP$ = "S" OR RESP$ = "s" THEN GOTO 3010
2980 C1 = 2
2990 C2 = 1.33/(1 + PR)
3000 GOTO 3060
3010 C1 = 3.41
3020 C2 = 1.37*(1.446-(.427*PR))
3030 GOTO 3060
3040 C1 = 4
3050 C2 = 8*(.957-(.208*PR))/3
3060 LOCATE 20,1
3070 PRINT "                                              "
3080 PRINT "                                              "
3090 PRINT "                                              "
3100 PRINT "                                              "
3110 LOCATE 20,1
3120 INPUT "What is the site width (in microns)";A
3130 LOCATE 20,1
3140 PRINT "                                    "
3150 LOCATE 20,1
3160 INPUT "What is the thickness of the film (in microns)";T
3170 RETURN 690
3180 LOCATE 20,1
3190 PRINT "                                         "
3200 PRINT "                                         "
3210 PRINT "                                         "
3220 PRINT "                                         "
3230 LOCATE 20,1
3240 PRINT "What filename do you wish to store the data under"
3250 INPUT "(format XXXXXXXX.XXX) or just hit ENTER if none";FILEN$
3260 IF FILEN$ = "" THEN GOTO 3360
3270 ON ERROR GOTO 2570
```

```
3280 OPEN PATH$ + FILEN$ FOR INPUT AS #2
3290 CLOSE #2
3300 ON ERROR GOTO 0
3310 INPUT "File already exists.  Do you wish to overwrite (y or n)";RESP$
3320 IF RESP$ <> "Y" AND RESP$ <> "y" AND RESP$ <> "N" AND RESP$ <>
     "n" THEN GOTO 3310
3330 IF RESP$ = "y" OR RESP$ = "Y" THEN GOTO 3360
3340 GOTO 3180
3350 ON ERROR GOTO 0
3360 RETURN 690
3370 LOCATE 20,1
3380 PRINT "30 psi, 5 psi, or other pressure sensor"
3390 PRINT
3400 INPUT "(h, l, or o)";RESP$
3410 IF RESP$ <> "H" AND RESP$ <> "h" AND RESP$ <> "l" AND RESP$
     <>"L" AND RESP$<> "o" AND RESP$ <> "O" THEN GOTO 3400
3420 IF RESP$ = "O" OR RESP$ = "o" THEN GOTO 3520
3430 IF RESP$ = "h" OR RESP$ = "H" THEN GOTO 3480
3440  P0=-44.456794#
3450  P1=44.022302#
3460  P2=1.084012
3470 GOTO 3620
3480  P0=-312.639674#
3490  P1=312.599394#
3500  P2=0
3510 GOTO 3620
3520 LOCATE 20,1
3530 PRINT "                                              "
3540 PRINT "                                              "
3550 PRINT "                                              "
3560 LOCATE 20,1
3570 PRINT "Please enter the new coefficients"
3580 PRINT
3590 INPUT "P0 = ";P0
3600 INPUT "P1 = ";P1
3610 INPUT "P2 = ";P2
3620 RETURN 690
3630 LOCATE 20,1
3640 INPUT "What is the Poisson Ratio of the film";PR
3650 IF C1 = 2 THEN C2 = 1.33
3660 IF C1 = 4 THEN C2 = 8/(3*(1.026+(.233*PR)))
3670 IF C1 = 3.41 THEN C2 = 1.37*(1.446-(.427*PR))
3680 RETURN 690
3690  TFACT=1
3700 IF EOF(1) THEN GOTO 3700
3710  LINE INPUT #1, DEFECT$
3720  TREF=TIMER
3730  RETURN
9010  A(1,1)=0
9020  A(2,2)=0
9030  A(1,2) = 0
9031  B(1) = 0
9032  B(2) = 0
9040 FOR I = 0 TO N
```

```
9050 A(1,1) = A(1,1) + D(I)^2
9060 A(2,2) = A(2,2) + D(I)^6
9070 A(1,2) = A(1,2) + D(I)^4
9071 B(1) = B(1) + P(I)*6894.75479#*D(I)
9072 B(2) = B(2) + P(I)*6894.75479#*D(I)^3
9080 NEXT I
9090 A(2,1) = A(1,2)
9100 DETA = A(1,1)*A(2,2)-A(1,2)*A(2,1)
9110 AI(1,1) = A(2,2)/DETA
9120 AI(1,2) = -1*A(1,2)/DETA
9130 AI(2,1) = -1*A(2,1)/DETA
9140 AI(2,2) = A(1,1)/DETA
9150 CONSTANT = 0
9160 A1 = 0
9170 A3 = 0
9180 FOR I = 1 TO 2
9190 A1 = A1 + B(I)*AI(1,I)
9200 A3 = A3 + B(I)*AI(2,I)
9210 NEXT I
9220 R = 0
9230 FOR I = 0 TO N
9240 K=P(I) - A1*D(I)/6894.75479#-A3*D(I)*D(I)*D(I)/6894.75479#
9250 R = R + K*K
9260 NEXT I
9270 R = R/(N-1)
9280 FOR I = 1 TO 2
9290 AI(I,I) = AI(I,I)*R
9300 AI(I,I) = SQR(AI(I,I))
9308 IF N > 50 THEN TSTAT = TS(50): GOTO 9310
9309 TSTAT = TS(N - 1)
9310 AI(I,I) = AI(I,I)*TSTAT
9320 NEXT I
9340 STRESS = A1*A^2/(C1*T):SERROR = AI(1,1)*6894.75479#*A^2/(C1*T)
9350 MODULUS = A3*A^4/(C2*T):MERROR = AI(2,2)*6894.75479#*A^4/(C2*T)
9360 PRINT "RESIDUAL STRESS: ";STRESS/1000000!;" MPa +/-
     ";SERROR/1000000!;" MPa"
9370 PRINT "BIAXIAL MODULUS: ";MODULUS/1000000000#;" GPa +/-
     ";MERROR/1000000000#;" GPa"
9380 LPRINT
9390 LPRINT "RESIDUAL STRESS: ";STRESS/1000000!;" MPa +/-
     ";SERROR/1000000!;" MPa"
9400 LPRINT "BIAXIAL MODULUS: ";MODULUS/1000000000#;" GPa +/-
     ";MERROR/1000000000#;" GPa"
9410 RETURN
```

B. Real-Time Mass-Uptake Data-Acquisition Program

The program *massup.bas* is a BASIC program used to acquire real-time data from a network analyzer on the zero-phase frequency of a mass-uptake SAW device. The network analyzer is initially set up with a marker tracking the zero-

131

phase point of the frequency response of the device. The program causes the computer to send a periodic trigger across the IEEE-488 bus as notification that the network analyzer is to send the marker frequency back to the computer for recording. The time of the measurement, taken from the computer's internal clock, and the frequency are then stored onto a hard disk. The period of the trigger is 100 msec. A complete listing of the program is given below.

MASSUP.BAS

```
10   CLEAR ,60000! : IBINIT1=60000! : IBINIT2=IBINIT1+3 : BLOAD
     "bib.m",IBINIT1
20   CALL
     IBINIT1(IBFIND,IBTRG,IBCLR,IBPCT,IBSIC,IBLOC,IBPPC,IBBNA,IBONL,IB
     RSC,IBSRE,IBRSV,IBPAD,IBSAD,IBIST,IBDMA,IBEOS,IBTMO,IBEOT,IBRDF
     ,IBWRTF,IBTRAP,IBDEV,IBLN)
30   CALL
     IBINIT2(IBGTS,IBCAC,IBWAIT,IBPOKE,IBWRT,IBWRTA,IBCMD,IBCMDA,
     IBRD,IBRDA,IBSTOP,IBRPP,IBRSP,IBDIAG,IBXTRC,IBRDI,IBWRTI,IBRDIA,
     IBWRTIA,IBSTA%,IBERR%,IBCNT%)
31 UDNAME$ = "gpib0"
32 CALL  IBFIND(UDNAME$,BRD0%)
33 V% = 0: CALL IBONL(UDNAME$,V%)
34 CALL  IBFIND(UDNAME$,BRD0%)
40 UDNAME$ = "NA"
50 CALL  IBFIND (UDNAME$,NA%)
60 CALL  IBCLR(NA%)
70 V% = 1 : CALL IBSRE (NA%,V%)
80 KEY(1) ON:KEY(2) ON
90 ON KEY(1) GOSUB 210
100 ON KEY(2) GOSUB 280
101 FLAG = 0
110 CLS
120 INPUT "Storage filename";RESP$
130 ON ERROR GOTO 190
140 OPEN RESP$ FOR INPUT AS #1
150 CLOSE #1
160 ON ERROR GOTO 0
170 INPUT "File already exists.  Do you wish to overwrite (y or n)";ANS$
180 IF ANS$ = "y" OR ANS$ = "Y" THEN GOTO 200
185 GOTO 110
190 RESUME 191
191 ON ERROR GOTO 0
200 OPEN RESP$ FOR OUTPUT AS #1
201 CLS
202 PRINT "Waiting for F1 start signal (F2 to stop)"
209 GOTO 209
210 START=TIMER
```

```
220 WRT$ = "outpmark;":CALL IBWRT(NA%,WRT$)
230 PNT=TIMER
240 VALUE$ = SPACE$(48) : CALL IBRD(NA%,VALUE$)
250 ELAPSE=PNT-START
260 PRINT ELAPSE,VALUE$
265 PRINT #1,ELAPSE;VALUE$
266 DELAY =0
267 DELAY = DELAY + 1
268 IF DELAY < 10 GOTO 267
269 IF FLAG=1 THEN GOTO 220
270 FLAG = 1
271 RETURN 220
279 GOTO 220
280 RETURN 290
290 END
```

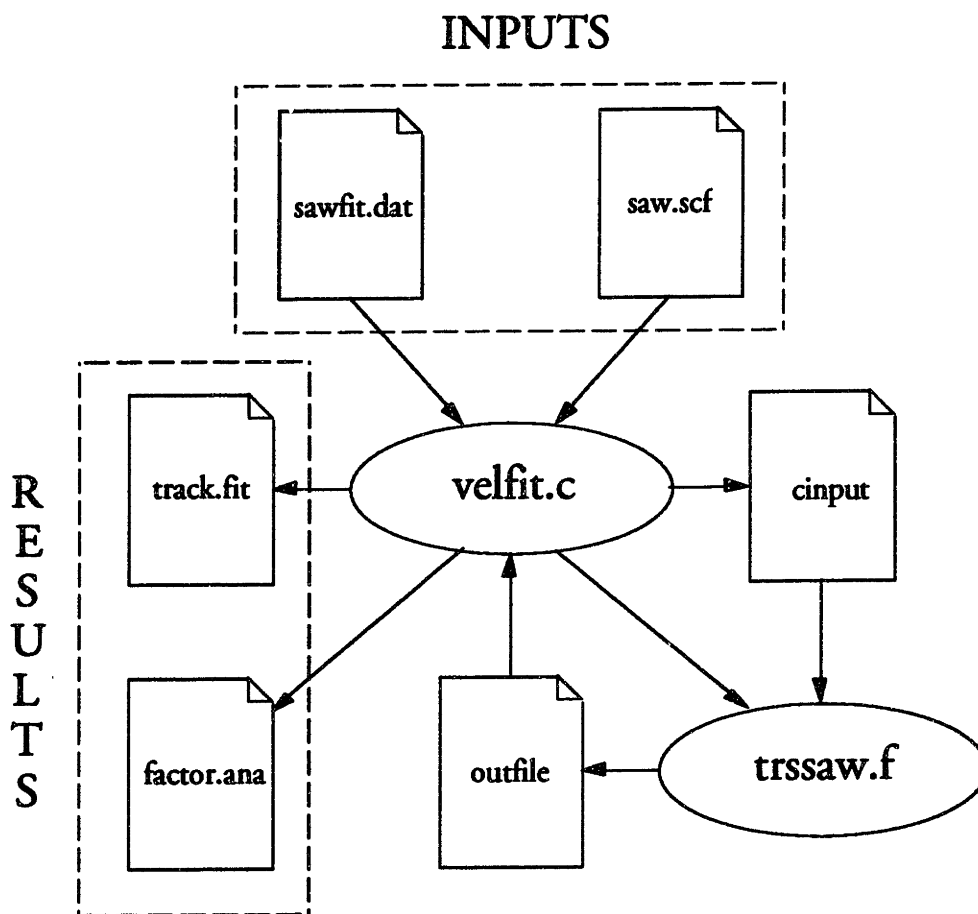## C. Program for Calculating Elastic Constants from Dispersion Data

Figure B.1: Organization of computer program for calculating elastic constants from dispersion data.

To compute the mechanical properties from experimental dispersion data, McGill SAW-simulation software [66] was called from a C program in which the elastic constants of the film are varied to minimize the squared difference between the experimental and simulated phase velocities. Direction set (Powell's) methods are used to determine how the constants are varied to find the minimum (the C code for this is given in [99]). A listing of the routines necessary for setting up the search and for calling the simulation code follows. When combined with the Powell's method routines, the code given in this Appendix completes the *velfit.c* program. Both the simulation software and the fitting program were compiled to run on a Cray-2 supercomputer.

Figure B.1 gives the organization of the program. The fitting program is called *velfit.c* whereas the simulation code is *trssaw.f*. The input file *sawfit.dat* contains the initial guesses of the film properties, the initial search directions, and the experimental velocities measured. The file *saw.scf* is the template for the input file to the simulation program. It contains the search ranges, the substrate material constants, and the film properties not being fitted such as thickness and density. Annotated samples of the two input files are given in this appendix.

Using the template, the fitting program writes another file, *cinput*, containing the search values of the elastic constants. The simulation program writes the list of simulated velocities and the associated boundary condition determinant for each velocity to the file *outfile*. The boundary condition determinant value, if greater than 10^{-4}, indicates that the velocity did not converge properly and that the associated velocity is suspect. This usually occurs when the search range was not wide enough to capture the correct value.

The fitting program reads in the simulated velocities, computes the squared error against the measured values, and adds the search step information to the file *track.fit*. The next search step is then computed and the process repeated until the

134

error is minimized. After the minimization is finished, the program then toggles the individual elastic constants by 1% to complete a two-level factorial design experimental grid [100, 101] and writes the result to *factor.ana*. The results can then be analyzed to determine the sensitivity of the velocities to each of the elastic constants as explained in Chapter 5.

SAWFIT.DAT INPUT FILE

5   **Number of Fit Elastic Constants**

.094871   e[1]

.113679   e[2]

.109427   e[3]   **Initial Guess of Elastic Constants**

.008890   e[4]

.017122   e[5]

.001 0.0 0.0 0.0 0.0

0.0 .001 0.0 0.0 0.0

0.0 0.0 .001 0.0 0.0   **Initial Search Vectors**

0.0 0.0 0.0 .001 0.0

0.0 0.0 0.0 0.0 .001

Dependencies

1 0 2.

1 8 4.   **Assignment of Elastic Constants:**

1 2 1.   First Int = 1: c[second int] = e[third int]

2 3 0.   First Int = 2: c[second int] = c[third int]

2 4 2.   First Int = 3: c[second int] = third #

1 5 3.   **c[1] = c[0] - 2c[8] always**

1 6 5.

2 7 6.

8 5   **# of velocities, # of fit constants**

2138.4   v[1]

3317.76   v[2]

1607.04   v[3]

2157.6   v[4]   **Experimentally measured velocities**

1183.2   v[5]

1353.024   v[6]

1059.66   v[7]

1195.728   v[8]

where the elastic constants, c_{ij}, have been assigned to the program array values,

c[i] according to:

$$
\begin{bmatrix}
c_0 & c_1 & c_2 & 0 & 0 & 0 \\
c_1 & c_3 & c_4 & 0 & 0 & 0 \\
c_2 & c_4 & c_5 & 0 & 0 & 0 \\
0 & 0 & 0 & c_6 & 0 & 0 \\
0 & 0 & 0 & 0 & c_7 & 0 \\
0 & 0 & 0 & 0 & 0 & c_8
\end{bmatrix}
=
\begin{bmatrix}
c_{11} & c_{12} & c_{13} & 0 & 0 & 0 \\
c_{12} & c_{22} & c_{23} & 0 & 0 & 0 \\
c_{12} & c_{23} & c_{33} & 0 & 0 & 0 \\
0 & 0 & 0 & c_{44} & 0 & 0 \\
0 & 0 & 0 & 0 & c_{55} & 0 \\
0 & 0 & 0 & 0 & 0 & c_{66}
\end{bmatrix}
\tag{B.6}
$$

Mode (1 = Both, 2 = Rayleigh, 3= Love)

1020000000000   **First Velocity Search Range**

```
                   .00          .00          .00          .00          .00
 1800.000    2700.000    .100E-05    .100E-14    .000         .000
LiNbO3    **    4700.000    .000000
  2.0300000    .5300000    .7500000    .0900000    .0000000    .0000000
   .5300000   2.0300000    .7500000   -.0900000    .0000000    .0000000
   .7500000    .7500000   2.4500000    .0000000    .0000000    .0000000
   .0900000   -.0900000    .0000000    .6000000    .0000000    .0000000
   .0000000    .0000000    .0000000    .0000000    .6000000    .0900000
   .0000000    .0000000    .0000000    .0000000    .0900000    .7500000
   .0000000    .0000000    .0000000    .0000000   3.7000000  -2.5000000
 -2.5000000   2.5000000    .0000000   3.7000000    .0000000    .0000000
   .2000000    .2000000   1.3000000    .0000000    .0000000    .0000000
 38.9000000    .0000000    .0000000    .000000038.9000000    .0000000
   .0000000    .000000025.7000000
  0  1  0  0  0  1  1             .000         .000         .000
Polyimid    1400.000    .1520062    First Layer Thickness(λ)
 0.1176855  0.0967277  0.0891833  0.0000000  0.0000000  0.0000000
 0.0967277  0.1176855  0.0891833  0.0000000  0.0000000  0.0000000
 0.0891833  0.0891833  0.1164392  0.0000000  0.0000000  0.0000000
 0.0000000  0.0000000  0.0000000  0.0107949  0.0000000  0.0000000
```

Layer elastic stiffness tensor (100 GPa)   0000 0.0107949 0.0000000
0000 0.0000000 0.0104789

```
   .0000000    .0000000    .0000000    .0000000    .0000000    .0000000
   .0000000    .0000000    .0000000    .0000000    .0000000    .0000000
   .0000000    .0000000    .0000000    .0000000    .0000000    .0000000
  3.1000000    .0000000    .0000000    .0000000   3.1000000    .0000000
   .0000000    .0000000   3.1000000
```

*S   3000.   3500.   — **Second Velocity Search Range**
*$
*S   1400.   1700.
*H   2   .1985887   — **Second Layer Thickness(λ)**
*$
*S   1700.   2400.
*$
*S   1130.   1350.
*H   2   .2830460
*$
*S   1350.   2000.
*$
*S   900.   1075.
*H   2   .4245690   — **Fourth Layer Thickness(λ)**
*$
*S   1075.   1300.   — **Eighth Velocity Search Range**
*$
*

velfit.c   Page 1
Printed on Monday, September 30, 1991 at 2:29 AM
Function main

#include <math.h>
#include <stdio.h>

```
main
```

main ()

```
{
        void powell(),factfind();
        FILE *fp,*fopen(),*wp;
        float *e,*p,**xi,ftol,fret,func(),tp[6];
        float *vector(),**matrix();
        int f[10],k,n,iter,i,j,ipow();
        char inline[200];

        fp = fopen("sawfit.dat","r");
        fgets(inline,200,fp);
        sscanf(inline,"%d",&n);

        p = vector(1,n);
        e = vector(1,n);
        for (i=1;i<=n;i++) {
           fgets(inline,200,fp);
           sscanf(inline,"%f",&p[i]);
        }

        xi = matrix(1,n,1,n);
        for (i=1;i<=n;i++) {
           fgets(inline,200,fp);
           sscanf(inline,"%f %f %f %f %f",&tp[1],&tp[2],&tp[3],&tp[4],&
...tp[5]);
           for (j=1;j<=n;j++)
              xi[j][i]=tp[j];
        }

        fclose(fp);

        ftol = 1e-6;

        powell(p,xi,n,ftol,&iter,&fret,func);
```

velfit.c   Page 2
Printed on Monday, September 30, 1991 at 2:35 AM
Functions main *(continued) and* ipow

```
for (i=1;i<=ipow(2,n);i++) {
    factfind(n,f,i);
    for(j=1;j<=n;j++) {
        e[j] = p[j] + 0.01*p[j]*f[j];
    }
    ftol = func(e);
    fp = fopen("outfile","r");
    wp = fopen("factor.ana","a");

    for (k=1;k<=n;k++) {
        fprintf(wp,"%f  ",e[k]);
    }
    fprintf(wp,"%f\n",ftol);

    while (fgets(inline,200,fp) != NULL) {
        fputs(inline,wp);
    }
    fclose(fp);
    fclose(wp);
}
ftol = func(p);
}
```

ipow

```
int ipow(a,b)
int a,b;

{
    int i,val;
    val = 1;
    for (i=1;i<=b;i++) {
        val = val*a;
    }
    return(val);
}
```

Functions factfind *and* func

factfind

```
void factfind(n,f,i)
int n,*f,i;

{
  int j,ipow(),k;
  i = i-1;
  for (j=1;j<=n;j++) {
    f[j] = 0;
  }
  for (j=n;j>=1;j--) {
    if(i >= ipow(2,j-1)) {
      f[j] = 1;
      i = i - ipow(2,j-1);
    }
  }
}
```

func

```
float func(p)
float p[];

{
        FILE *fp, *wp, *fopen(), *dp;
        char inline[200];
        char *prog,*file;
        float e[9];
        int spawnl();
        int np,n,i,j,k,m;
        float vs[10],d[10],r,a,err,l,vo,vf,dz,df;
        void modify();

        dp = fopen("sawfit.dat","r");
        fgets(inline,200,dp);
        while(inline[0] != 'D') {
          fgets(inline,200,dp);
        }

        for(i=1;i<=8;i++) {
          fgets(inline,200,dp);
          sscanf(inline,"%d  %d  %f",&j,&k,&l);
          if(j == 1) {
            m = (int)l;
            e[k] = p[m];
          }
```

velfit.c   Page 4
Printed on Monday, September 30, 1991 at 2:35 AM
Function func *(continued)*

```c
      if(j == 2) {
         m = (int)l;
         e[k] = e[m];
      }
      if(j == 3) {
         e[k] = l;
      }
      if(i == 2) {
         e[1] = e[0]-e[8]*2.0;
      }
   }

   fp = fopen("saw.scf","r");
   wp = fopen("cinput","w");
   while(fgets(inline,200,fp) != NULL) {
         fputs(inline,wp);
         if (inline[0] == 'P') {
                   modify(fp,wp,e);
         }
   }
   fclose(fp);
   fclose(wp);

   system("trssaw");

   wp = fopen("outfile","r");

   fgets(inline,200,dp);
   sscanf(inline,"%d  %d",&n,&np);

   for (i=0;i<=n-1;i++) {
         fscanf(wp,"%f  %f",&vs[i],&d[i]);
   }
   fclose(wp);

   err = 0;
   for(i=0;i<=n-1;i++) {
      fgets(inline,200,dp);
      sscanf(inline,"%f",&r);
      err = err + (r-vs[i])*(r-vs[i]);
   }
   fclose(dp);
```

141

```c
        fp = fopen("track.fit", "a");
        for(i=1;i<=np;i++) {
            fprintf(fp,"%.7f  ",p[i]);
        }
        fprintf(fp,"%.7f\n",err);
        fclose(fp);
        return(err);

}
```

modify

```c
void modify(fp,wp,c)

FILE *fp,*wp;
float c[];

{

        char inline[200];

        fgets(inline,200,fp);
        fprintf(wp,"%10.7f%10.7f%10.7f%10.7f%10.7f%10.7f\n",c[0],c[
...1],c[2],0.0,0.0,0.0);

        fgets(inline,200,fp);
        fprintf(wp,"%10.7f%10.7f%10.7f%10.7f%10.7f%10.7f\n",c[1],c[
...3],c[4],0.0,0.0,0.0);

        fgets(inline,200,fp);
        fprintf(wp,"%10.7f%10.7f%10.7f%10.7f%10.7f%10.7f\n",c[2],c[
...4],c[5],0.0,0.0,0.0);

        fgets(inline,200,fp);
        fprintf(wp,"%10.7f%10.7f%10.7f%10.7f%10.7f%10.7f\n",0.0,
...0.0,0.0,c[6],0.0,0.0);

        fgets(inline,200,fp);
        fprintf(wp,"%10.7f%10.7f%10.7f%10.7f%10.7f%10.7f\n",0.0,
...0.0,0.0,0.0,c[7],0.0);

        fgets(inline,200,fp);
        fprintf(wp,"%10.7f%10.7f%10.7f%10.7f%10.7f%10.7f\n",0.0,
...0.0,0.0,0.0,0.0,c[8]);

}
```

APPENDIX C: ADINA INPUT FILE FOR FEM SIMULATION OF LOAD-DEFLECTION OF A RECTANGULAR MEMBRANE

ADINA (ADINA Engineering Inc., Watertown, MA) running on a Sun-4 workstation was the FEM program used to analyze the membranes. A typical input file for simulating the load-deflection of a rectangular membrane is given below. To account for the residual stress, the material is designated to be thermo-elastic, and a temperature load is applied. The large deflection solution is then computed by applying the pressure load in a number of small steps, computing a solution after each load step. To save on computing time, only one quarter of a rectangular membrane with length 2", width 1/4", thickness 5 μm, and circular ends was simulated with 1296 four-noded shell elements.

ADINA INPUT FILE

```
DATABASE CREATE
HEAD 'RECTANGULAR MEMBRANE'
*
MASTER IDOF=000001 NSTEP=18 TSTART=0.0 ITP56=2 REACTIONS=NO
KINEMATICS DISPLACEMENT=LARGE STRAIN=SMALL
ITERATION METHOD=FULL-NEWTON LINE-SEARCH=YES
TOLERANCES ITEMAX=99
PRINTOUT VOLUME=MINIMUM PRINTDEFAULT=NO
PRINTNODES 1 4
*
TIMEFUNCTION 1
  0.0   0.0
  1     0.3
  2     0.7
  3     1.000000
  4     2.027025
  5     3.365500
  6     4.633262
  7     6.476830
  8     9.114032
  9     12.404360
  10    16.423928
  11    18.280490
  12    21.467910
  13    25.097240
  14    28.030548
  15    31.309172
```

```
   16    35.471095
   17    41.427173
   18    45.932141
*
COORINDATES
ENTRIES NODES   X     Y     Z
        1    0.   0.    .0
        2   25.4  0.    .0
        3   25.4  3.175 .0
        4    0.   3.175 .0
        5   28.575 3.175  .0
LINE STRAIGHT 1 2 30
LINE STRAIGHT 2 3 24
LINE STRAIGHT 3 4 30
LINE STRAIGHT 1 4 24
LINE STRAIGHT 3 5 24
LINE ARC 2 5 3 24
SHELLNODESDOF DOF-DEFAULT=FIVE DOF-INPUT=SIX TYPE=LINES
 1 2 / 2 5 / 3 5 / 3 4 / 4 1
*
MATERIAL 1 THERMO-ELASTIC TREF=0.0 DENSITY=1.42E-6
-10.0  3000.  0.40  0.0060000
  0.0  3000.  0.40  0.0060000
 22.0  3000.  0.40  0.0060000
*
EGROUP 1 SHELL RESULTS=FORCE
GSURFACE 1 2 3 4 30 24 4 NCOINCIDE=ALL
THICKNESS 1 THICK1=0.0050
LOADS ELEMENTS
     1  -3  0.000279451 0.000279451 0.000279451 0.000279451 1
     STEP 1 TO
     720  -3  0.000279451 0.000279451 0.000279451 0.000279451 1
*
EGROUP 2 SHELL RESULTS=FORCE
GSURFACE 2 5 3 2 24 24 4 NCOINCIDE=ALL
THICKNESS 1 THICK1=0.0050
LOADS ELEMENTS
     1  -3  0.000279451 0.000279451 0.000279451 0.000279451 1
     STEP 1 TO
     576  -3  0.000279451 0.000279451 0.000279451 0.000279451 1
*
FIXBOUNDARIES 123456 TYPE=LINES / 2 5
FIXBOUNDARIES 123456 TYPE=LINES / 1 2
FIXBOUNDARIES 246 TYPE=LINES / 3 4
FIXBOUNDARIES 246 TYPE=LINES / 3 5
FIXBOUNDARIES 156 TYPE=LINES / 4 1
*
LOAD TEMPERATURE TREFN=-1
*
ADINA
```